April 2019

Controlled Wetting Using Ultrasonic Vibration

Matthew A. Trapuzzano
University of South Florida, m_trapuzzano@yahoo.com

Controlled Wetting Using Ultrasonic Vibration

by

Matthew A. Trapuzzano

A dissertation submitted in partial fulfillment
of the requirements for the degree of
Doctor of Philosophy in Mechanical Engineering
Department of Mechanical Engineering
College of Engineering
University of South Florida

Co-Major Professor: Nathan B. Crane, Ph.D.
Co-Major Professor: Rasim Guldiken, Ph.D.
Andrés Tejada-Martínez, Ph.D.
Zhimin Shi, Ph.D.
Daniel Hess, Ph.D.

Date of Approval:
December 7, 2018

Keywords: Resonance, Transducer, Contact Angle, Contact Line, Droplet

DEDICATION

This thesis and work is dedicated to my late brother Nathan Benjamin Trapuzzano, for whom without, I would not be where I am today. The love, friendship, help, and guidance you provided me in the short time I was blessed to have with you will always be cherished. I hope you are proud of me. Euge serve bone et fidelis, I love you brother.

ACKNOWLEDGEMENTS

First, I would like to thank the National Science Foundation for supporting this work under Grant No. 1361919, for without the aid, I would not have been able to afford to continue my graduate studies. My committee members also deserve acknowledgment for their constant support and guidance: Dr. Rasim Guldiken for the fluids and acoustics background; Dr. Andrés Tejada-Martínez for insightful numerical simulations; Dr. Daniel Hess for the help and insight with acceleration measurement; And Dr. Zhimin Shi for insight provided for optical measurements. I would like to especially thank my advisor, Dr. Nathan Crane, for his time and guidance. I would also like to thank my lab mates Qi Ni, Jose Carabllo, Efe Yayoglu, Mohsen Ziaee, Clayton Neff, and Justin Nussbaum for their companionship along the way. The insight and humor they provide helped to make my work environment enjoyable and fruitful; they have become life-long friends. I am thankful for my family for their support and everything they have done for me, and am especially thankful for my lovely wife, Molly Catherine, for always believing in me and putting up with my absence. Lastly, and most importantly, I give thanks to God for blessing me with opportunity and abilities that have allowed me to be where I am today. At times I have doubts that I make the right decisions, but I trust that there is a greater plan for my life. Trust in the LORD with all your heart and lean not on your own understanding; in all your ways submit to him, and he will make your paths straight – Proverbs 3:5-6.

TABLE OF CONTENTS

LIST OF TABLES

LIST OF FIGURES

ABSTRACT

Many industrial processes such as printing and cleaning, as well as products like adhesives, coatings, and biological testing devices, rely on the wetting of liquids on a surfaces. Wetting is commonly controlled through material selection, coatings, and/or surface texture, but these means are sensitive to environmental conditions. Wetting is influenced by variables like surface tension, density, the surface chemistry, local energy barriers like surface roughness, and how the droplet is placed on the surface. Wetting of droplets can also be influenced externally in many ways such as introducing surfactants, applying electrical fields, or by dynamically excitation. Low-frequency, high amplitude vibration can initiate wetting changes prompted by droplet contact line oscillations that exceed the range of stable contact angles inherent of a droplet on a solid surface.

The study of ultrasonic vibration wetting and spreading effects is sparse [1, 2], and is usually only qualitatively analyzed. Therefore, the specific goal of this thesis is somewhat unique, but also has potential as a means to controllably reverse surface adhesion.

High frequency vibration effects and the governing mechanisms are relatively uncharacterized due to difficulties posed by the spatial and temporal scales. To investigate, droplets of 10, 20, and 30 µL are imaged as they vibrate on a hydrophobic surface forced via a piezoelectric transducer over different high frequencies (>10 kHz). Wetting transitions occur abruptly over a range of parameters, but coincide with transducer resonance modes. The

magnitude of contact angle change is dependent on droplet volume and surface acceleration, and remains after cessation of vibration, however new droplets wet with the original contact angle.

A more detailed investigation of this phenomenon was necessary to obtain a better understanding. This required repeatable testing conditions, which relies heavily on surface integrity. However, some "hydrophobic" coatings are sensitive to extended water exposure. To determine which hydrophobic coatings may be appropriate for investigating dynamic wetting phenomena, samples of glass slides coated with a series of fluoropolymer coatings were tested by measuring water contact angle before, during, and after extended submersion in deionized water and compared to the same coatings subjected to ultrasonic vibration while covered in deionized water. Both methods caused changes in advancing and receding contact angle, but degradation rates of vibrated coatings, when apparent, were significantly increased. Prolonged soaking caused significant decreases in the contact angle of most coatings, but experienced significant recovery of hydrophobicity when later heat-treated at 160 C. Dissimilar trends apparent in receding contact angles suggests a unique degradation cause in each case. Roughening and smoothing of coatings was noted for coatings that were submerged and heat-treated respectively, but this did not correlate well with the changing water contact angle. Degradation did not correspond to surface acceleration levels, but may be related to how well coatings adhere to the substrate, indicative of a dissolved coating. Most coatings suffered from contact angle degradation between 20-70% when exposed to water over a long period of time, however the hydrophobic fluoropolymer coating FluoroSyl was found to remain unchanged. For this reason it was found to be the most robust coating for providing long term wetting repeatability of vibrated droplets.

Droplets (10 to 70 µL) were imaged on hydrophobic surfaces as they were vibrated with ultrasonic piezoelectric transducers. Droplets were vibrated at a constant frequency with ramped amplitude. Spreading of droplets occurs abruptly when a threshold surface acceleration is exceeded of approximately 20,000 m/s^2. Droplet contact area (diameter) can be controlled by varying acceleration levels above the threshold. The threshold acceleration was relatively independent of droplet volume, while initial contact angle impacts the extent of spreading. Wetting changes remain after cessation of vibration as long as the vibrated droplet remained within the equilibrium contact angle range for the surface (> the receding contact angle), however new droplets wet with the original contact angle except for some cases where vibration of liquid can affect the integrity of the coating. Reversible wettability of textured surfaces is a desired effect that has various industry applications where droplet manipulation is used, like biomedical devices, coating technologies, and agriculture [3-5].

CHAPTER 1:

INTRODUCTION

1.1 Abstract

This chapter provides a brief overview of the interactions that occur between liquids and solids. The importance of these interactions to many processes, and the possible benefits of controlling these interactions is discussed. The goal of this work is stated, and at the end, the main topic of each chapter will be summarized.

1.2 Wetting Background

'Wetting' is the term used for the process of a liquid making contact with a solid. While the effects of these interactions are noticeable to the human eye (like the rise of a liquid in a capillary), they are actually determined by phenomena occurring on the microscopic scale (Figure 1). The complex interactions between a liquid and a solid are often overlooked even though they are a crucial aspect of many processes such as printing [6], coating [7], cleaning [8], lubrication [9], and adhesion [10]. In nature, it is critical to self-cleaning properties such as those found on the leaves of a lotus plant [11], the ability for spiders and insects to walk on water [12], and fog harvesting capabilities like those exploited by the Namib Desert beetle [13], are a result of the interactions between liquids and solids.

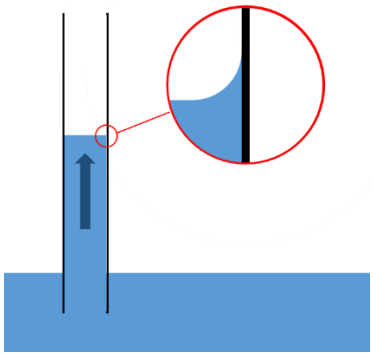

Figure 1. Microscopic effect of liquid-solid interaction in a capillary tube inserted in a liquid as the liquid rises.

1.3 Surface Free Energy

Wetting is the physical manifestation of the minimization of surface free energy at the phase boundaries of the interacting materials. Surface free energy (γ) emerges from the interaction of intermolecular cohesive forces [14-16]. Molecules in the bulk of a liquid are subject to attractive forces in all directions from other molecules in the bulk. However, molecules at or near an interface are missing neighboring bulk molecules on one side. This imbalance in cohesive forces results in free surface energy and a surface tension force (σ) at the 'skin' of the liquid generated from the net force on the molecules at the liquid interface (Figure 2).

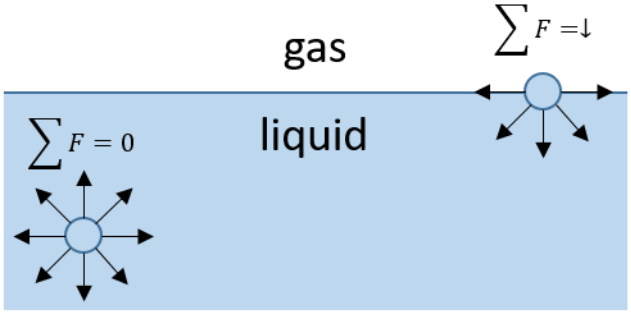

Figure 2. Imbalance of intermolecular cohesive forces in a liquid that are responsible for the surface tension phenomenon.

These interactions are most often observed between a liquid and a gas or a liquid and a solid, because of the formation of an interface. However, the minimization of energy applies to interactions between all media, and interfaces can even form between two liquids or two gases [17].

1.4 Wetting on Solid Surfaces

When a liquid wets a solid, the resulting shape of the liquid varies based on the interfacial tensions of the interacting mediums [18], other mechanical properties of the liquid like density and viscosity, hysteretic effects like surface roughness [19] and the liquid dispensing methods [20], as well as gravity. If the liquid wets the solid as a droplet, the liquid-gas interface forms an apparent angle with the solid-liquid phase along the perimeter of the droplet. The droplet perimeter is known as the contact line, and the angle is known as the contact angle or wetting angle θ (Figure 3).

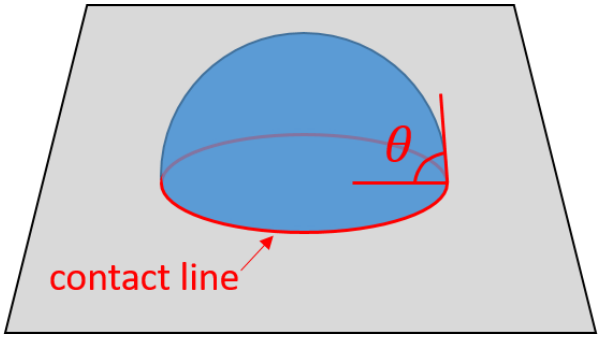

Figure 3. Angle formed between the liquid-gas and solid-liquid interfaces when a liquid wets a solid.

The contact angle useful in the characterization of different liquids and solid surfaces [21]. For instance, surfaces are commonly referred to as hydrophobic or hydrophilic if water wets the surface at an angle greater or less than 90 ° respectively. However, as mentioned before,

the wetting state depends on different factors, and becomes much more complicated if the surface is not smooth.

1.5 Wetting on Textured Surfaces

Liquid on a surface that is sufficiently rough can wet in more than one state; the liquid can be partially suspended by surface features in a slick state or wet into the texture in a sticky state (Figure 4).

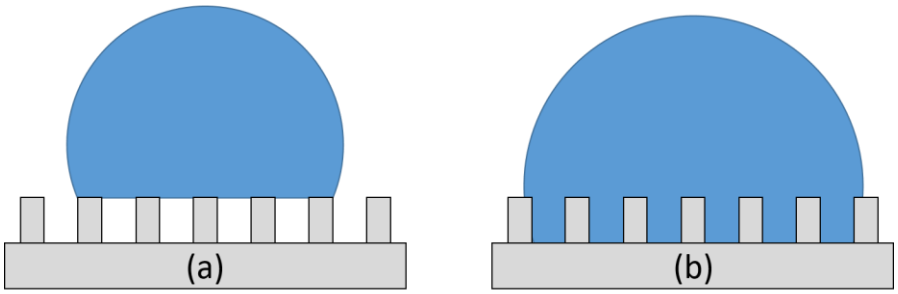

Figure 4. Different wetting states of a liquid on a solid with a rough texture. A droplet can be partially suspended by the surface features of the solid (a), or wet into the texture of the surface (b).

The texture can make determination of the contact angle very difficult because of the microscopic menisci that can form. However, textured surfaces can be useful in changing the wetting state of a liquid, but controlling the effects is complicated. While varying the wetting of liquids on smooth surfaces can be done with the use of electrical fields and mechanical agitation, as well as by chemically altering the mechanical properties of the solid of liquid, surface features can promote the movement of a droplet's contact line or inversely act as energy barriers to the movement. Careful combination of mechanical agitation of the liquid's contact line, with specific surface energy barriers could allow the contact line to transition between surface features to

numerous stable wetting states. The ability to control the wetting state of droplets on a solid would have value in applications such as self-cleaning surfaces, tailored corrosion of materials, and to increase or decrease adhesion of liquids on a surface.

1.6 Wetting Dynamics

External forcing with large amplitude vibration, at low frequencies that correspond to droplet volume resonance, is one way to alter the contact lines of droplets on a solid. However, large oscillations in the surface are not usually desired, so lower amplitude oscillations, like those provided by higher frequency vibration would be preferred. However, the interactions between liquids and rough surfaces is very complex and not well understood, so wetting transitions on smooth surfaces is an ideal starting point for initial investigation of the dynamic contact line effects.

1.7 Dissertation Objective

The objective of this thesis is to controllably wet liquid droplets with ultrasonic vibration. Comprehension of the complex interactions between liquids and textured surfaces will allow the use of mechanical vibration to precisely control droplet contact line dynamics and influence interactions to obtain numerable stable liquid wetting states. To that end, this work investigates the use of ultrasonic vibration (> 20 kHz) to controllably and repeatedly wet droplets initially on smooth hydrophobic surfaces and troubleshoots some of the inherent difficulties that ultrasonic vibrations produce.

1.8 Dissertation Outline

The next chapter entails a background of basic wetting terminology, measurement methods, and related research necessary to form a foundation for the basis of this work. This includes an explanation of static and dynamic contact line interactions, a report of interactions between liquids and rough surfaces with application of switchable adhesion, and a broad discussion of the effects of vibration on liquid droplets.

Chapter 3 is an experimental validation and qualitative analysis of the accuracy of the measurement systems utilized in this work. The focus of this chapter is the reliability of acceleration measurement with a piezoelectric accelerometer and a dynamic analyzer. Other set-backs and measurement difficulties, like the inherent error of using an adhesive coupling with high power are also discussed in this chapter. An emphasis on the stability of hydrophobic coatings and the importance for using robust coatings to obtain meaningful results while experimenting with ultrasonic vibration is introduced.

Chapter 4 is a detailed study of the robustness of hydrophobic fluoropolymer coatings – used in this work and elsewhere in common industrial applications – and their resistance to contact angle change when exposed to water and ultrasonic vibration. The findings are discussed, and the different degradation from both mechanisms are compared. Application of the results from the testing of ultrasonically-vibrated wet coatings is used to implement an accurate testing method for vibrating droplets at high frequencies.

In chapter 5, the most robust, readily available hydrophobic coatings were used to determine the effects that ultrasonic vibration frequency has on the wetting of droplets on the smooth hydrophobic surfaces. The effects of vibration frequency, droplet volume, and surface

acceleration on the wetting of water droplets are compared qualitatively, and a new method of investigation is conceived to characterize the wetting transitions.

Chapter 6 applies the initial comprehension of the ultrasonic wetting phenomena to a different method for the control of droplet spreading using ultrasonic vibration. By controlling the level of acceleration generated by high frequency vibration, droplets are controllably spread over a range of frequencies. Droplet size and shape, as well as mechanical properties are varied to characterize this process to adapt its use to switchable adhesion of droplets in the future.

Finally in chapter 7, the control of droplet spreading using ultrasonic vibration is proposed as a means to reversibly wet and de-wet textured surfaces, and the future work and direction of this research is discussed.

CHAPTER 2:

BACKGROUND

2.1 Abstract

The objective of this dissertation is to characterize the wetting effects caused by ultrasonically vibrated surfaces. This chapter details background information on liquid-solid interactions, surface energy measurement methods, and droplet dynamics that are closely related to the later work described in this manuscript. The importance of liquid-solid interaction (artificial and natural) is the cause for the recent increase of the investigation of wetting phenomena. A more specific background on wetting is necessary to form an understanding of the scope of the problem, and is necessary to guide future work. Wetting on non-ideal surfaces is discussed in detail; this includes textured surface fabrication methods and interactions of wetting transitions. Vibration resonance prediction, and validation of measurement methods are discussed. The effects of vibration on liquid wetting on solid surfaces, specifically contact line motion, are summarized. Finally, we propose a method for the adhesive control of liquids on textured surfaces with ultrasonic vibration.

2.2 Wetting

Wetting of a fluid on a surface may seem trivial, but in fact, it is an extremely complex interaction that takes place on a range of size scales. Freely suspended liquid takes on a shape which minimizes the free energy of the system (liquid and air in this case). For liquid water in

the absence of gravity, this equilibrium shape is a perfect sphere that minimizes the surface area of the droplet. In the presence of gravity however, liquid droplets can deform under their own weight. The capillary length (K) of a liquid describes a characteristic interface length, which when exceeded, begins to be influenced by gravitational forces. It is defined as

$$K = \sqrt{\frac{\sigma}{\rho g}} \tag{1}$$

where σ is the liquid-gas surface tension, ρ is the liquid density, and g is the gravitational constant. For water, the capillary length is ~2.73 mm. Droplets of water with a diameter greater than the capillary length will not be spherical, but rather flatten out as they wet a surface. A liquid droplet placed in a static position on a surface that is smooth and homogeneous throughout, forms an equilibrium contact angle (θ_E) between the liquid-solid and liquid-air interface at the triple point where the liquid, solid, and air meet (Figure 5).

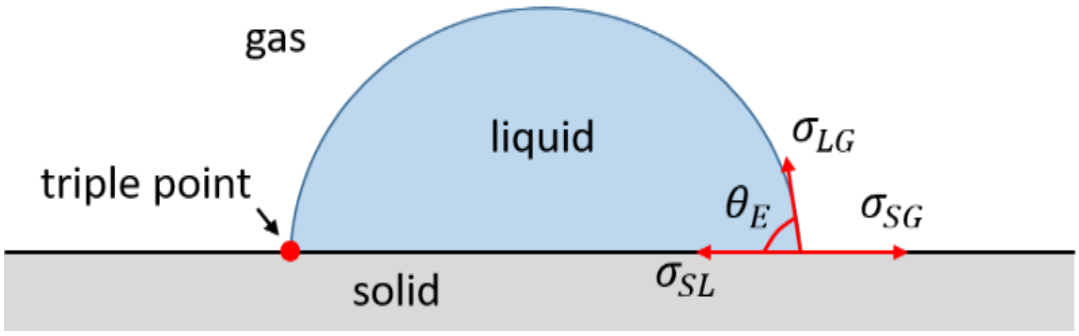

Figure 5. Schematic of surface tension forces for a droplet that can wet a surface with a range of equilibrium contact angles (θ_E). The triple point is shown as a red dot.

This angle is known as the wetting angle (or contact angle), and was first described by Thomas Young [18] in 1805. The contact angle of a droplet on a solid surface depends on the balance of interfacial surface tension forces acting at the triple point:

$$\sigma_{SG} = \sigma_{LG} * cos\theta_E + \sigma_{SL} \quad (2)$$

where σ_{SG}, σ_{LG}, σ_{SL} are the solid-gas, liquid-gas, and solid-liquid interfacial tensions, and θ_E is the Young's equilibrium angle. This equation is well known and is referred to as Young's equation. Alternatively, this angle can be conceptualized in terms of the free energies per unit area (γ) at the liquid-solid, liquid-gas, and solid-gas interfaces [22]. Lower wetting results in a liquid forming a droplet on a surface and strong adhesion forces result in a liquid spreading out on a surface. If $\gamma_{SL} > \gamma_{SG} + \gamma_{LG}$, the minimization of the large free energy at the liquid-solid interface results in a 180 ° contact angle that causes the liquid not to wet the solid at all, but 'bead' up on the surface of the solid. If $\gamma_{SL} < \gamma_{SG} - \gamma_{LG}$ the low free energy at the liquid-solid interface results in a 0 ° contact angle that cause the droplet to spread out to cover the solid surface.

Use of the contact angle is very common method to characterize the wettability of materials. High contact angles correspond to low wettability, and low contact angles correspond to high wettability. The wettability of a surface to a specific liquid is critical for many manufacturing processes like soldering of integrated circuits, adhesive bonding, and surface coating such as painting. It is also vital to lab-on-chip medical devices used for biological testing.

Prediction of a droplet's wetting state on a surface can be done by considering the spreading coefficient [23].

$$S = \gamma_{SG} - (\gamma_{SL} + \gamma_{LG}) \quad (3)$$

When $S > 0$, the liquid will completely wet the substrate, and when $S < 0$, the liquid partially wets the substrate (Figure 6).

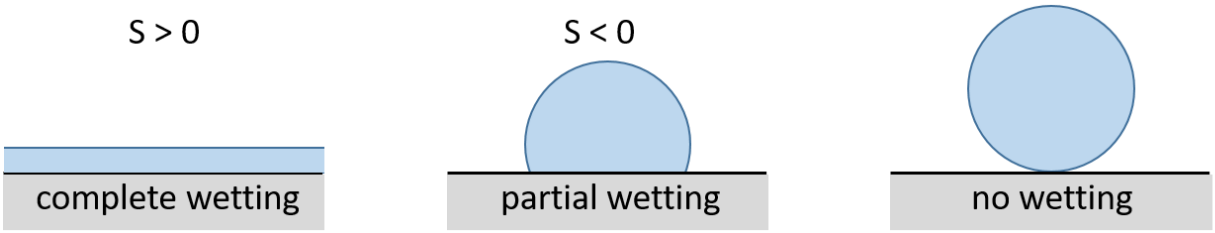

Figure 6. Wetting regimes defined by the spreading coefficient. When S > 0 complete wetting of the solid surface occurs. When S > 0 partial wetting of the solid surface occurs.

If complete spreading does not occur, Young's equation can be used to solve for the contact angle. The spreading coefficient can be combined with Young's equation to form the Young-Dupré equation [24], which also only has valid solutions for θ when $S < 0$.

$$S = \gamma_{LG}(cos(\theta) - 1) \quad (4)$$

2.3 Contact Angle Measurement

If prediction of a liquid's wetting angle on a solid surface is not feasible, measurement of the contact angle can be done experimentally by various methods [21, 25]. Optical measurement of contact angles is a simple method. One way this can be done is by projecting a scaled-up

version of the droplet's shape laterally on to a surface where the contact angle is measured directly (Figure 7).

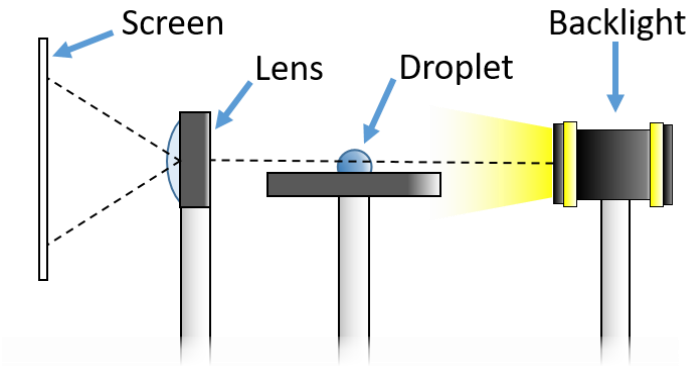

Figure 7. Optical projection contact angle measurement method.

Direct optical measurement of contact angle can be accomplished by using high resolution imaging equipment and a backlight to provide high contrast images of the droplet's shape (Figure 8). Calculation of the contact angle is then completed by post-processing images. Typically, this is done semi-automatically using sophisticated edge detection algorithms and curve fitting, but can be approximated manually with triangulation at the contact line (Figure 9).

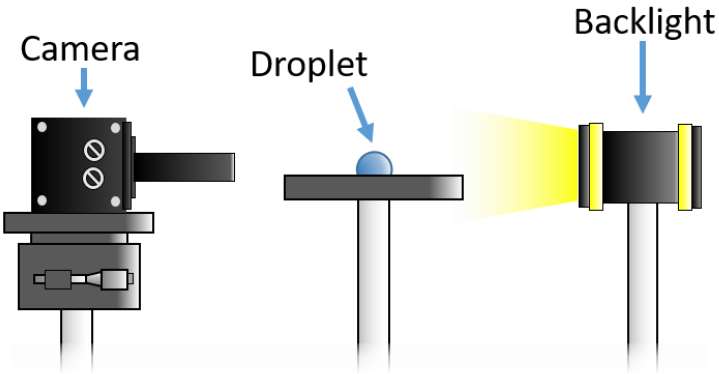

Figure 8. Direct optical measurement of contact angle using a camera and backlight.

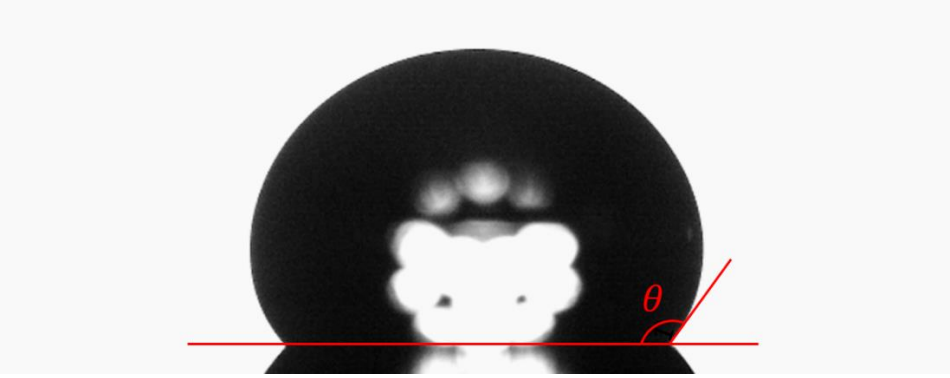

Figure 9. Direct optical measurement of contact angle using back-lit droplet profiles.

Direct optical measurement of contact angles is used prolifically for the characterization of surfaces [7]. All of the optical measurement methods are relatively simple and low-cost, and can be applied in most situations. Accuracy is typically approximately ± 2 ° [25]. More accurate contact angle measurement methods do exist, however. Vertical interferometric microscopy of droplet contact angle is performed with sophisticated equipment that determines the phase shift of an optical beam that is partially reflected into a photo detector off of the surface of the liquid droplet, and partially refracted through the liquid and then reflected off of the solid surface underneath the droplet. Using the interference pattern created by the split beam incident on the photo detector, the profile can be reconstructed, and the contact angle calculated. The previously described method has approximately ± 0.1 ° accuracy, but its application is restricted to scenarios where the contact angle is less than 45 °, so it is not very commonly used. Other methods, like capillary rise measurement, or the Wilhelmy method [26] can be used to measure the surface energy of a liquid/solid combination and then calculate the contact angle of liquids on solids indirectly, but these are not applicable to droplets. Measurement of contact angle is a useful way to characterize a surface, but because a liquid moves when wetting occurs, a unique wetting state

does not generally exist and the use of a single static contact angle is not completely adequate to describe the wetting state.

2.4 Contact Angle Hysteresis

As wetting occurs, a moving contact line produces a dynamic contact angle. A solid-liquid interface moving away, or advancing from the liquid will have a larger contact angle than the same interface moving toward, or receding into the liquid. The angles formed at the interface of the advancing and receding liquid are called the advancing contact angle (θ_A) and the receding contact angle (θ_R), respectively (Figure 10).

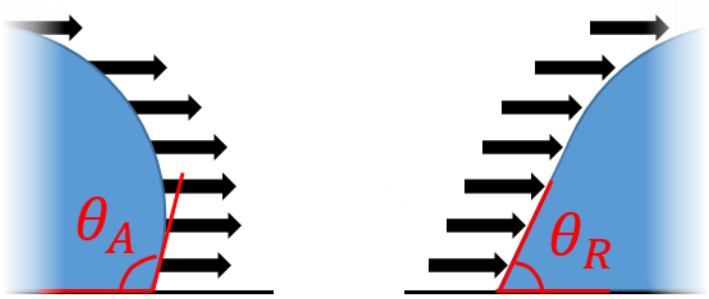

Figure 10. Advancing (θ_A) and receding (θ_R) contact angle of a liquid interface that is advancing and receding, respectively.

This effect is called contact angle hysteresis (H), and it is usually attributed to the presence of surface defects or heterogeneities in the topography or chemical make-up of a surface [19, 27-30]. The contact angle hysteresis is defined as the difference between the advancing and receding contact angles [31].

$$H = \theta_A - \theta_R \tag{5}$$

Hysteresis gives the range of possible equilibrium contact angles of a liquid on a surface. Unlike an ideal surface, any real surface is inherently rough to some extent. This roughness can be non-homogeneous, so that when a liquid wets, the contact line may have to overcome local energy barriers in different locations. These barriers can cause local pinning of the contact line that may lock the droplet in place. This makes interpretation of the contact angle on a rough surface by means of Young's equation misleading and essentially meaningless because it does not account for surface topography.

Along with contact angle, contact angle hysteresis is the second quantity that is commonly used to characterize the wettability of a surface. However, when liquid wets a textured surface, these quantities can become ambiguous.

2.5 Wetting and Textured Surfaces

When a droplet is placed on a flat homogeneous surface, it wets the surface uniformly with a contact angle that can be determined by Young's equation. When the same droplet is placed on a rough surface, wetting becomes much more complicated. For rough surfaces, measurement of contact angle by projection of the droplet shape, or by interferometric methods can be difficult because of the presence of heterogeneities. These can cause the local angle to vary due to deformation along the contact line, which is anchored to small defects [32]. However, if the scale of the heterogeneities is orders of magnitude smaller in comparison to the characteristic length of the droplet, the aforementioned measurement methods work well. A liquid typically exhibits one, or a mixture of the following behaviors when wetting a rough surface. Firstly, it is possible that the droplet may completely wet, or come into full contact with

the solid surface (Figure 11). In this case, the entire surface area of the liquid within the perimeter of the contact line is in contact with the solid surface.

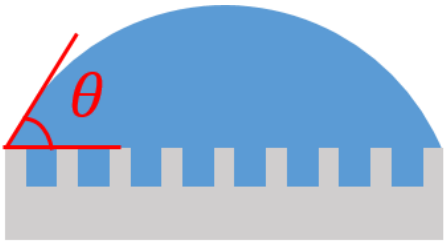

Figure 11. Wenzel state of a droplet wetting a textured surface.

Even if the rough surface is of the same composition as the ideal smooth surface, the surface energy will differ and the liquid will wet differently on each surface. In 1936, Robert Wenzel described a simple model for this type of homogeneous wetting of a rough surface [33].

$$cos\theta^* = rcos\theta_E \quad (6)$$

The symbol θ^* is the apparent contact angle, r is the ratio of the area of the liquid-solid interface to the projected area within the contact line of the droplet, and θ_E is the Young contact angle for the ideal surface. The roughness of the surface can act to pin the droplet in place, but also increases the area of contact between the liquid and air phases, thereby causing the free energy to affect the wetting state.

Secondly, if the surface has certain combinations of texture and surface energy, the liquid may not penetrate into the textured surface entirely, but rather float along the tops of protruding surface features forming a make-shift, or composite solid-liquid-air interface (Figure 12). A

surface that causes liquid to form a composite interface usually repels liquid well due to air gaps that remain under the droplet, allowing it to slip along the top of the surface with low friction.

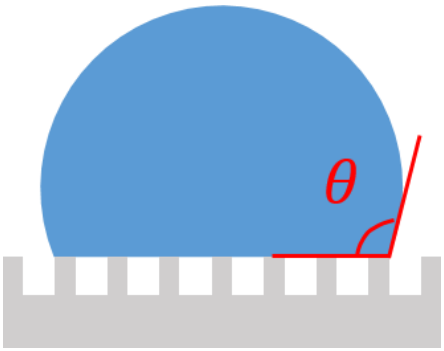

Figure 12. Cassie-Baxter state of a droplet wetting a textured surface.

A more complicated approach is needed in this case to determine the contact angle. A model for the apparent equilibrium contact angle θ^*_E on a heterogeneous surface was proposed by Cassie and Baxter in 1944 [34].

$$cos\theta^*_E = r_\emptyset \emptyset_S cos\theta_1 + (1 - \emptyset_S) cos\theta_2 \quad (7)$$

where θ_1 and θ_2 are equilibrium contact angles on the ideal solid surface (θ_E) and air (180°), and $r_\emptyset \emptyset_S$ and $(1 - \emptyset_S)$ are the ratio of liquid-solid and liquid-air interface respectively (Figure 13).

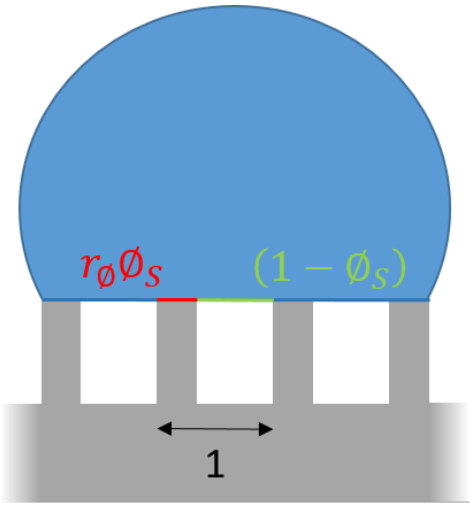

Figure 13. Ratio of liquid-solid liquid-air used to calculate contact angle with the Cassie-Baxter model.

The Wenzel and Cassie-Baxter equations are traditional methods for predicting the apparent contact angle on textured surfaces. However, there are many pitfalls with both of these methods. The Wenzel and Cassie-Baxter methods both demonstrate that the contact angle of a liquid wetting a rough surface is different than a smooth surface, but they do not take into account contact angle hysteresis and only predict a single value of the apparent contact angle. One study demonstrated that these theories should only be used when the droplet size is about 40 times larger than the characteristic roughness scale [35]. More recent studies of wetting interactions on textured surfaces provide more accurate theories for predicting the apparent contact angle of small droplets on textured surfaces [35]. But, even though there have been improvements in the prediction of apparent contact angle for specific cases of liquids wetting textured surfaces, the interactions of every case are too variable and complex to predict with just a few different equations.

The favorability of one state or the other depends on the inherent surface roughness, but both states can exist on the same 'bi-stable' surface due to wetting transitions between energy

barriers, where one state is in a free energy local minimum (metastable) and the other state is in a free energy global minimum (thermodynamically stable) [36]. Applications of textured surfaces that exhibit these characteristics are profound, and include high-performance optics [37], self-cleaning surfaces [38], separation of liquids in medical devices [39], as well as surfaces that lower drag forces [40].

The range and composition of textured surfaces used in wetting studies, as well as the fabrication method, varies greatly. Typically, surfaces are manufactured with easily replicable features, like arrays of cylindrical and rectangular posts [41, 42] or holes, patterned on various length scales (Figure 14). Wetting states of these surfaces vary, but they are useful to study because droplet sizes and wetting effects can be related to geometrical dimensions and feature spacing.

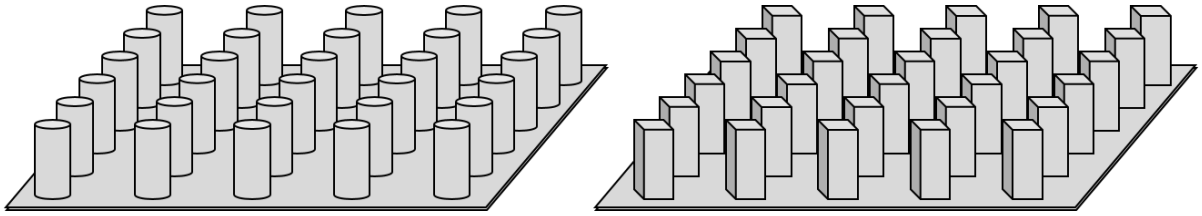

Figure 14. Typical textured surfaces used for investigation of wetting behavior.

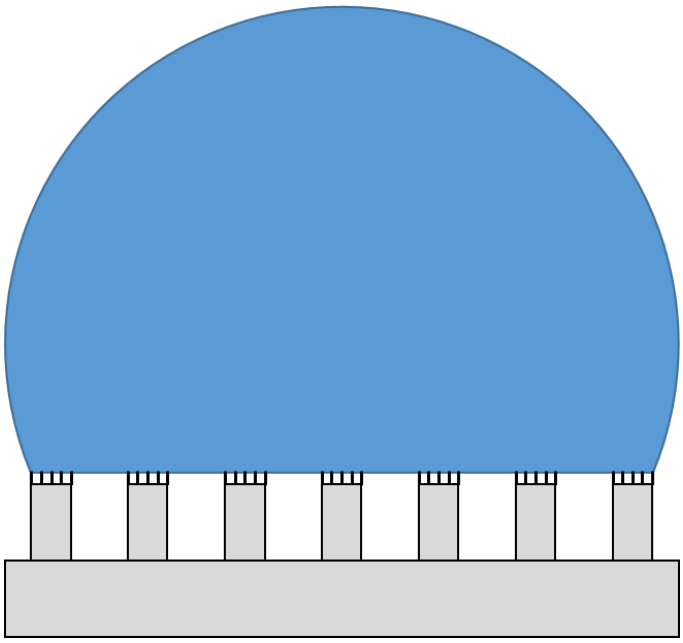

Figure 15. Hierarchical structures of liquid repelling manufactured surfaces.

Hierarchical structures consisting of a composite of both the micro and nano-scale features [43-45] are usually a mimic of natural water-repellant surfaces found in nature [11], and have similar liquid-repelling effects to their natural counterparts (Figure 15). Porous surfaces or honeycomb structures have also been used as surface structures to study wetting of liquids [34].

Hierarchical surfaces can be made from a range of materials including silicon [41, 42, 46], metals [47], glass [48], and other ceramics. Surfaces with arrays of features can be made easily by dicing the surface with a saw blade [41]. Polydimethylsiloxane (PDMS) is a polymer commonly used for creating micro channels for lab-on-chip devices, but is also ideal for creating intricate textured surfaces by casting into silicon molds and then curing in to a solid [49]. Silicon can be patterned with a photoresist and wet-etched to form surface features [46], or plasma etched using dry reactive ion etching (DRIE) [42] via the Bosch process; the latter method produces more identical, smoother, higher aspect ratio features. Hierarchical surfaces can be manufactured by first creating the micro features and then patterning smaller features; this can be

done with anodic oxidation [45] or other methods. Pulsed laser etching [48] and electron beam lithography [50] are additional methods for ultra-fine patterning of textured surfaces. Additionally, textured surfaces can be coated to tailor the wetting properties of the different surface components.

The use of textured surfaces to influence the wetting behavior of liquids is commonly studied in the scientific literature due to the beneficial effects to many processes previously mentioned. Wetting transitions from the Cassie state to the Wenzel state are commonplace, however, reversing this process is difficult; thus, the Cassie-Wenzel state is usually considered to be irreversible. Wetting transitions have been studied using simple geometrical features consisting of square or cylindrical posts (Figure 16), and droplet sizes significantly larger than the scale of the surface features. A wetting transition on a similar texture can be broken down into two interactions: the liquid starting to penetrate the texture, and then the liquid wetting the base surface. When the contact angle for the base (smooth) surface is greater than 90 ° ($\theta_E >$ 90 °), an energy barrier to the Cassie-Wenzel transition always exists and cannot occur without some external stimuli [51]. Gravity potential energy has been found to be able to decrease or eliminate the barrier for Cassie-Wenzel transitions.

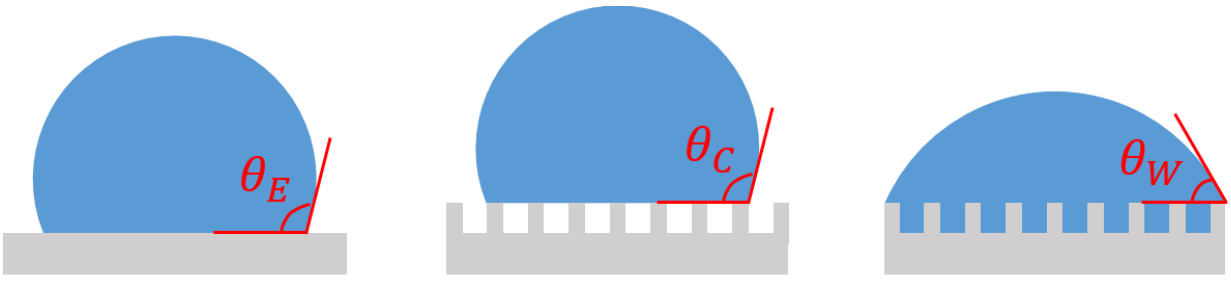

Figure 16. Wetting states of smooth and textured surfaces. On the left, a droplet wets a smooth surface with contact angle, θ_E. In the center, a droplet wets a textured surface in the Cassie-Baxter state with apparent contact angle, θ_C. On the right, a droplet wets a textured surface in the Wenzel state with apparent contact angle, θ_W.

If the contact angle of the base surface is greater than 90 °, but less than the apparent contact angle in the Cassie-Baxter state ($90\ ° < \theta_E < \theta_C$), both states may exist under the assumption that an equilibrium state occurs when the free energy is minimized (meta-stable), but the Wenzel state is more favorable as it is in a condition of lower global energy comparatively ($e_C > e_W$) [51]. If the contact angle of the base surface is greater than the apparent contact angle in the Cassie-Baxter state ($\theta_E > \theta_C$), both states are again meta-stable, but the Cassie-Baxter state is in a condition of lower global energy ($e_W > e_C$), so the droplet would not transition to the Wenzel state without outside influence. Additionally, hierarchical roughness in the reliefs of a surface has been shown to increase the energy barrier between the Cassie and Wenzel states [52]. The favorability of the Wenzel state over the Cassie state was shown to increase with hole diameter on nano-porous surfaces while maintaining the hole interval and depth, and can even facilitate Wenzel-Cassie transitions [53]. For base surfaces with a contact angle of less than 90 °, where the free energy of the Cassie-Baxter state is higher than that of the Wenzel state, the Cassie-Baxter state is not achievable [51].

While texturing of surfaces is a viable means for changing the wetting properties of a base material to some extent, texture does not necessarily facilitate the change of wetting states on a given surface because features act to pin the contact line of the droplet or do not allow the penetration of liquid into the surface at all. This is where additional energy input from an outside source could be useful in transitioning between wetting states on a surface.

2.6 Wetting and Vibration

Various methods for the dynamic excitation of liquids to alter the wetting state on a surface have been demonstrated by means of electrowetting [54], boiling/phase change [55], and

vibration excitation [56, 57]. Electrowetting actuation is not always feasible depending on the ability to fabricate integrated circuits on or in the wetting surface, and the use of the Leidenfrost effect to change the wetting state [58] is usually accompanied with unwanted phase change. However, the use of vibration to affect the wetting state of droplets has been shown to be easy to implement and can aid in pinning and de-pinning of droplets on textured surfaces to obtain a desired wetting state. However, sufficient and precise oscillation is necessary to allow controllable contact line motion between surface-specific pinning features. Mode shape and the directionality of droplet oscillation – i.e. horizontal or vertical – is also important to control the motion of the contact line or droplet surface in the desired manner. Just as solids have inherent resonance frequencies and vibration modes, liquids also resonate at specific frequencies, and with different mode shapes. In a solid, the natural frequency is related to the material's stiffness and mass. In a liquid, this is essentially still true, however a liquid is free to shear, making determination of natural frequency more complicated. In addition to the mass of a liquid, other factors such as surface tension, viscous damping, contact angle, and shape affect the natural frequency of a liquid. Predetermination of natural frequencies and mode shapes of liquid bodies would be beneficial to pinpoint vibration frequencies that amplify the oscillations to a sufficient level to accommodate desired droplet motion to affect wetting changes.

2.7 Droplet Resonance

2.7.1 Vibration Modes of Free Levitated Droplets

The natural vibration of liquids has been a common field of study for well over a century now. The resonance of free, levitated droplets was first studied by Lord Kelvin [59] and

subsequently by Lord Rayleigh [60], and then by Horace Lamb [61], who developed a general equation for the vibrational modes of free levitated droplets ignoring viscous damping:

$$f_j = \sqrt{\frac{j(j-1)(j+2)\sigma}{4\rho\pi^2 R^3}} \tag{8}$$

where f is the resonance frequency, σ is the surface tension, m is the mass of the droplet, and j is an integer greater than or equal to 2. While levitated droplets are useful in chemical or biological analysis [62] and mechanical property estimation [63, 64], the application of oscillating droplets (or other bodies of liquids) wetting a solid surface are much more applicable (as mentioned in the previous chapter). Potential applications are the driving factor behind the more recent proliferation of studies on the vibration of droplets wetting a solid surface, and rightly so because with the addition of liquid-solid interaction, the dynamics gain an additional component of complexity that requires much attention to gain understanding.

Vibration excitation of droplets on a solid surface has been studied to some extent. Most of the fundamental studies involve a low frequency (0-100s Hz) and high amplitude (> ~100 μm) vertical excitation [32, 49, 56, 57, 65-70] or horizontal shaking [68, 71-78], but the effect of high frequency vibration on liquid droplets has also been investigated [1, 2, 79-81]. Low frequency vibration excitation is commonly used to study the effects of droplet contact line oscillations and spreading [32, 56, 57, 65], but also for droplet locomotion [67-69] and particle collection [82].

2.7.2 Surface Orthogonal Vibration Modes of Sessile Droplets

A droplet on a flat surface is typically vibrated by applying a periodic oscillation to the solid surface. Sufficient surface displacements at low frequencies are required to generate forces large enough to initiate the motion of the liquid. However, if the droplet were vibrated at a frequency close to its resonance, the solid surface amplitudes would not need to be as large to obtain the same amplitude of liquid oscillation.

Noblin et al. [57] observed complicated three-dimensional wave patterns on the surface of droplets during vertical, low frequency vibration. While no analytical expression is available to calculate the resonance frequencies of vertically vibrated droplets, a simplification of the problem was proposed by considering the waves as one-dimensional (1-D) capillary waves. A volume-dependent wave vector $q_j(V)$ can be calculated for each mode and droplet size combination (Figure 17).

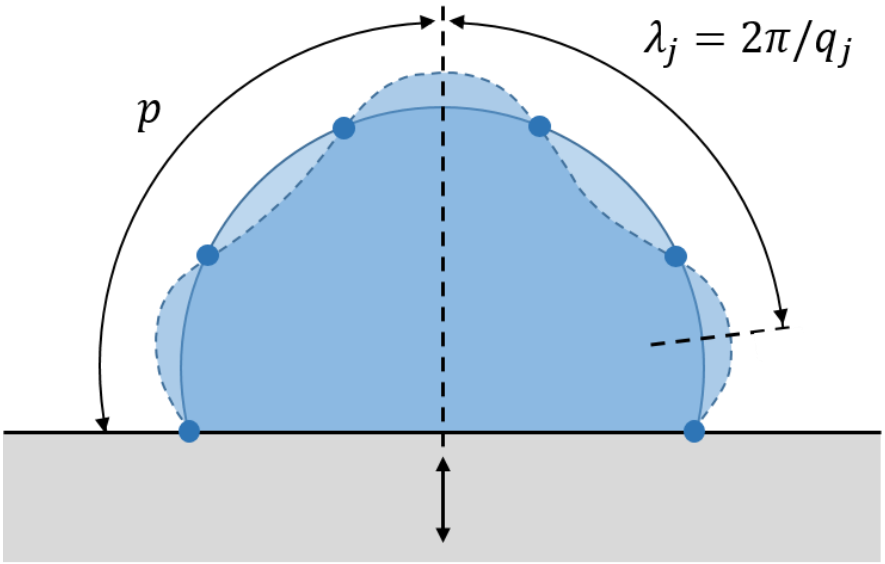

Figure 17. Capillary waves on a droplet that is vibrated vertically on a flat surface. The droplet meridian arc length (p), and wave length (λ) are defined schematically.

The wavelength, $\lambda_j = 2\pi/q_j$ is taken as the mean distance between 3 consecutive nodes along the surface of the droplet, and p is the arc length of the meridian curve from the center of the droplet, to its edge at equilibrium (Figure 17). Considering j to be the half number of nodal points along a droplet, the relation $(j - 1/2)\lambda_j = 2p$ is then determined and re-expressed as

$$\frac{2\pi}{\lambda_j} = \frac{\pi(j - 1/2)}{p} \tag{9}$$

For a sessile droplet at equilibrium, p is dependent on droplet volume and contact angle. The well-known dispersion relation for 1-D capillary waves on a flat liquid surface [25]

$$f = \left(\frac{2\pi\sigma}{\rho\lambda^3}\right)^{1/2} \tag{10}$$

where f is the vibration frequency and σ is the liquid's surface tension, can then be used to obtain the following equation:

$$f = \sqrt{\left(gq + \frac{\sigma}{\rho}q^3\right)\tanh(qh)} \tag{11}$$

For the depth of the liquid under the flat liquid surface (h), the mean height of the droplet can be considered as $h_m = V/\pi R^2$ and substituted to obtain:

$$f_j = \sqrt{\left(gq_j + \frac{\sigma}{\rho} q_j{}^3\right) \tanh\left(q_j \frac{V}{\pi R^2}\right)} \tag{12}$$

This analytical method has good agreement with experimental measurements for the resonance frequencies in both the gravity and capillary regime, with the exception of the mode where $j = 1$, however this mode does not implicitly account for the contact angle of the droplet as the contact line boundary condition is not taken into account.

A simple theory for the resonance of sessile droplets vibrated vertically is described by Sharp et al. [83], and considers frequencies associated with standing waves around the profile of a droplet and the dependence of frequency on contact angle (Figure 18).

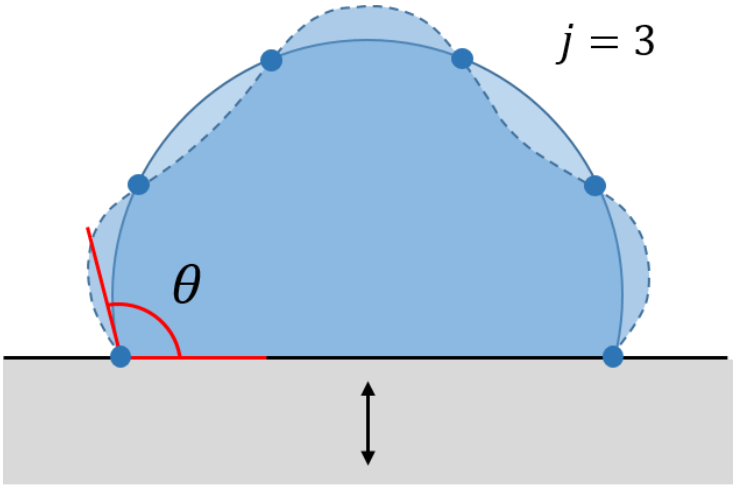

Figure 18. Resonance of a sessile droplet vibrated vertically on a flat surface with initial contact angle θ.

Under the condition of resonance, the profile length (s) of a droplet will be an integer multiple of one half the wavelength (λ) on the droplet's surface.

$$s = 2R\theta = \frac{j\lambda}{2} \tag{13}$$

Here, R is the radius of curvature, θ is the contact angle, and j is the integer half number of nodal points along the droplet surface ($j = 2,3,4, \ldots$) that corresponds to the vibration mode. Droplets smaller than the capillary length (~3 mm for water) can be approximated accurately to the shape of a spherical cap where the contact angle dependent volume (V) can be determined by:

$$\mathrm{V} = \frac{\mathrm{m}}{\rho} = \frac{\pi R^3}{3}(cos^3\theta - 3cos\theta + 2) \tag{14}$$

Here, m and ρ are the droplet mass and liquid density, respectively. The dispersion relation for 1-D capillary waves on a liquid ((10) can be combined with ((13) and ((14) to obtain an analytical solution for resonance frequency of the j^{th} mode of a sessile droplet with dependence on contact angle:

$$f_j = \frac{\pi}{2}\left(\frac{j^3\sigma}{24m}\frac{(cos^3\theta - 3cos\theta + 2)}{\theta^3}\right)^{1/2} \tag{15}$$

Experimentally measured resonance frequencies of vibrated sessile droplets show good agreement (within a factor of 0.81) with this analytical method [83]. The use of this method to determine the natural frequency of sessile droplets is limited, however due to the stipulation of symmetrical droplet oscillations. Under careful laboratory conditions, symmetrical excitation of droplets is possible, but would be irrelevant in real-world applications where heterogeneous

surfaces, dynamic air currents, contaminants, and many other uncontrollable factors exist. The use of this method is satisfactory to approximate the eigen-frequencies for small millimeter-sized droplets subject to low frequency vertical vibration, and thus use this frequency to supply sufficient energy to affect the wetting state of the droplet.

2.7.3 Surface Parallel Vibration Modes of Sessile Droplets

Lyubimov et al. [74] predicted the low frequency horizontal rocking mode of a droplet on a solid surface, and derived a solution for resonance frequencies of laterally oscillated inviscid droplets by taking into account the oscillation of contact line. Celestini and Kaufman [78] attempted to characterize the fundamental vibration mode of sessile droplets excited with in-plane surface oscillation (rocking mode), and achieved good success for droplets of radius larger than 0.1 mm. Droplets vibrated with a sufficiently weak force parallel to the surface undergo surface deformations, while the contact line remains pinned. The deformation is characterized as the displacement (dx) of the center of mass and the change ($d\theta$) of the advancing (θ_A) and receding (θ_R) contact angles (Figure 19).

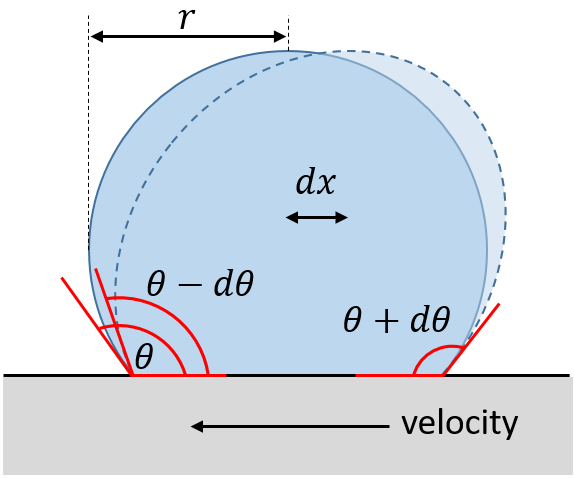

Figure 19. Rocking mode caused by horizontal vibration of a sessile droplet.

The symbol θ is the equilibrium contact angle, and a symmetric variation of contact angle hysteresis is assumed ($\theta_A = \theta + d\theta$, and $\theta_R = \theta - d\theta$). The surface variation (ΔS) due to deformation is taken as the difference between the surface under the influence of and external force (S), and the surface of the droplet at equilibrium (S_0). ΔS can be expressed as

$$\Delta S = S_0 f(\theta) d\theta^2 \tag{16}$$

by including the linear relations between ΔS and S_0 and between ΔS and $d\theta^2$. The function $f(\theta)$ accounts for the dependence of these quantities on the equilibrium contact angle. In the scenario where θ goes to π, the droplet has a small area of contact with the surface. When $\theta = \pi$, the contact area of the droplet and the surface reduces to a point, and the droplet can rotate without deforming. The limiting value of $f(\theta)$, when θ goes to π, is zero. The displacement of the center of mass can be written as

$$dx = g(\theta) r d\theta \tag{17}$$

where r is the spherical radius formed by the droplet and $g(\theta)$ is another function that depends on the geometry of the system. Combination of (16) and (17) yields

$$\Delta S = \frac{S_0 h(\theta)}{r^2} dx^2 \tag{18}$$

where $h(\theta) = f(\theta)/g(\theta)^2$. A restoring force, $F_r = -\sigma \Delta S/dx$ is related to the deformation by

$$F_r = -\frac{\sigma S_0 h(\theta)}{r^2} dx \tag{19}$$

where σ is the surface tension between the liquid and gas interface. Because the restoring force is linear with the displacement of the droplet center of mass, an effective spring constant (k_e) can be defined. The eigen-frequency of the droplet ($f_0 = \sqrt{k_e/\rho V}$) using the expression for the equilibrium droplet surface (S_0) and volume (V) of a partial sphere (similar to ((14)), is then defined as

$$f_0 = \mathrm{r}^{-3/2} \sqrt{\frac{6\sigma h(\theta)}{\rho(1-cos\theta)(2+cos\theta)}} \tag{20}$$

where ρ is the density of the liquid, and the dependence on geometry $h(\theta)$ is included. Computation of $h(\theta)$ can be done under the condition that the deformation is obtained at equilibrium, where this deformation is responsible for minimizing the free energy of the droplet under a constant external force. This would be the case when the ratio of viscous forces to surface tension forces is much less than 1 ($\eta v/\sigma \ll 1$, where η is the dynamic viscosity, and v is the characteristic velocity). The method for determining the value of $h(\theta)$ is complicated, but it is detailed by Celestini and Kaufman [78]. Determination of dx and $d\theta$ can be accomplished by imaging vibrated droplets with an exposure time greater than the period of vibration. This expression in combination with numerical values of $h(\theta)$ could be used to obtain a reasonable prediction of the eigen-frequencies for any condition of wetting angle. However, when contact line motion occurs in addition to droplet deformation, this method breaks down. Because of the ambiguous geometrical dependencies that affect the motion of longitudinally-vibrated droplets,

pre-determination of eigen-frequencies with this type of excitation is nearly impossible to do, especially in the presence of surface roughness where wetting transitions are of interest.

As a result of horizontal vibration, surface waves appear on the surface of a vibrated droplet extending over the surface parallel to the direction of vibration. Bormeshanko et al. [77] demonstrated that these waves could be described with the same framework developed by Noblin et al. [57] for vertical vibration of droplets. Similar to equation (11), the 1-D dispersion relation for capillary waves is given as

$$f = \sqrt{\left(gq + \frac{\sigma}{\rho}q^3\right)\tanh(qH)} \tag{21}$$

where the mean depth of the droplet H can be set to $H = V/\pi(Rsin\theta)^2$, with V being the droplet volume.

2.7.4 High Frequency Vibration Modes of Sessile Droplets

While low frequency vibration of droplets has been investigated thoroughly, and many approximations reported for the eigen-frequencies, high frequency vibration of droplets is less studied [1, 2, 79], while being more complicated. Droplets vibrating at high frequencies can undergo very asymmetrical deformations and the inherent high surface accelerations can cause droplets to break up [79]. Low amplitude, high frequency vibration may not cause droplet ejection, but the shorter vibration wavelength initiates higher order vibration modes that are more unstable. This makes the calculation of droplet resonance very difficult.

2.8 Vibration Effects

Low frequency excitation of droplets is known to excite volume modes of the liquid where standing waves appear on the surface of the droplet; the nature of these waves depends on the boundary condition at the contact line. The amplitude of vibration seems to play a big role in the effects of exciting droplets. Using low frequencies vibrations, produces large wavelengths on the solid, and so similarly-sized droplets experience a similar excitation over a large surface area [56].

The use of low frequency, high amplitude vibration has been demonstrated as a means to dynamically change the wetting angle of droplets by oscillation of the contact line. Sufficient levels of vibration can cause the dynamic contact angle to exceed the range of the surface hysteresis, causing the contact line to move (Figure 20).

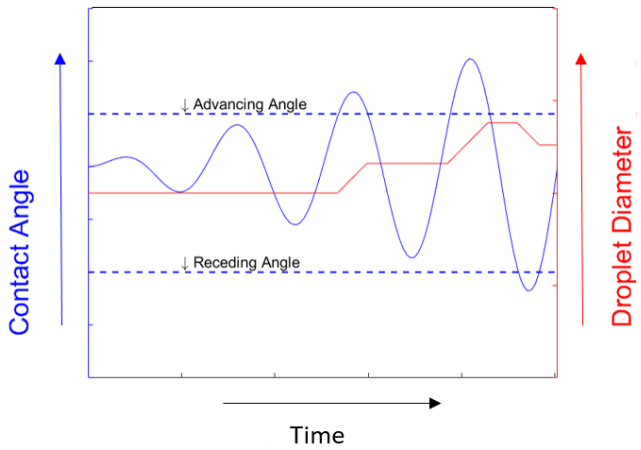

Figure 20. Contact line oscillations (blue solid line) causing droplet spreading (red solid line) when the CAH range (distance between the two horizontal blue dashed lines) is exceeded.

Droplet spreading will occur during periods where the contact angle exceeds the contact angle hysteresis of the surface [84]. The momentum carried by the oscillation of the droplet has

been used as additional energy input to help overcome fluid contact line pinning caused by rough surfaces.

Contact line motion, or the spreading of a droplet using low frequency vibration is perhaps the most studied effect of vibrating droplets. Droplet spreading has been adapted to a range of applications where it has improved the efficiency of a given process. Chong et al. [3] demonstrated the controlled filling of microplate wells with the help of mechanical vibrations (a range of amplitudes and low frequencies) to reduce the volume of fluid needed (by almost 50%) to fill the surface of the well regardless of initial droplet shape and vibration frequency. Whitehill et al. [65] noted that as droplets are continuously vibrated, the size of the surface waves decreased as spreading occurred, and the spreading was more extensive and less axisymmetric in higher amplitude cases. This demonstrates that spreading is dependent on amplitude of the liquid surface deformations.

Sufficient levels of low frequency vibration can result in ratchet motion of droplets on a flat surface using both vertical and horizontal vibration [68, 75]. Gravity-defying climbing of droplets has also been demonstrated. Vertical vibration of 30 - 200 Hz and up to 50 g was used to move a droplet up an incline plane due to droplet deformation [69]. The maximum contact angle on the high side is greater than the maximum contact angle on the low side, so the droplet experiences a net force upward. In this case, higher viscosity fluids exhibited slower climbing speeds, while lower viscosity fluids break up due to the high accelerations before they can begin to move. The resulting mean motion was dependent on the acceleration and frequency

High frequency vibration of droplets, while not as commonly studied or adapter to processes, can be useful in applications where dissimilar fluids can be made into an emulsion, separation [4] and sorting of particles, adhesion of coatings, and liquid spreading [1]. If low

frequencies vibrations excite similarly-sized droplets equally over a large surface area [56], high frequency vibration, producing shorter wavelengths, could better isolate droplet actuation. Studies that investigate the spreading of droplets, or contact line motion using high frequency vibration excitation are rare, most likely because of the difficulties posed by the small scale phenomena that take place on a small time scale, and effects like cavitation that can occur due to acoustic waves in a liquid. If droplets are excited by some other means other than the displacement of the solid surface, droplet resonance could be measured by passing an optical beam through the droplet and allowing it to reflect off of the substrate and scatter the beam into a photo detector [83] where the time-dependent signal can be transformed into the frequency domain with a Fourier transform. However, characterizing the dynamics of a vibrating droplet in relation to a moving reference is very difficult.

Sophisticated measurement equipment is required to be able to study the effect of high frequency vibration on contact line motion and the spreading of droplets on a solid surface, and consequently the effects are studied qualitatively.

Surface roughness can affect the motion of the contact line and the equilibrium state of droplets on the surface due to the local pinning of the contact line (as explained in the previous sections of this chapter). The shape of droplets pumped on to a surface is influenced by pinning of the contact line on surface defects. Sufficiently high vibration can supply enough energy for the contact line to un-pin locally from a metastable state and move to the most stable global equilibrium. In this manner, vibration of droplets provides the most repeatable shape for a sessile droplet of a given volume on a rough surface and can be used to calculate the most stable equilibrium contact angle [65, 85]. Un-pinning the contact line from defects on a heterogeneously rough surface by vertical vibration is also a repeatable method to measure the

average spreading parameter of the surface [32]. The new location of the contact line could also result in a lowered contact angle hysteresis if the contact line was moved from a higher energy metastable state to a lower one, but this would depend on the heterogeneity of the surface roughness.

2.8.1 Decreasing Contact Angle Hysteresis

Sufficient vibration amplitude has been shown to reduce the contact angle hysteresis of a surface [32, 86, 87]. Li et al. were able to increase the electrowetting velocity of sandwiched droplets three-fold using a low frequency (tens of Hz) orthogonally vibrating top plate [66]. Andrieu et al. [32] measured the advancing and receding contact angle of liquid puddles on various heterogeneous horizontal surfaces before and after undergoing vertical vibration at a low frequency (50 Hz and amplitude 0.3 - 2.5 mm) and noted that as the vibration amplitude increased, the post-vibration advancing and receding contact angle decreased and increased respectively until they reached the same value at an amplitude of 1 mm. Surface tension driven flow was discovered by James Thomson (the brother of Lord Kelvin) in 1855 while observing the “tears of wine” effect [88]. Since then, this effect has been studied intensively and is named after Italian physicist Carlo Marangoni who studied it for his doctoral dissertation. Greenspan first predicted that a droplet placed on a chemically anisotropic surface would move towards the region of greater wettability [89]. If a continuous wetting gradient is present, the droplet will move at a constant rate of speed toward the area of greater wettability. The movement of the droplet is due to a surface tension gradient, but the velocity of the droplet is limited by the contact angle hysteresis of the surface [76]. Daniel et al. [76] demonstrated a 5 fold increase in the average speed of 1-2 µL droplets moving on a wetting gradient by using an in-plane square-

wave vibration. This resulted in the average droplet velocity magnitude to exceed the expected magnitude for the case where there was an absence of contact angle hysteresis.

2.8.2 Vibration-Induced Wetting Transitions

Cassie-Wenzel wetting transitions have been induced with low frequency vibration, both orthogonally and in-plane, to wet droplets on micro-scale, porous, honeycomb polymer [90]. In the case of vertical vibration, the effect of water penetration is attributed to the inertial force caused by the vibration, where the amplitude of the additional pressure (p) exerted on the substrate is

$$p = \frac{\rho V A f^2}{\pi [r(\theta)]^2 \sin^2 \theta} \tag{22}$$

where ρ is the liquid density, V is the droplet volume, A and f are the vertical amplitude and frequency of vibration. The radius of the contact line, $r(\theta)$ is dependent on the apparent contact angle, θ. Cassie-Wenzel transitions were experimentally observed for similarly-sized droplets at the same value of Af^2, which is synonymous to the surface acceleration caused by the vertical oscillation. The transition was then attributed to the increase in pressure exerted by the droplet on the substrate. Cassie-Wenzel transitions are more complicated when in-plane oscillations excite the liquid. The increase in Laplace pressure due to droplet deformation, and the displacement of the contact line seem to be the driving mechanisms in this case as noted by Celestini and Kofman [78]. Bormeshanko et al. [77] demonstrated that only droplet surface modes are responsible for Cassie-Wenzel transitions that occur on a porous surface while vibrating droplets horizontally.

Wenzel-Cassie transitions are less observed and studied in the scientific literature, however these transitions can occur on textured surfaces with the aid of external forcing like heating [58], and vibration [91]. A given increase in the spacing of square pillars of PDMS at a given vibration frequency, was shown to decrease the critical amplitude to transition a vertically vibrated droplet from the Wenzel to the Cassie state [91]. For an unchanging surface, $R(\theta){f_j}^2{A_{cr}}^2$ is approximately constant where $R(\theta)$ is the spherical radius of the droplet, f_j is the resonant frequency, and A_{cr} is the critical amplitude of vertical vibration to initiate the Wenzel-Cassie transition [91].

2.9 Summary

Reversible wetting of textured surfaces has many applications, from drag reduction, self-cleaning, and lab-on-chip medical devices. Vibration-induced wetting transitions on textured surfaces can be accomplished with the right combinations of contact line motion and surface features. A contact angle greater than 90 ° for the base surface is favorable for reversibly transitioning between Cassie and Wenzel states on textured surfaces consisting of arrays of cylindrical or rectangular posts [51]. Hierarchical texturing of reliefs, may be well-suited for inducing the hard to achieve Wenzel-Cassie transition [52]. For textured surfaces consisting of reliefs rather than posts, the favorability of the Wenzel state over the Cassie state was shown to increase with relief diameter on nano-porous surfaces that maintained a constant feature interval and depth [53].

The magnitude of different vibration wetting effects (i.e. spreading) has been shown to depend on the level of acceleration [69]. For low frequency vibration, spreading of droplets is dependent on amplitude of the liquid surface deformations, where as a droplet undergoes

spreading, the amplitude of the of the surface waves diminish as it reaches its final spread diameter [65]. Cassie-Wenzel transitions that were induced by vibration seem to occur at constant level of surface acceleration [90]. Droplet spreading using low frequency vertical vibration occurs over a range of amplitudes and frequencies, regardless of the initial shape of the droplet and whether vibration frequency is resonant [3].

The vibration frequencies that could be useful to provide sufficient levels of liquid surface deformation and contact line motion could be approximated using some of the methods detailed in the previous sections of this chapter if the use of low frequency vibrations was utilized. However, much scientific literature on the effects of the low frequency vibration exists, so the investigation of the high frequency effects are of much higher interest.

The work in the successive chapters of this thesis detail a method for using ultrasonic (> 20 kHz) vibration to control the spreading of droplets on smooth hydrophobic surfaces. Large deformations on the surface of a droplet (as produced by low frequency, high amplitude vibration) may be desirable in transitioning wetting states on some surfaces. However, large deformations can be responsible for unpredictable droplet dynamics, especially when contact line motion occurs. Ultrasonic vibration has not been commonly used to move contact lines and spreading droplets, nor has it been commonly used in vibration-assisted wetting transitions on textured surfaces. While ultrasonic vibration of liquids can have undesired effects like cavitation and droplet ejection, sufficiently high levels of accelerations could supply enough energy to initiate wetting transitions while remaining under the threshold of the undesired effects. The amplitude of the waves on the surface of droplets vibrated with high frequency are small in comparison to low frequency vibrations of the same acceleration level. This makes ultrasonic

vibration attractive as a method for moving droplet contact lines with the least effect on the droplet shape.

The well-studied, low frequency vibration excitation effects on droplet spreading and general droplet dynamics provide initial areas of investigation for the droplet effects of high frequency vibration excitation.

CHAPTER 3:

EXPERIMENTAL VALIDATION AND RECOMMENDATIONS

3.1 Abstract

The goal of this thesis is to characterize how droplets spread under ultrasonic surface vibration. Low frequency droplet spreading has been studied generally [32, 56, 65] and found useful for applications in biological analysis previously [56]. The study of ultrasonic vibration wetting and spreading effects is sparse [1, 2], and is usually only qualitatively analyzed. Therefore, the specific goal of this thesis is somewhat unique, but also has potential as a means to controllably reverse surface adhesion. In order to characterize ultrasonic wetting effects, measurement methods needed to be repeatable and accurate. In this chapter, measurement methods for characterizing the physical interactions between droplets and a solid surface under ultrasonic vibration are evaluated. The repeatability of acceleration measurement with an adhesive-mounted accelerometer was found to be sufficient after a recommended application method, including significant adhesive cure time, was instituted. The mass of the accelerometer does not affect the surface frequency response when measuring acceleration, and charging and heating of piezoelectric elements is not an issue for repeatable measurements. Some inherent issues exist with characterizing vibration using an accelerometer, but these are secondary to the effects introduced by ultrasonic vibration.

3.2 Generation of Ultrasonic Vibration

Ultrasonic vibration is generated by using piezoelectric transducers like those typically found in ultrasonic cleaning equipment. This equipment produces high frequency pressure waves that cause small bubbles to oscillated and implode. This creates many small shockwaves that dislodge contaminants from a surface being cleaned. These ultrasonic transducers (Figure 21) are comprised of a stack of two piezoelectric transducers (PZTs) with a positive-biased electrode between them. Two masses, usually made from steel alloy, are attached (with high strength epoxy) to each side of the transducer stack with a negative-biased electrode between one of the masses and the transducers. Masses vary in shape and size and give the transducer specific resonance properties. The whole assembly is pre-loaded with a large bolt to keep the piezoelectric elements loaded in compression, and to ground the other side of the transducer stack, where no electrode exists.

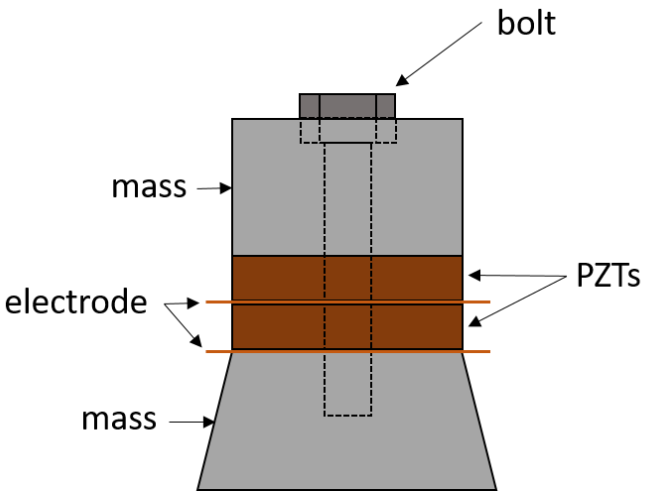

Figure 21. Schematic of an ultrasonic transducer taken from an ultrasonic cleaner.

Transducers manufactured for cleaning purposes are designed to function in the ultrasonic range (> 20 kHz) at their resonance frequency, and are typically fixed to the oscillating bath container with high strength epoxy.

These ultrasonic transducers can be adapted to facilitate the study of vibrating droplets (Figure 22). A threaded hole, made in the bottom of the mass opposite the protruding pre-load bolt allows this end of the system to act as a base that can be mounted securely to a stationary surface. Cylindrical caps were machined from 6061 aluminum alloy in order to provide a flat vibrating surface. These caps were mounted to the top of the steel alloy mass with four M4-0.7 bolts, and utilized a small internal cavity to cover the protrusion of the pre-load bolt. The top surface of the aluminum cap provides a smooth, flat surface, ideal for sample mounting (discussed later in the next section). The caps were made sufficiently thick (> 12 mm) to maximize the surface stiffness, and reduce the phase variation of vibration over its surface (35 mm diameter).

To study the effects of ultrasonic vibration on the spreading of droplets, it is logical that the initial wetting state of a droplet be non-wetting. This can be accomplished using a combination of high surface energy liquids, or low surface energy substrates. Pure, deionized water was chosen for its availability and practical uses. Water does not have a particularly high free energy, so a variety of low free energy 'hydrophobic' fluoropolymer coatings fulfill the requirement of an initial non-wetting droplet state. Since a variety of different low energy coatings would be used in vibration testing, a means to interchangeably attach different surfaces to the vibrating transducer was needed. Coating the smooth surface of the aluminum cap continuously with different coatings would be tedious. Alternatively, substrates could be coated with different coatings and then attached to the top of the aluminum cap.

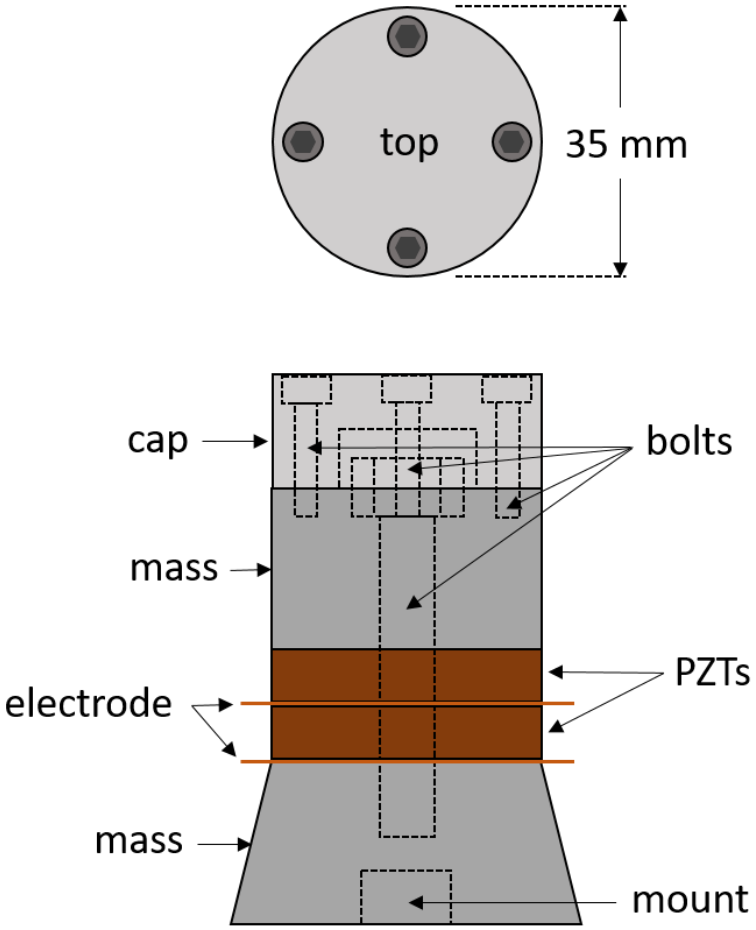

Figure 22. Schematic of an adapted ultrasonic transducer used to study the high frequency vibration effects on liquid droplets.

3.3 Substrate Mounting

Glass microscope slides were diced into squares (18.25 mm x 18.25 mm and 1 mm thick) to use as the substrate surface for hydrophobic coating application. Once coated, these glass slides needed to be fixed to the top surface of the aluminum cap, where they would be used in later testing of vibrating droplets (Figure 23).

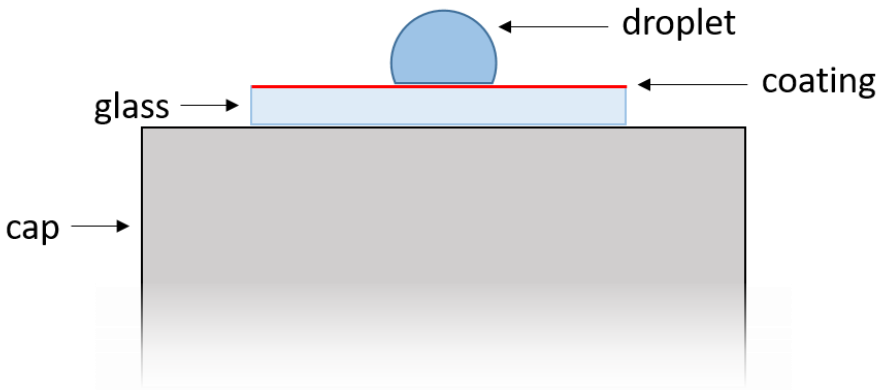

Figure 23. Square glass slides are used as a coating substrate and were mounted to the top of the aluminum cap attached to a piezoelectric transducer by adhesive as discussed later in this section.

To do this, glass slides needed to be fixed rigidly to the aluminum cap to allow the transmission of vibration from the piezoelectric transducer to the surface of the coating interacting with droplets. The best method for attachment of glass substrates needed to be determined.

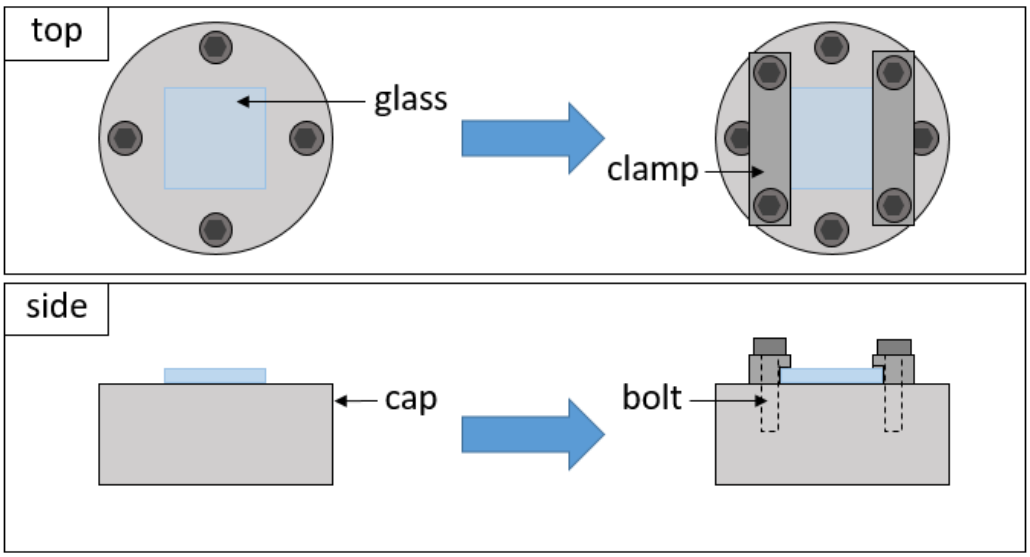

Figure 24. Glass substrate attachment method using a clamp.

Clamping, or bolting glass slides to the aluminum cap is one method to mount them rigidly to the ultrasonic transducer. This could be done with a fixture similar to Figure 24. The transmission of vibration from the transducer through the cap and to the surface of the glass depends on how much clamping force is used to keep the glass rigidly against the surface of the cap. One benefit to this method is the ease of switching out glass substrates with different coatings for testing. However, there are some inherent issues with this method as well. Careful clamping was needed to supply enough pressure to the delicate substrates, but this can only be done on two edges of the glass while still allowing for imaging of the droplet profile.

Sufficient clamping force would be necessary to hold the substrate in place without cracking the brittle material, and even though glass is a stiff material, two sides of the substrate are not restrained and are free to move with different amplitudes and phases. This would induce high tensile stresses at the substrate surface that could facilitate the propagation of cracks and destroy the coating or substrate. To mount glass substrates repeatably, clamping bolts needed to be pre-loaded with the same consistent torque level, otherwise the transmission of vibration from the transducer to the glass plate will vary from substrate to substrate.

Bonding the glass substrates to the aluminum cap with an adhesive is another method to rigidly mount them to the ultrasonic transducer (Figure 25). The transmission of vibration from the transducer through the cap and to the glass surface partially depends on how rigid the adhesive is. This stiffness property of an adhesive can be determined from the mechanical properties section of the data sheet provided by the manufacturer. Stiffness can vary from adhesive to adhesive, but will also vary with curing time, thickness, temperature, humidity, and other parameters.

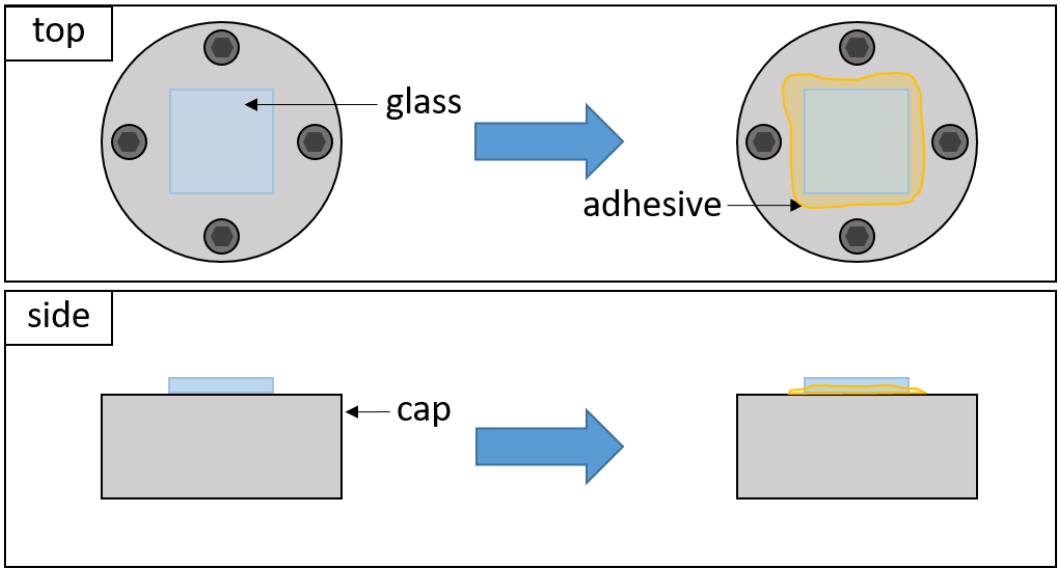

Figure 25. Glass substrate attachment method using adhesive.

Surface preparation also plays an important role when bonding anything with adhesives. If the surface is not clean and free of oil and contaminants, the strength of the bond will diminish. Adhesive also acts to fill in non-contact gaps between two bonding surfaces, thereby increasing the transmission of the vibration signal. Different adhesives require different methods to initiate cross-linking (i.e. mixture of a resin and hardener for epoxy), and so different types of adhesives are best adapted for particular applications.

Use of a high strength adhesive to bond glass substrates to the transducer seems like a promising method for vibration coupling. Many adhesives can be cured rapidly with exposure to ultraviolet light, and can be dissolved in a solvent, thereby enabling speedy mounting and dismounting of substrates during testing. An adhesive bond will also penetrate surface and substrate roughness to assure an even fixturing across the entire surface.

The qualities of adhesive bonding made it appear to be the most viable method for fixing glass substrates with repeatable vibration transmission to the surface of the coating. However, this needed to be verified. The measurement of vibration is typically done using a surface-mount

micro-electromechanical system (MEMS) device called an accelerometer, or with sophisticated equipment that uses optical beams to track the surface as it moves. The latter of these methods utilizes sophisticated equipment like a laser Doppler vibrometer (LDV), and is usually the best method to quantify vibration due to its high spatial and temporal resolution and non-contact measurement, but the cost of this equipment makes the use of relatively inexpensive accelerometers the method of choice in this work.

3.4 Accelerometer Mounting

Various types of accelerometers exist for different applications. One main difference is the mounting method used to fix the accelerometer to a vibrating surface. An accelerometer can be manufactured to mount with the use of adhesives, magnets, or studs. The appropriate accelerometer mounting method depends on the application, but also plays an integral role on the transmission of vibration from the vibrating surface and the amplification of the response measured by the accelerometer.

The damping of the signal, and the quality of frequency response measurements obtained by an accelerometer depends on how the accelerometer is mounted to the vibrating surface. In order to obtain the most accurate measurement, it is important that the accelerometer and mounting surface are rigidly coupled – especially at high vibration frequencies – to avoid loss of signal transmissibility and response [92]. Rigidly mounting an accelerometer transmits the signal from the vibrating surface to the accelerometer with the greatest certainty. Stud mounting is one example of rigid mounting, however the necessity to characterize the vibration at specific locations on the surface of the glass substrate where droplets are excited does not facilitate this mounting method as the smooth substrate cannot have an attachment point. Alternatively,

clamping the accelerometer may affect the entire system by changing the mass and damping characteristics substantially, and because the acceleration measurement with an accelerometer cannot be done simultaneously while droplets are vibrated on the surface, the acceleration levels measured would be different from the acceleration levels used to excite droplets on the surface.

Using adhesives, as with substrate mounting, an accelerometer can be mounted to any location to characterize vibration with little impact on the vibration characteristics of the surface. Similar to wax mounting, adhesives will provide relatively good transmission of vibration in comparison to stud mounting and should act as a means to replicate the vibration characteristics when mounting different substrates.

3.5 Surface Acceleration Measurement

3.5.1 Measurement Equipment

Characterization of vibrating surfaces was done with a small adhesive-mount accelerometer (Model: 352A92, PCB Piezotronics). Some key characteristics of this transducer are taken from the data sheet supplied by the manufacturer [93], and are shown in Table 1.

Table 1. 352A92 accelerometer characteristics.

Size – Length x Width x Height	5.46 x 3.43 x 2.54 mm
Weight	0.16 gm
Sensing Element	Ceramic
Sensitivity	~ 0.025 mV/(m/s^2)
Measurement Range	$\pm$196,200 m/s^2 pk
Frequency Range ($\pm$10%)	1 to 20,0000 Hz
Resonant Frequency	$\geq$ 100 kHz
Overload Limit (Shock)	$\pm$294,300 m/s^2 pk
Discharge Time Constant	0.4 to 1.2 sec

The accelerometer is mounted to the top cap of the vibrating transducer with an ultraviolet (UV) light-cure cyanoacrylate adhesive (Loctite 4310, Loctite) (The specific mounting procedure is discussed in the next section). As the surface vibrates, a ceramic piezoelectric element inside the accelerometer is compressed and expanded due to inertial forces. This element generates a voltage signal proportional to its strain. This signal is conditioned and then processed by a dynamic analyzer (Model 50-21, SigLab) that computes the ratio of the cross-spectrum and the reference auto spectrum to obtain the surface frequency response (Figure 26).

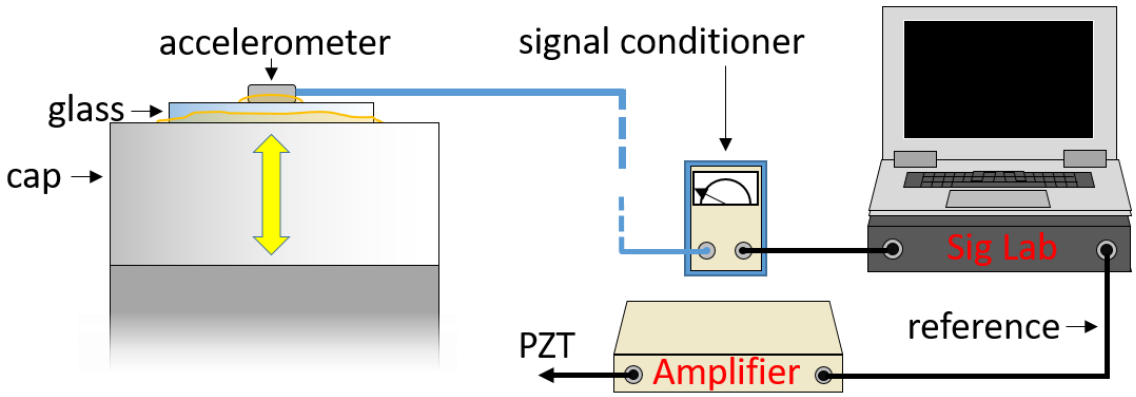

Figure 26. Surface vibration characterization with an adhesive mount accelerometer. A dynamic analyzer computes the ratio of the cross-spectrum and the reference auto spectrum to obtain the frequency response.

The frequency response signal can then be converted into approximate acceleration levels at a given frequency using the accelerometer sensitivity conversion in Table 1. This acceleration (a) can then be used to determine an approximate vibration amplitude (A)

$$A = \frac{a}{f^2} \tag{23}$$

and maximum velocity (v_{max})

$$v_{max} = \frac{a}{f} \tag{24}$$

at a given frequency (f).

3.5.2 Measurement Repeatability

3.5.2.1 Adhesive Mounting Effects

The measurement of acceleration with an accelerometer will have to be repeatable in order to rely on this method to characterize the vibration at the surface of glass substrates. To determine whether this was the case, accelerometer and PZT cap surfaces were solvent cleaned, and the accelerometer was glued to a glass substrate (Figure 26) with a patch of adhesive that was large enough to run out from beneath while applying moderate pressure. The adhesive was exposed to UV light (365 nm wavelength and 3 mW/cm^2) for ~5 minutes and then allowed to cure for ~48 hours. The glass substrate was then glued to the cap on top of the piezoelectric transducer (Figure 26) with a patch of adhesive large enough to run out from beneath while applying moderate pressure. The adhesive curing time was selected based on a study of varying cure times. In these experiments, the adhesive was exposed to UV light for ~5 minutes and the frequency response for a driving swept sine wave signal with amplitude of 200 V was measured from 18 to 23 kHz, periodically as the adhesive cured over time. The left side of Figure 27 shows frequency response measurements 0.5 hours, 4.5 hours, and 20.5 hours after the adhesive was initially cured with UV light for ~5 minutes. The frequency shift in the measured frequency

response clearly portrays a dependence on adhesive cure time. The adhesive was allowed to cure for a longer length of time to determine whether the frequency response could be measured repeatably. The right side of Figure 27 shows frequency response measurements 20.5 hours, 52.5 hours, and 119.5 hours after the adhesive was initially cured with UV light for ~5 minutes.

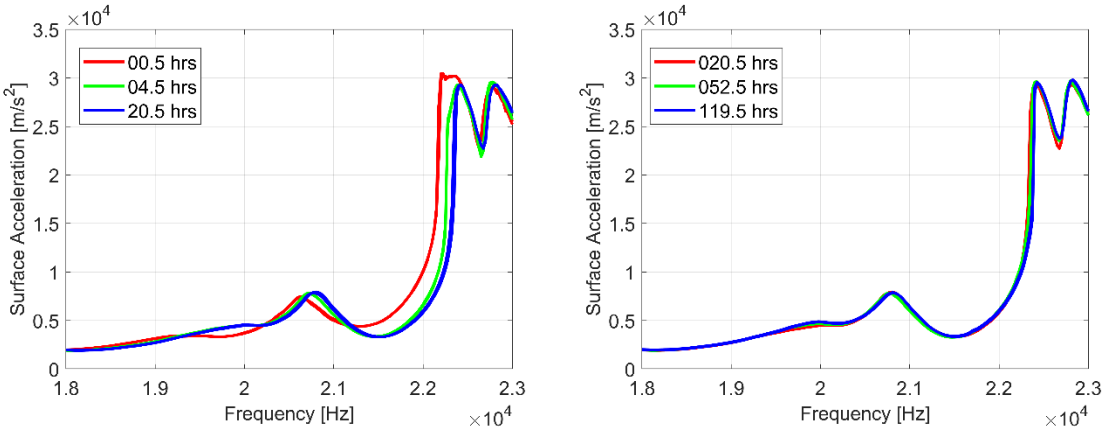

Figure 27. Comparison of frequency response measurements as the bonding adhesive between the glass substrate and piezoelectric transducer cap is cured. Good repeatability was achieved after ~20 hours of cure time in addition to the initial ~5 minutes of UV exposure.

Repeatable frequency response measurements were attained for an adhesive that cured for ~20 hours or longer in addition to ~5 minutes of initial UV exposure. Under these conditions, frequency response measurements had just 4.1% average relative variation in the magnitude of the surface acceleration over the entire frequency range between samples.

3.5.2.1.1 Recommended Adhesive Mounting Method

These results suggest that an adhesive fixturing method needed to be instated to assure repeatable acceleration transmission through the adhesive. First, surfaces to be bonded are solvent-cleaned in acetone, and then methanol. This is followed by a bath in deionized water and a subsequent cleaning with isopropyl alcohol before drying with a jet of compressed air to remove any contaminants. A patch of UV light-cure adhesive (Loctite 4310, Loctite), is applied

between the bonding surfaces; the amount of adhesive was to be large enough to run out from beneath the bonding surfaces as moderate pressure is applied. The adhesive should be exposed with UV light (365 nm wavelength and 3 mW/cm^2) for ~5 minutes and then allowed to cure for at least ~24 hours. This method produces a repeatable fixation method for glass substrates and accelerometers on the piezoelectric transducer. This previously described method was subsequently used for the fixturing of glass substrates and accelerometers in the rest of this work in order to obtain the most reliable data.

3.5.2.2 Transducer Mounting

In addition to possible frequency response change due to changes in the adhesive coupling between vibrating surfaces, frequency response is expected to change when mounting different parts of the piezoelectric transducer. The top cap mounted with four bolts on to the piezoelectric transducer was designed to be removable so that multiple caps of the same design could be interchangeable. Because ~24 hours of cure time is required for bonding of vibrating surfaces, this facilitates the data acquisition rate by allowing different coated glass substrates to be mounted on different caps in advance preparation for testing. This requires a cap to be unbolted and different caps to be re-attached by bolting again. It is important, but mostly convenient that different caps are attached in a repeatable manner to obtain similar and predictable frequency responses for testing. A few things were to be considered.

First, the method of bolting caps to the piezoelectric transducer was addressed. Relatively repeatable pre-load of bolted joints can be accomplished in different ways, but one simple way is the use of a torque wrench. The effect of varying bolt pre-load between the cap and piezoelectric transducer is shown in Figure 28. All four bolts are tightened incrementally in a cross pattern,

from 10, 15, and 20 inch-pound pre-loads, to assure even clamping. Frequency response measurements of each pre-load were taken for a driving sine wave of 200 V amplitude between 20-25 kHz.

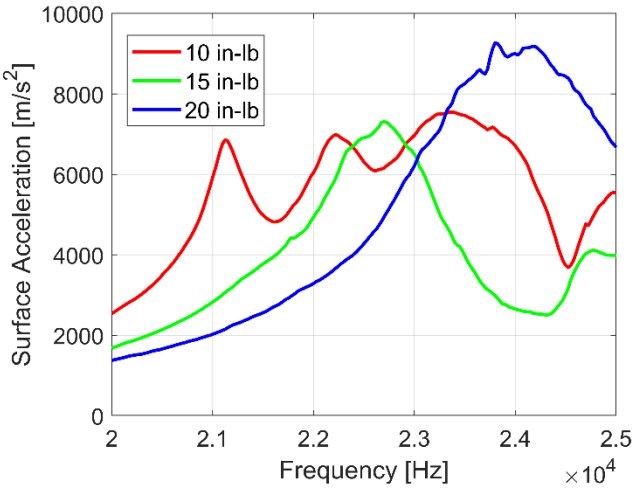

Figure 28. Frequency response change as the pre-load of bolts coupling the piezoelectric transducer to the cap is increased.

This data clearly shows the magnitude and frequency of the surface response changes dramatically as bolt pre-load is increased. The average relative error between the magnitudes of the three measurements is 69.9%. This effect does not seem to diminish as the clamping force is increased, either. A pre-load of 20 inch-pounds seems more than sufficient to couple the two surfaces without having to worry about bolts backing out. Also, increasing the pre-load more may be approaching a limit where bolts may begin to shear. So, this pre-load was used to determine how substantially the frequency response of the vibrating surface is changed when the aluminum cap is removed from the piezoelectric transducer and then replaced.

A single aluminum cap was bolted to a piezoelectric transducer in the same orientation 7 different times using a bolt pre-load of 20 in-lb applied incrementally in a cross pattern. An

accelerometer attached to the top of the cap (with methods detailed in section 3.5.2.1.1) measured the frequency response of the surface to a driving sine wave of 200 V amplitude between 17-22 kHz (Figure 29).

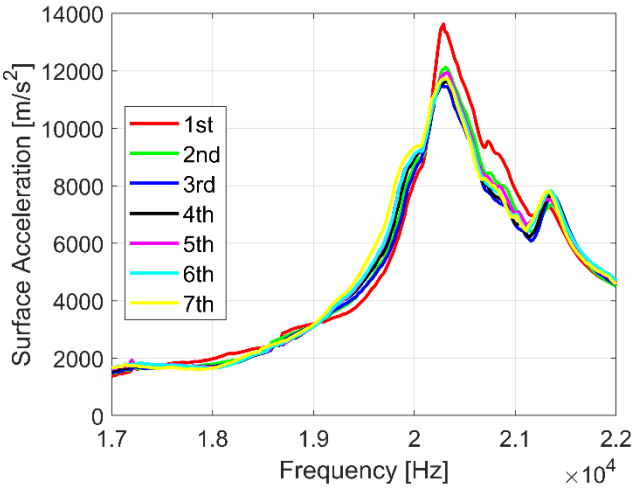

Figure 29. Repeatable frequency response measurements using a torque wrench to apply a pre-load of 20 inch-pounds to the bolts holding the cap and transducer together. Between each set of data (1st, 2nd, etc.) that was measured, the cap was removed and subsequently attached to the transducer again using the pre-load of 20 inch-pounds.

From Figure 29, it is clear that using a torque wrench to bolt the piezoelectric transducer to the cap is beneficial for repeatable and predictable frequency response at the surface of the cap. The average relative error in the acceleration magnitude of the frequency response between all seven measurements is 13.8%, and is improved to 8.4% with the exclusion of the first measurement. This error could be caused by variations in the mating surfaces due to very fine roughness, but it is most likely just inherent accelerometer noise. Based off of these results, a pre-load of 20 inch-pounds was used from this point on when bolting caps to the transducer.

The noticeable effect of bolt pre-load on surface frequency response brought up the possibility of threadlock improving repeatability. Medium strength threadlocker (Permatex) was

applied to the threads of bolts used to attach the cap and transducer together. A single cap was attached and removed three times in the same orientation using a pre-load of 20 inch-pounds to fasten the cap and transducer together. The threadlocker was given ~24 hours to cure each time. The frequency response of the surface to a driving sine wave of 200 V amplitude between 17-22 kHz was again measured each time with an accelerometer attached to the top of the cap (with methods detailed in section 3.5.2.1.1). Figure 30 shows slight, but negligible variation in the three frequency response measurements taken. However, the average relative error of the magnitudes between the measurements was 8.9%, so the repeatability of the response was not improved relative to controlling pre-load alone. For this reason, threadlocker was not utilized in any further testing.

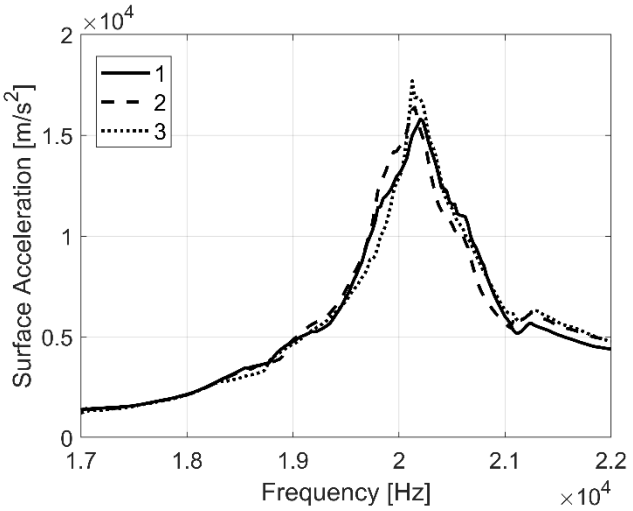

Figure 30. Frequency response repeatability using threadlocker on the threads of bolts that are pre-loaded at 20 inch-pounds. The three data sets plotted represent three separate instances where the cap and transducer were assembled with threadlocker and measurements were taken.

3.5.2.3 Piezoelectric Charging and Heating

Another concern for repeatable acceleration measurements would be the charging or heating of piezoelectric elements. The conversion of electrical energy into mechanical energy (or vice versa) done by a piezoelectric transducer element results in an increase in temperature from mechanical damping and dielectric loss. This could be exacerbated by operation at resonance or with high levels of electrical field, and could manifest as accelerated aging or thermal damage of the piezoelectric element [94]. Heating results in expansion and contraction of materials which can cause piezoelectric material to build a charge that alters its driving signal. In this instance, charging could occur for either the vibration transducer, or the measurement transducer (accelerometer). To determine whether charging or heating would be an issue for either piezoelectric transducer, an accelerometer was mounted to the top cap of the piezoelectric transducer with the recommended method detailed in the previous section. The frequency response for a driving swept sine wave signal swept from 16 to 26 kHz was measured four times with 5 minutes between each measurement, and four times again consecutively (no time between each measurement). Charging and heating will be related to the amplitude of the signal powering the transducer, so both a low voltage sine wave of 100 V amplitude, and a high voltage sine wave of 300 V amplitude (the maximum voltage that can be generated at high frequencies with available equipment) were tested. Figure 31 shows four frequency responses for the lower amplitude case (100 V amplitude driving sine wave) taken with 5 minutes between each measurement (left), and consecutively (right). Both cases show good agreement with 3.7 and 3.5% average relative error for the 5 minute rest and consecutive cases, respectively, however there appears to be some noticeable variation in the higher frequency range of measurements that were taken consecutively.

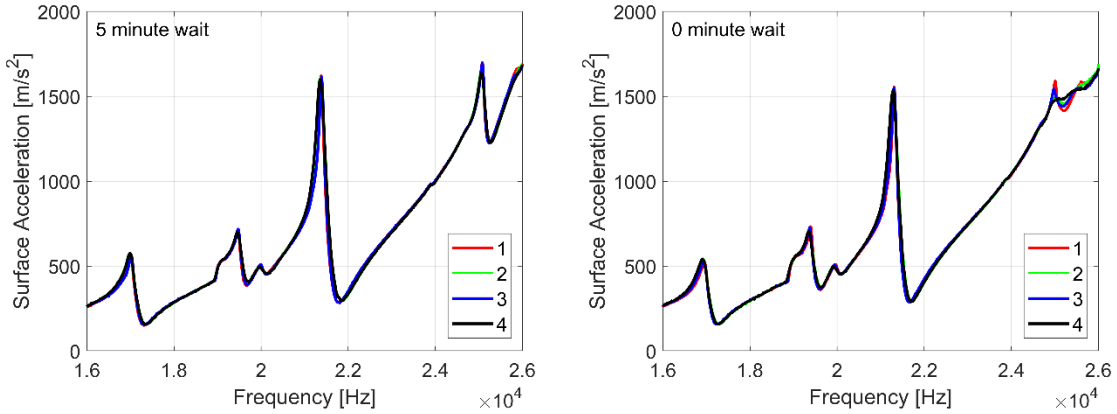

Figure 31. Four frequency response measurements of a driving swept sine wave signal with amplitude of 100 V from 16 and 26 kHz taken consecutively with 5 minutes between each measurement (left) and no time between each measurement (right).

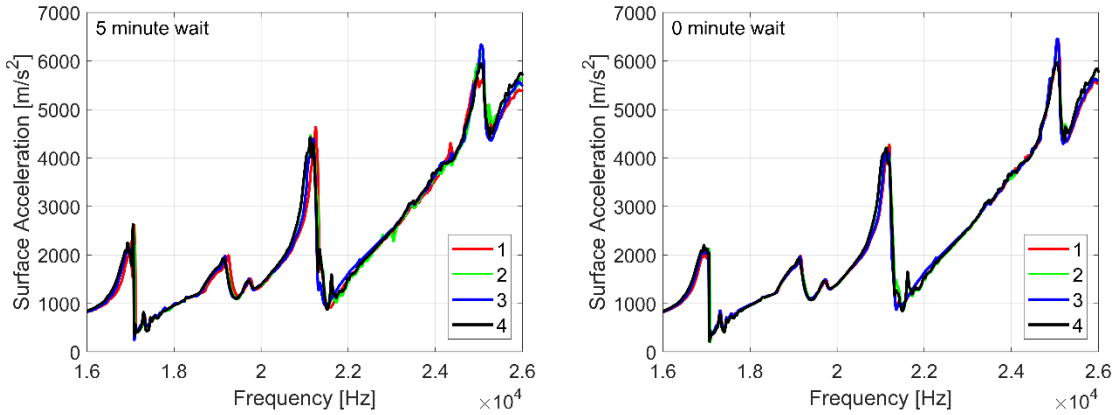

Figure 32. Four frequency response measurements of a driving swept sine wave signal with amplitude of 300 V from 16 and 26 kHz taken consecutively with 5 minutes between each measurement (left) and no time between each measurement (right).

Figure 32 shows four frequency responses for the higher amplitude case (300 V amplitude driving sine wave) taken with 5 minutes between each measurement (left), and consecutively (right). Noise is more noticeable in both cases of higher amplitude especially above 20 kHz (whether 5 minutes was allowed between measurements or not), with 9.3 and 5.8% average relative error for the 5 minute rest and consecutive cases, respectively. This increase in noise could be a sign of charging due to the higher level electric field, however the

lower average relative error for measurements taken consecutively suggests that the cause of the noise is not heating or charging. In addition, the accelerometer's maximum discharge time constant of 1.2 seconds allows ample time for over 99% of built up charge to dissipate in the 5 minutes between each measurement.

While charging does not seem to be an issue, even under the most severe conditions (300 V amplitude driving signal), there does still seem to be significant levels of noise in the frequency response measurement at higher frequencies and with higher amplitude driving signals. The cause is unknown, but may be related of the high frequency error (> +/- 10%) inherent to the accelerometer used to take measurements. Regardless, this increase in noise must be noted for later analyzing the accuracy of data.

3.5.3 Measurement Accuracy

3.5.3.1 Spatial Variation in Acceleration Measurement

Prior results have shown that measurement repeatability can reach levels of <10% through control of the measurement process. Making sure measurements are accurate is just as, if not more important. While the transducer and substrate mounting top cap are rigidly coupled with four bolts to transmit the vibration signal between the surfaces, the mode shape of the surface vibration may not be an even piston-like oscillation. A non-piston like motion could cause spatial variation in the magnitude or phase of vibrations across the surface that would result in a varying frequency response over the surface of the cap attached to the piezoelectric transducer. Because the accelerometer is not infinitesimally small, when it is fixed to the surface with adhesive, it will measure an average frequency response of acceleration over its area. If

significant variation in acceleration is apparent over the vibrating surface, the simultaneous measurement of acceleration and droplet effects will be impossible with an accelerometer as this would require the accelerometer to be placed in the precise location where the droplet is vibrated to obtain the most accurate acceleration measurement.

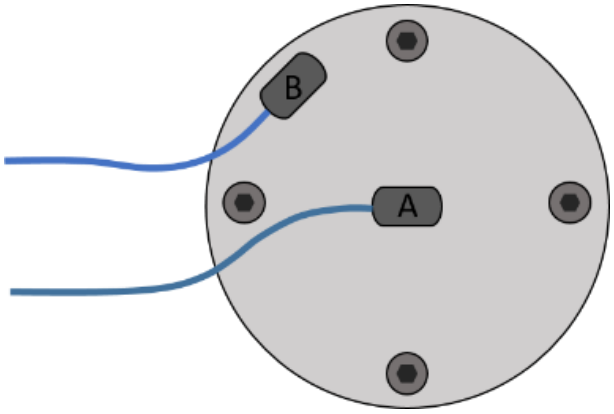

Figure 33. Mounting locations of two accelerometers on the top cap attached to the piezoelectric transducer to determine how the frequency response varies over the surface.

To determine if the frequency response varies spatially, two accelerometers (accelerometer A and B) were glued to the top of the cap attached to the piezoelectric transducer in two separate locations (Figure 33) with the method detailed in section 3.5.2.1.1. The frequency response was measured by both accelerometers for a driving swept sine wave signal with amplitude of 200 V from 18 to 23 kHz. Figure 34 shows a different frequency response measurement between the center location (B) and the outer location (A). These measurements were performed in additional locations on the surface with a similar effect, but two examples are shown here for simplicity.

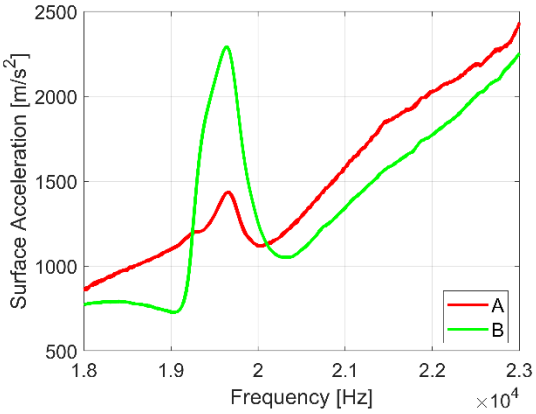

Figure 34. Spatial variation in frequency response of the top of a PZT cap measured with an accelerometer.

Both locations on the surface respond in the same manner at a given frequency, but the magnitude of the response differs. An average relative error of 19.7% is quite large and demonstrates that an accelerometer must be mounted in the exact location on the surface where droplets are vibrated to characterize the vibration excitation of the droplet correctly. This result also unfortunately eliminates the possibility of mounting an accelerometer on the side of the surface to simultaneously measure acceleration levels while testing with droplets. This is a detrimental result that could affect the accuracy of acceleration measurement due to changes in the coupling of vibrating surfaces precipitated by high power ultrasonic vibration. In light of the findings in the chapter thus far, acceleration measurement has to be done in the exact location on the surface where droplets are vibrated, and after the droplets are vibrated due to the destructive nature of the recommended accelerometer mounting method.

3.5.3.2 Measurement Effect of Accelerometer Mass

Droplets used in vibration testing will range from of 10 to 70 µL and about 2 to 6 mm in diameter at their contact line. The dimensions of the accelerometer used for frequency response

measurement is 5.46 x 3.43 x 2.54 mm (L x W x H). These dimensions are similar to the droplet sizes, however the mass of the droplets range between 0.01 and 0.07 grams while the mass of the accelerometer is 0.16 grams. While the difference between the mass of droplets and the accelerometer seems small, the accelerometer is at least 2 times more massive. This difference could result in a variation of the frequency response due to the difference of the mass on the surface. This could transpire as a shift in frequency or change in the magnitude of measured acceleration.

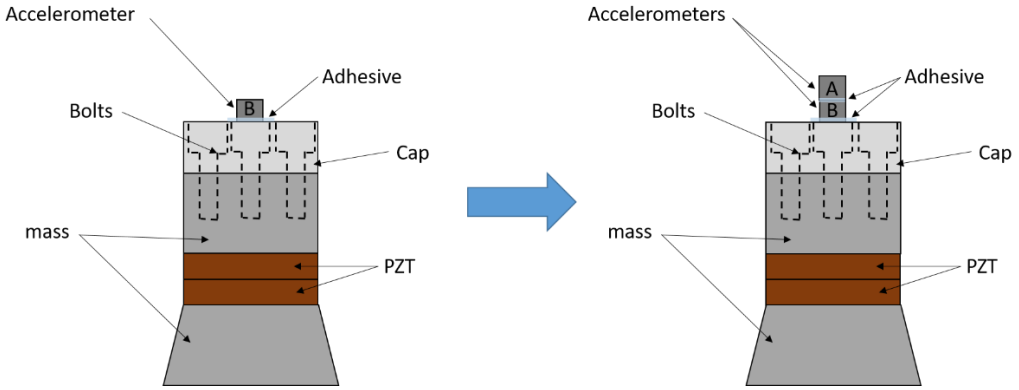

Figure 35. Method used to test the effect of accelerometer mass on the frequency response. Frequency response was measured with one accelerometer fixed to the surface using a small amount of adhesive. Another accelerometer was fixed on top of the first accelerometer with a small amount of adhesive so that frequency response could be measured again to compare the difference.

The effect of mass difference was tested using the method illustrated in Figure 35. One accelerometer (accelerometer B) was mounted with adhesive to the top surface of the cap on the piezoelectric transducer with the method described in section 3.5.2.1.1. The frequency response of the surface was measured for a driving swept sine wave signal of 200 V amplitude from 18 to 23 kHz using accelerometer B. A second, identical accelerometer (accelerometer A) was then mounted to the top surface of the first accelerometer (accelerometer B) already mounted to the

top cap of the piezoelectric transducer. This was again done with the method in 3.5.2.1.1. The frequency response of the surface was measured for a driving swept sine wave signal of 200 V amplitude from 18 to 23 kHz using accelerometer B. Figure 36 shows the difference between the frequency response measurements before and after adding the second accelerometer is negligible in acceleration magnitude and frequency shift with an average relative error of 4.1%.

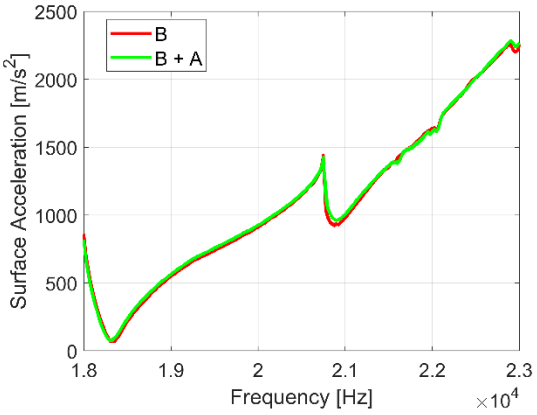

Figure 36. Measurement of frequency response to determine if accelerometer mass makes an impact. The red line shows the frequency response of the first accelerometer fixed to the surface by itself. Blue and cyan lines show the frequency response after the second accelerometer was fixed to the first accelerometer after varying times of adhesive cure time.

The addition of an accelerometer on the top of the first accelerometer represents the additional mass that one accelerometer adds to the surface when the frequency response is measured. This data provides reassurance that the additional mass of the accelerometer used to measure the frequency response does not affect the measurement significantly.

3.5.4 Validation of Accelerometer Measurements

A 3D scanning laser Doppler vibrometer (LDV) (Polytec, PSV-500-3D-HV) was used to obtain non-contact acceleration, velocity, and displacement measurements of the top surface of

the cap of three separate vibrating transducers (Figure 37). Laser vibrometry uses the Doppler effect to compare the phase and frequency shift of laser light reflected from a moving surface to a reference beam to determine the displacement, velocity, and acceleration of the moving surface.

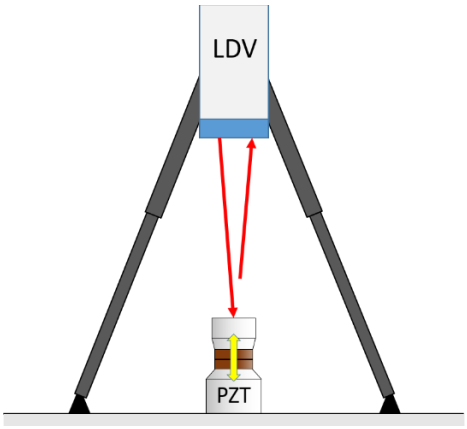

Figure 37. Laser Doppler vibrometry measurement of piezoelectric transducers. Laser vibrometry uses the Doppler effect to compare the phase and frequency shift of laser light reflected from a moving surface to a reference beam to determine the displacement, velocity, and acceleration of the moving surface.

These results are compared with acceleration measurements obtained by using an accelerometer as previously detailed in this chapter (Figure 38). The frequency response determined by LDV was an average of multiple points over the surface and is shown in each figure as a blue line. The frequency response measured with an accelerometer fixed to the center of the surface of each of the three different PZTs is shown in each figure as a red line. The absolute magnitude of the measurements taken with LDV and with an accelerometer cannot be compared because of different equipment used in the excitation. However, the response difference can be examined in terms of frequency. The first piezoelectric transducer shows relatively good response agreement in terms of frequency. The second and third piezoelectric

transducers appear to respond differently according to the acceleration methods. This may not necessarily be a physical difference in the vibration of the transducer, but rather a measurement effect.

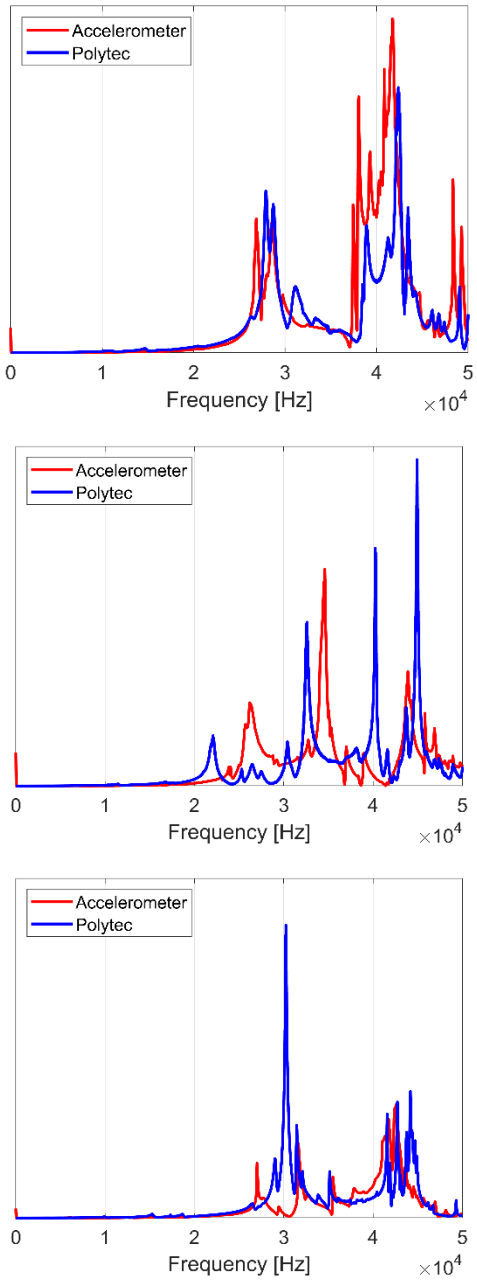

Figure 38. Comparison of accelerometer and Polytec laser vibrometer surface acceleration measurements for three different piezoelectric transducers.

An inherent limitation of accelerometer measurements are that it only measures acceleration in one direction. LDV can measure tilting/angled modes (Figure 39) to obtain a different, more conclusive result.

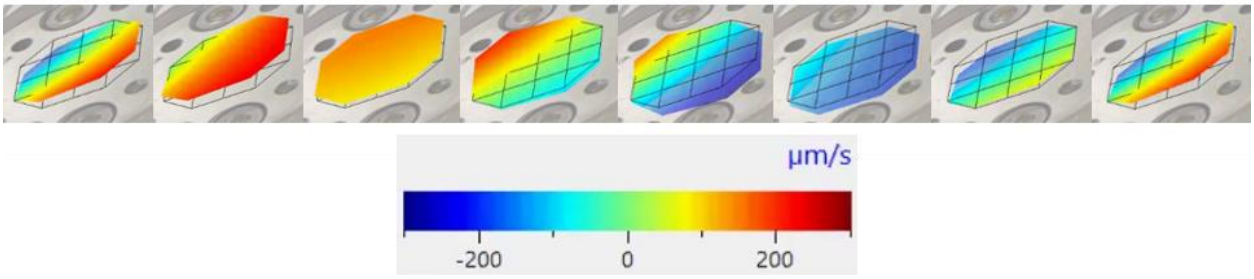

Figure 39. One cycle of a wave-like oscillating mode on the top surface of the piezoelectric transducer when vibrated at 32.1 kHz as measured by 3D scanning laser Doppler vibrometry.

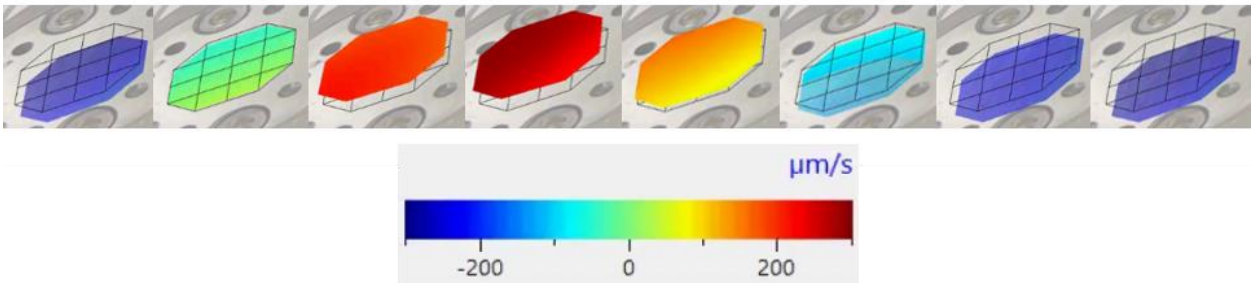

Figure 40. One cycle of a piston-like oscillating mode on the top surface of the piezoelectric transducer when vibrated at 29.0 kHz as measured by 3D scanning laser Doppler vibrometry.

The error may also be due to LDV measurements averaging over multiple points on the vibrating surface, while acceleration measurement from the accelerometer is taken at a single location on the center of the surface. This theory is further reinforced from acceleration data taken from accelerometers placed at different locations on the top of a piezoelectric transducer (Figure 34). The vibration mode shape of the PZT caps were noted to usually exhibit a piston-like surface mode (Figure 40) at frequencies near the resonance peaks of the transducers.

3.6 Other Measurements

One variable that was found to be well-controlled was the dispensing of droplets with the use of a syringe pump (Legato 180, KD Scientific). Droplet target volumes of 10, 30, and 50 µL had an average relative error of about 1.5% over the range of volume as measured by a high precision scale (PA313, Ohaus).

The dynamic analyzer has also helped to determine that the adhesion method used for attaching glass substrates to the top cap is not always repeatable, meaning that when a different glass substrate is glued to the top cap, the frequency response needed to be measured again. Glass substrates of the same size were always placed in approximately the same location on the cap of the transducer, but spreading of adhesive and applying the same pressure while curing was difficult to do given the nature of the delicate surface.

Delamination of glass substrates and accelerometers, while infrequent did occur. This would occur very suddenly without much warning. It was important to check the adhesion of substrates and accelerometers periodically to assure continued bonding. A change in vibration noise was apparent to the ear, and was able to give occasional warnings of impending problems. If delamination occurred while testing, the data set was rendered useless because the substrate-specific acceleration measurement becomes unavailable. The problem of delamination is relatively rare however, and can be somewhat controlled with good surface preparation.

One key issue that most frequently arose was the integrity of hydrophobic coatings used in testing. As mentioned in an earlier chapter, surfaces are commonly characterized by the contact angle formed by a liquid wetting the surface. This angle is usually relatively stable, especially for smooth surfaces. While ultrasonically vibrating hydrophobic-coated glass substrates with droplets of water wetting the surface, the equilibrium contact angle was observed

to change significantly. As contact angle is an indication of a surface's free energy, a changing contact angle designates a change in the surface's free energy. This change would result in very different physical interactions between a liquid and the surface as the contact angle degradation takes place. To determine the effects of ultrasonic vibration on the wetting of droplets, the surface free energy must be consistent, so in order to be successful with this objective, the cause of the coating degradation needed to be understood and avoided. The degradation of several hydrophobic fluoropolymer coatings are evaluated in the next chapter, and the most robust coatings are used for ultrasonic wetting studies to acquire the most reliable data

3.7 Recommended Testing Procedures

Based on the previous studies, the following general test procedures were utilized in order to minimize the errors and uncertainty for surface acceleration measurement:

- The recommended method for bonding two vibrating surfaces is outlined in section 3.5.2.1.1.
- A pre-load of 20 inch-pounds was used to attach the top cap to the piezoelectric transducer each time a different cap was mounted.
- To best approximate the level of vibration that a droplet is excited with, accelerometers were mounted to the surface where droplets were vibrated during testing.
- Contact angle hysteresis measurements were taken before and after coatings were used in testing to determine if significant changes to surface energy might have occurred, thereby affecting the accuracy of the data.

- Frequency response measurements with an accelerometer to characterize the acceleration of a surface were taken as quickly as possible after testing with droplets was complete. This frequency response measurement was used to interpret the response of all droplets tested on that substrate.
- Each frequency response measurement was taken twice so that if an issue with delamination was occurring, significant difference (> 10%) would be apparent between measurements taken for the same level vibration signal.

3.8 Summary

Measurement methods and their repeatability were assessed. Adhesives used to mount testing equipment should be allowed 24 hours to cure. The addition of the mass of the accelerometer does not affect frequency response when measuring acceleration. Charging and heating of piezoelectric elements is not an issue for repeatable frequency response measurement, but the high frequency accuracy of the accelerometer may be a source of measurement error. Surface preparation and careful observation during testing is important to acquire good data, but the possible change in surface free energy due to ultrasonic vibration of wet coatings is an issue that needs to be investigated. The next chapter will evaluate the degradation of several hydrophobic fluoropolymer coatings due to exposure to droplets of water and ultrasonic vibration.

CHAPTER 4:

DEGRADATION OF HYDROPHOBIC COATINGS

4.1 Abstract

Many important processes, from manufacturing of integrated circuit boards to an insect's ability to walk on water, depend on the wetting of liquids on surfaces. Wetting is commonly controlled through material selection, coatings, and/or surface texture. However, wetting is sensitive to environmental conditions. In particular, some hydrophobic fluoropolymer coatings are sensitive to extended water exposure as evidenced by a declining contact angle and increasing contact angle hysteresis.[1] Understanding "degradation" of these coatings is critical to applications that employ them. Samples of glass slides coated with a series of fluoropolymer coatings were tested by measuring the contact angle before, during, and after extended submersion in deionized water. These measurements were compared to similar measurements taken before, during, and after the same coatings were subject to ultrasonic vibration while covered in deionized water. Both methods caused changes in advancing and receding contact angles, but degradation rates of vibrated coatings were significantly increased. Prolonged soaking caused significant decreases in the contact angle of most of the samples, though most experienced significant recovery of hydrophobicity when heat-treated at 160 °C after

[1] This chapter was published in the proceedings of ASME 2018 International Mechanical Engineering Congress and Exposition (Trapuzzano MA, Guldiken R, Tejada-Martínez A, Crane NB. Degradation of Hydrophobic Surface Coatings Under Water Exposure. ASME. ASME International Mechanical Engineering Congress and Exposition, *Volume 7: Fluids Engineering* ():V007T09A064. doi:10.1115/IMECE2018-87860). Permission is included in Appendix A.

submersion. Some coatings appear noticeably more resistant to degradation by one or both methods. The FluoroSyl coating showed no clear change under submersion, while other coatings experienced significant contact angle change. Degradation of wet-vibrated coatings is inconsistent for different coatings, but is not simply an acceleration of the degradation resulting from submerging coatings in water. This is apparent as some coatings are affected by one method but not the other. Atomic force microscopy showed a roughening and smoothing effect when coatings were submerged and heat-treated respectively, but the magnitude of this change does not correlate with the changes in wetting on the coatings. The magnitude of vibration acceleration between 700 and 7000 g did not significantly alter the rate of contact angle degradation.

4.2 Introduction

Wetting is commonly controlled through material selection, coatings, and/or surface texture, however these means are sensitive to environmental conditions (heat, light, moisture, abrasion), especially in monolayer coatings. Much scientific literature exists on the degradation of coatings, including effects of UV exposure [95, 96], temperature [97-99], exposure to water [100-103], or mechanical erosion [104]. The effects of various means of degradation varies from coating to coating, suggesting that coating composition plays a major role in the robustness of the coating.

Hydrophobic, or water-repellant coatings are one type of coating that has become increasingly common in every-day applications. Fluoropolymer, coatings, especially polytetrofluoroethelyne (PTFE), are perhaps the most common types of hydrophobic coatings. The low surface energy of fluoropolymer coatings causes liquids wetting the surface to “bead”

up and easily roll off of the surface. Hydrophobic coatings can be found in nature [105], and have been used for the prevention of biofouling [106] and corrosion [107], as well as encapsulants for electronic components to improve the reliability when such components are exposed to moisture while in operation [108, 109]. Use of hydrophobic coatings, specifically PTFE and Cytop, are common in research and industry applications like electrowetting [110] due to their low friction characteristics. These coatings are usually easy to apply and relatively inexpensive.

While hydrophobic coatings have many applications, reliability of the coatings is crucial to repeatable long-term wetting. Therefore, changes in contact angle (CA) and/or contact angle hysteresis (CAH) of the coating is of great importance. Degradation of fluoropolymer coatings like FluoroPel, Cytop, and Teflon due to electrowetting actuation has been documented [111]. Some hydrophobic fluoropolymer coatings are also sensitive to extended water exposure as evidenced by an increase in coating thickness or weight [112]. This could be a cause for concern if water uptake is found to have an effect on the CA of these coatings. Cytop is reported to have a minimal water absorptivity at less than 0.01 percent at 60 °C in water [113], so it may seem like a good candidate coating for applications where prolonged exposure to water occurs. However, this type of data is not readily available for many coatings, so information about how water exposure affects the CA of hydrophobic fluoropolymer coatings could be useful to determine which coatings would be appropriate for specific applications.

Sonication is a common method used for a variety of cleaning and preparatory processes due to the generation of high frequency pressure waves that create oscillating gas bubbles that implode, dislodging contaminants from a surface. Sonication has also been shown to increase mass transport in and out of permeable solids [114]. If degradation of CA for hydrophobic

fluoropolymer coatings can be attributed to uptake of water, sonication of these coatings under water exposure could accelerate this process by increasing transport at the coating/liquid interface. If so, this method could provide quick insight on coating performance under prolonged exposure to water.

This work uses standard CA and surface energy measurement methods to characterize the degradation of hydrophobic fluoropolymer coatings due to long term water exposure over the course of many days, and contrasts these with measurements from short term exposure under high frequency vibration (> 20 kHz) over a period of minutes. The goal is to quantify the wetting effects of coatings exposed to water for long periods of time, understand the causes, and determine if ultrasonic vibration provides an expedited method to predict the effects of long term water exposure for a given coating.

4.3 Experimental Methods

Glass microscope slides (1 mm thick) were coated with several different commercial hydrophobic fluoropolymer coatings (Table 2). All coatings were purchased from manufacturers and are proprietary, so the exact constituents of each coating is unknown. Coatings listed in this table without an application method indicate that the slides were purchased with a pre-applied coating, while other coatings were applied to glass slides using the manufacturer recommended application methods. All glass slides were solvent-cleaned with acetone and then methanol, followed by rinsing with deionized water and then isopropyl alcohol before drying with N_2. The glass slides were then plasma-cleaned for 2 minutes with an O_2 plasma.

Table 2. Hydrophobic coatings used for testing, their application method, and their manufacturer.

Coating	Application	Manufacturer
Cytop CTX-809A	Spin	Bellex
FluoroPel 1601V	Spin	Cytonix
FluoroSyl 3750	Dip	Cytonix
FluorAcryl 3298	Dip	Cytonix
PTFE	N/A	EMS
AFC 2101	N/A	AFT Fluorotec
AFC 2206	N/A	AFT Fluorotec

Cytop is an amorphous fluoropolymer coating that can be applied by spin-coating, dip-coating, or by potting [115]. Spin-coating was done at 2000 rpm for 40 seconds. A soft-bake at 100 ºC on a hot plate for 90 seconds, and a hard-bake at 180 ºC for 30 minutes followed, resulting in a coating of ~ 1 µm thickness [115]. FluoroPel is a polymer in a fluorosolvent. The recommended application method is spin-coating [116]. For deposition, a drop of FluoroPel was placed in the center of the glass slide before spinning at 2000 rpm for 40 seconds. A soft-bake at 100 ºC on a hot plate for 90 seconds, and a hard-bake at 150 ºC for 30 minutes followed. FluorAcryl is a fluoroacrylate UV-curable oligomer that can be applied by dip-coating, or spray-coating [117]. Slides were coated by a manual dipping method. Once the coating settled flat, it was cured with 420 nm UV light to a pencil hardness greater than #2. FluoroSyl is a perfluoropolyether coating that can be applied by dip-coating, or spray-coating [118]. Slides were submerged into the FluoroSyl liquid for 1 minute. After 1 minute, glass slides were removed and hard-baked at 100 ºC for 20 minutes. Coatings that came pre-applied on glass slides were already prepared for testing, and were simply diced to manageable sizes.

Samples of all coated glass slides were tested for degradation by two methods (Figure 41). The first degradation method was continuous submersion of hydrophobic coatings in water.

Coated glass slides were covered with deionized water and sealed in glass containers for a period of 130 days (Figure 41 (2a)). A total of 6 slides (18.25 mm x 18.25 mm) of each coating were used for submersion testing. Each coating type was submerged in a separate container to prevent cross-contamination. Thrtoughout the 130 days, samples were removed at intervals for characterization, where advancing and receding CA measurements were taken at 2 arbitrary locations on the surface of each sample, resulting in a total of twelve measurements for each coating at each point of characterization. The coatings were then re-submerged until they were removed again for characterization. After 130 days of submersion, one submerged sample of each coating was removed from the water bath, dried with compressed air, and heat-treated in an oven at 160 ºC for up to 20 days. Samples were again removed from the oven at intervals to measure advancing and receding CA at 4 arbitrary locations on the surface of each sample.

The second degradation method was vibration-accelerated degradation. This was tested by bonding samples of each coating on a glass slide to a piezoelectric transducer (PZT) actuation stack (Figure 41 (2b)) with adhesive (Loctite 4310). The coated glass slide was covered with a puddle of deionized water, and then vibrated orthogonally to the coated surface (Figure 41(3b)) at a frequency of 24 kHz (near one of the transducer's resonance frequencies) with a sine wave generating ~ 500 g of surface acceleration for a total of 50 minutes using a function generator (33250A, Agilent Technologies) and driver/amplifier (PZD350A, Trek Inc.). Four advancing and receding CA measurements were taken at random locations and averaged for one coating data point. Measurements were taken before vibration and at intervals during vibration.

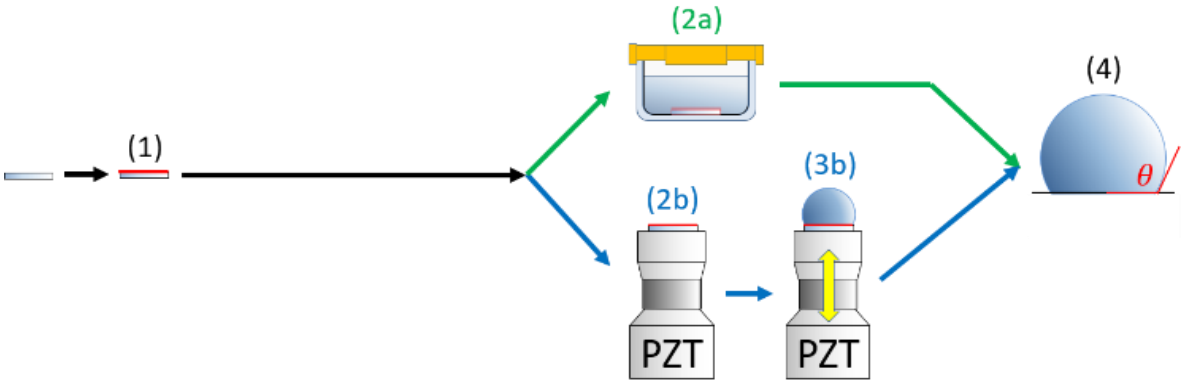

Figure 41. Flow-chart schematic of experimental testing. Glass microscope slides were coated with a hydrophobic coating (1). Coated glass slides were then either submerged in deionized water (2a), or fixed to a PZT (2b), then vibrated while covered with deionized water (3b). Advancing and receding CA was measured before, during, and after testing (4).

CA measurements were taken using the sliding angle (tilted plate) method. In this method, droplets were pumped on to the coating surface while the surface is oriented horizontally. The surface was tilted while the droplet shape was imaged. The advancing angle (θ_A) was taken as the angle at the leading edge of the droplet just before the leading edge of the droplet becomes un-pinned, and the receding angle (θ_R) was taken similarly at the trailing edge of the droplet (Figure 42(b). The CAH was taken as the angle difference between the advancing and receding angle. Coated glass slides were fixed to a tilting goniometer to take CA measurements (Figure 42(a)). Deionized water droplets of 20 µL were pumped onto the slides with a syringe pump (Legato 180, KD Scientific). A camera (NX8-S2, IDT Vision), and backlight were used to image droplets as the goniometer stage was tilted. Images of droplets were recorded at 30 Hz. An edge detection algorithm [119-122] was used to track the CA at two sides of the droplet (Figure 42(c)).

While this measurement method is sufficient for characterization, it has its shortcomings. On a hydrophobic surface, the minimum CA is approximately equal to the receding CA, while

the maximum CA can be lower than the actual advancing CA [30]. Drop placement also has an impact on sliding angle measurements due to surface heterogeneities and non-repeatable sliding behavior. Differing contact line lengths for a given droplet volume can cause for a range of equilibrium CAs on a surface [123]. Despite these CAH measurement limitations, this method will suffice for detecting changes in CAH due to water exposure.

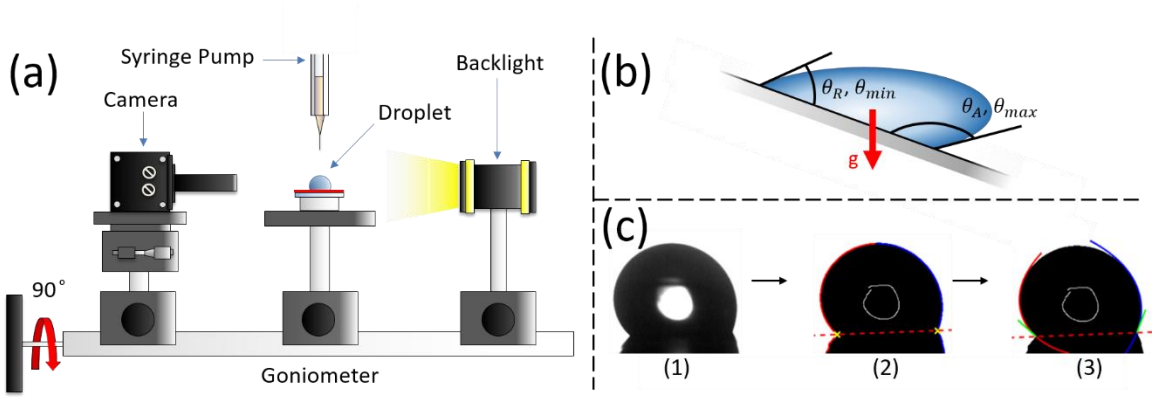

Figure 42. Experimental setup used to track droplet CA (a). Deionized water droplets were pumped onto hydrophobic-coated glass slides that were fixed to a tilting stage used to align imaging equipment. Images were recorded at 30 fps as the stage is tilted. CA measurement diagram (b). Advancing (θ_A, θ_{max}), and receding (θ_R, θ_{min}) CAs of a droplet the moment before it unpins and slides down a tilted surface. The direction of the gravitational force is represented with a red arrow for orientation purposes. MATLAB algorithm (c) used for tracking droplet position and CA. An image of a droplet (1) was separated into left and right sides and the contact line was plotted as a red dashed line through both yellow 'x' marks (2). Then, polynomial fitting of the droplet was used to find the CA of the droplet on each side (3).

4.4 Results and Discussion

4.4.1 Submersion of Coatings

Figure 43 shows advancing and receding CA data for coatings that were submerged in water as a function of time. All coatings but the FluoroSyl experienced degradation of their

advancing and receding angles as a result of submersion in water. The decline of both CAs degrades rapidly but moves toward a limiting value after 40 to 50 days of submersion in water.

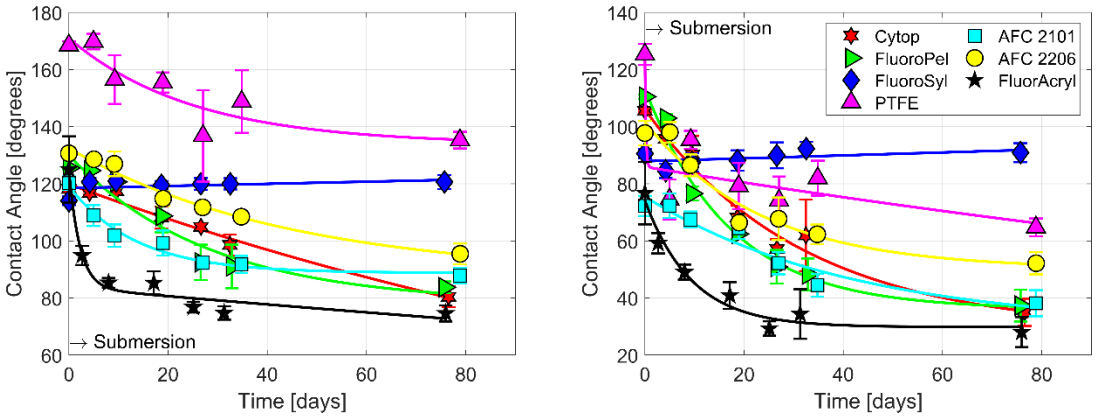

Figure 43. Advancing (left) and receding (right) CAs for coatings that were submerged in water. Exponential, polynomial, or linear fits are used to show data trends for each coating.

While decreasing advancing and receding angles was a common trend for 6 coatings, an increasing CAH for these coatings is not always manifest (Figure 44). An increase in CAH is only apparent for Cytop, FluoroPel, and AFC 2206 coatings. These three coatings experienced a more drastic decline of receding angle when compared to advancing angle, which in turn increases their CAH. Submersion of AFC 2101 and FluorAcryl results in similar degradation of advancing and receding CA. Thus, a change in CAH is not apparent under the CA measurement uncertainty. Variation in CA measurements was particularly large for submerged PTFE results which could be a significant application issue itself.

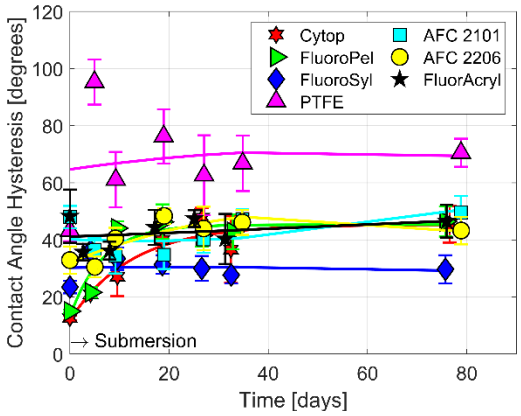

Figure 44. Change in CAH for coatings submerged in water.

Because the exact composition of each proprietary coating is not known, it is difficult to hypothesize about the difference between the degradation trends of FluoroSyl and all other coatings tested. Boinovich et al. [103] noted mechanisms (reversible and non-reversible) for the degradation of water CA on siloxane–based hydrophobic surfaces that were in continuous contact with water, including the growth of wetting films, reversible hydration creating hydrogen bonds, hydrolysis of molecule-specific free end groups with hydroxyl end groups, and non-reversible hydration of hydrogen bonding active groups inside the material. One possibility for the change in CA could be the absorption or adsorption of water during submersion. These effects could change surface energy, perhaps as a result of hydroxyl groups from water molecules changing the energy of the free surface by means of weak hydrogen bonding. Absorption might be evidenced by a change in film thickness as the coating is submerged in water. A contact profilometer (Dektak 150, Veeco) was used to measure the thickness of the Cytop coating. The initial Cytop coating thickness of 622 nm (6 nm standard deviation) increased to a thickness of 653 nm (30 nm standard deviation) after the coating was submerged for 12 days. The results of these measurements show that there may be a slight increase in step

height, but the measurement standard deviation is also increasing, so these results are insufficient to conclude that the change in wetting properties are due to the absorption of water.

4.4.2 Heat Treatment of Submerged Coatings

It is possible for the coatings tested to absorb or adhere to hydroxyl groups of water molecules without causing a detectable film thickness change. Heating the submerged samples above 100 °C could remove absorbed/adsorbed water and restore the initial wetting characteristics. Figure 45 shows the impact heating has on samples after submersion. The data suggests that the degradation of CA is at least partially thermally reversible for most coatings. This provides some evidence that coatings are absorbing or reacting with water, as heating coatings at 160 °C seems to have a restoring effect. While the improvement may be due to evaporation of water from the coatings, the mechanism of the CA change is unclear. Heating produced significant CA recovery in all coatings tested in this study except for FluoroSyl, and FluorAcryl. Heat treatment of FluorAcryl and FluoroSyl may have been beneficial in restoring the CA if a lower temperature heating condition were chosen, however wetting characteristics of Cytop and PTFE were nearly completely restored as a result of heating at the given temperature. The heat treatment rapidly restores the coatings compared to the rate at which they were degraded. While advancing and receding CA are improved individually, Figure 46 shows that the CAH for coatings except Cytop and PTFE are still increasing while undergoing heat treatment. AFC 2101, AFC 2206, and FluoroPel benefit from a restoration of advancing and receding angle as a result of heat treatment, however the rate of restoration for the receding angle lags the advancing angle, manifesting as an increase in CAH as heat treatment ensues.

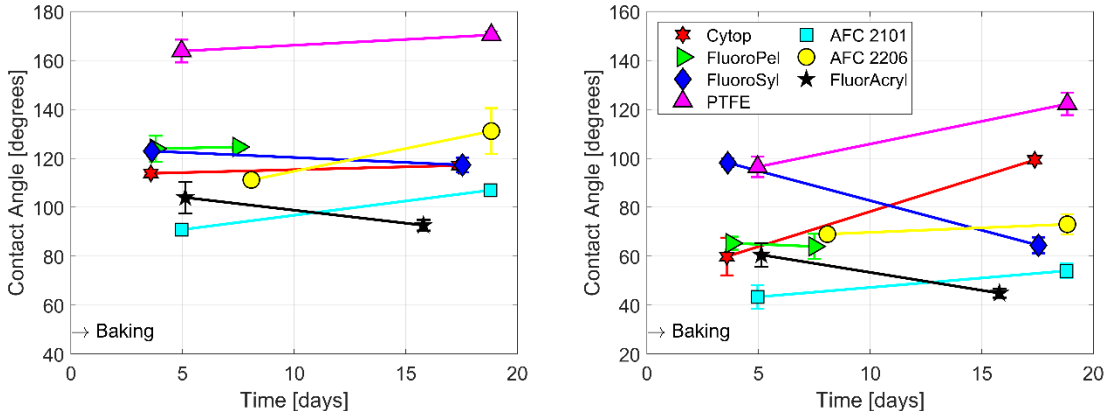

Figure 45. Change in advancing (left) and receding (right) CA by heating previously submerged samples at 160 ºC for varying lengths of time. Coatings remained submerged and were taken out of water and heat-treated after approximately 130 days. CAs were measured periodically as coatings were heat-treated.

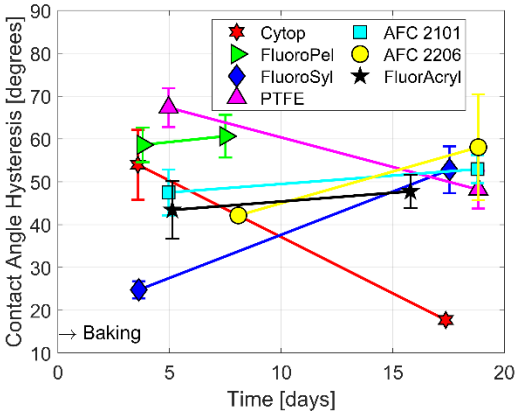

Figure 46. Change in CAH by heating previously submerged samples at 160 ºC for varying lengths of time. Coatings remained submerged and were taken out of water and heat-treated around 130 days. CAH was measured periodically as coatings were heat-treated.

When FluorAcryl is heat-treated at 160 °C, the advancing and receding CA is initially restored very close to initial values, but as the heat treatment continues, the coating begins to degrade again. This coating yellowed when heat-treated, indicating some chemical/structural changes. Degradation of Fluorosyl receding CA during heat treatment, is attributed to exceeding

the recommended 100 °C curing temperature. However, this coating did not degrade due to water submersion, so heating to restore the coating is unnecessary.

One cause for CA change could be a change in surface topology, specifically roughness. Surfaces with micrometer and nanometer-scale roughness can exhibit hydrophobic and oleophobic properties due to contact line pinning and trapping of gas between the solid and liquid [43, 44, 124]. If submersion of coatings in water results in a change in surface roughness, this could help explain the change in CAs. Table 3 summarizes roughness data obtained with atomic force microscopy for both FluoroSyl and Cytop coatings before and after long-term submersion in water, and then again after being restored by heat treatment.

Table 3. Average and RMS roughness change of submerged and heat-treated coatings.

	Avg. R_a (Std. Dev.) [nm]	**Avg. R_q (Std. Dev.) [nm]**
Cytop (Virgin)	0.5 (0.0)	0.7 (0.0)
Cytop (Submerged)	19.8 (2.1)	42.8 (4.7)
Cytop (Heated 160 °C)	10.7 (5.3)	15.3 (7.3)
FluoroSyl (Virgin)	15.4 (11.9)	40.0 (29.9)
FluoroSyl (Submerged)	16.8 (3.8)	31.4 (5.4)
FluoroSyl (Heated 160 °C)	2.7 (0.8)	6.8 (1.6)

The average and RMS roughness of Cytop were both increased more than 10x due to submersion. The Cytop coating was only partially re-smoothed by heat treatment, but the advancing and receding CA were essentially restored in full. Roughness of FluoroSyl was not changed significantly due to submersion however, but remained close to the original roughness value. After heat-treating these two coatings at 160 °C, the average and RMS roughness were reduced significantly. The CA characteristics of FluoroSyl were not affected by soaking the

coating in water, however after heating the coating, the receding angle of water on this coating decreased. Roughness changes with heating are inconsistent between both materials, therefore the roughness change that occurs as a result of submerging the coatings in water, and from heat-treating the coatings at 160 °C, does not appear to be the primary source of the CA changes.

Water submersion provides valuable insight into the performance of the materials during water exposure, but the tests are time consuming. Methods of accelerated testing are of great value in shortening testing times and predicting long term coating performance. While temperature is widely used in accelerated degradation testing, it can cause unexpected changes such as a phase change. Alternatively, acceleration of coating degradation from additional motion could occur as a result of increased transport between water and substrate.

4.4.3 Comparison of Ultrasonically Vibrated Wet Coatings

Ultrasonic vibration of coated substrates covered with water is capable of altering the hydrophobic properties of fluoropolymer coatings as seen in Figure 47, though generally the changes are smaller than long term submersion.

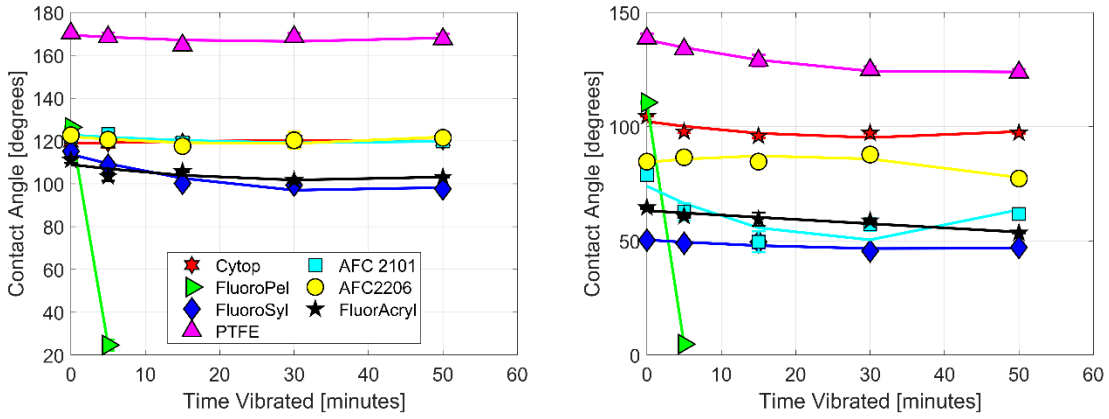

Figure 47. Advancing (left) and receding (right) CA for coatings that were covered in water and vibrated with a piezoelectric transducer (sine wave, 24 kHz, ~ 500 g surface acceleration).

Vibrating these coatings while covered in water produced varying results in comparison to soaking tests. Most coatings showed negligible degradation from water-covered vibration, however FluoroPel degraded quickly compared to all other coatings. While the degradation of some coatings is apparent at just a fraction of the time, some coatings like Cytop do not begin to degrade in the amount of time vibrated, but did degrade when submerged in water. It is apparent that ultrasonic vibration increases the degradation rate of coatings that degraded substantially in the time vibrated, but the degradation of each coating in one method is not proportional to the corresponding degradation in the other method over the range of conditions studied. Figure 48 compares the final measured advancing and receding CA for each method of degradation. Distinctive degradation of FluoroPel and FluoroSyl demonstrate that vibration does not simply accelerate the changes observed from water immersion. This data, like the data in Figure 43, also shows that the receding CA degrades more than the advancing CA. Surface acceleration levels and rate/amount of coating CA degradation were not apparently related when comparing samples that were vibrated between 700 and 7000 g. FluoroPel degraded most substantially and at the highest rate due to ultrasonic agitation while covered in water. While the advancing and receding CAs for FluoroPel were restored significantly by heat treatment after submersion, this coating showed no restoration after being subsequently heat-treated for 72 hours at 160 °C. Follow-up profilometry testing confirmed that FluoroPel was removed in the regions covered by water when vibrated.

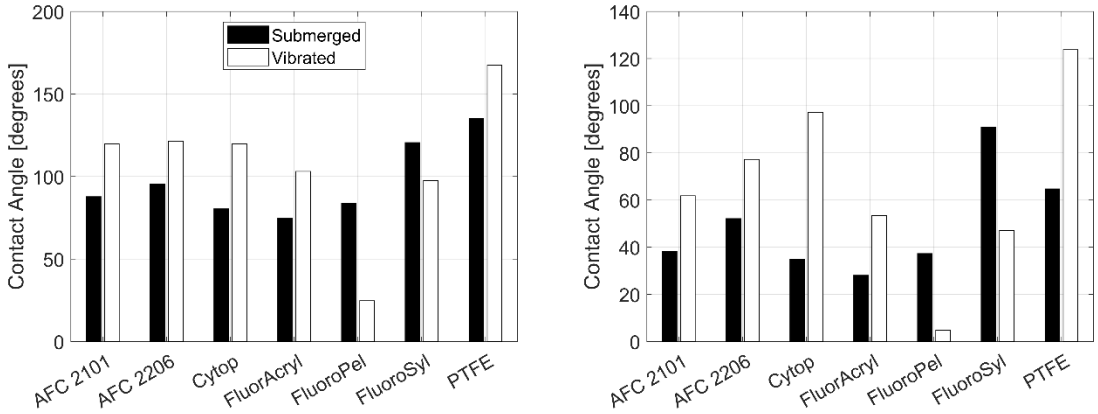

Figure 48. Final measured advancing (left) and receding (right) CA of coatings that were tested by both means of degradation.

4.5 Conclusion

Degradation of seven hydrophobic fluoropolymer coatings were tested with two different methods: submersion of the coating in deionized water over time, and ultrasonic vibration of the coating while covered in deionized water. These two scenarios represent real conditions that a hydrophobic coating may be exposed to in various applications. While FluoroSyl experienced negligible CA change while submerged in water, advancing and receding CA, the CA in all other coatings tested was reduced by 20-70%. Heat treatment was shown to restore the CA of submerged coatings over a shorter time scale – as compared to degradation – when coatings were not sensitive to high temperatures, and careful selection of heating conditions were chosen. Submersion of coatings in water results in a slow degradation of CA occurring over the course of days to weeks, while vibration of most coatings showed some modest degrading effects from a short exposure (minutes instead of days) to vibration while covered in water. High frequency vibration of wet coatings is not simply an acceleration of the degradation that occurs as a result of submerging the coatings in water – as distinct trends are apparent for FluoroPel and FluoroSyl – but it could be useful as an accelerated indication of how hydrophobic coatings subjected to

vibration or agitation in industrial applications will degrade. Surface profilometry measurements did not reveal a recognizable trend that would be useful for determining a possible cause for the changing CA. It does not appear that vibration of coatings submerged in water is promising as a speedy method to determine if coatings will degrade at all due to water exposure or submersion over the lifetime of the coating.

CHAPTER 5:

DROPLET WETTING WITH ULTRASONIC VIBRATION

5.1 Abstract

Many processes rely on wetting of liquids on surfaces. The way a liquid wets a solid depends on chemistry, geometry, and local energy inputs. Low-frequency surface vibrations can effect wetting changes prompted by droplet oscillations. High-frequency (ultrasonic) surface vibration can also cause a liquid to wet or spread out on a solid, but governing mechanisms are relatively uncharacterized.[2] To investigate, droplets are imaged as they vibrate on a hydrophobic surface over different high frequencies (>10 kHz). Wetting transitions occur abruptly over a range of parameters, but coincide with surface resonance modes. The wetting change is proportional to droplet volume and surface acceleration, and remains after cessation of vibration, however new droplets wet with the original contact angle. Wetting control has various industry applications, and understanding these basic phenomena will help develop a deeper understanding of how ultrasonic vibration can be utilized to tune the behavior of liquids on any surface.

[2] This chapter was published in the proceedings of ASME 2018 International Mechanical Engineering Congress and Exposition (Trapuzzano MA, Crane NB, Guldiken R, Tejada-Martínez A. Forced Wetting of Liquids Using Ultrasonic Surface Vibration. ASME. ASME International Mechanical Engineering Congress and Exposition, *Volume 7: Fluids Engineering* ():V007T09A063. doi:10.1115/IMECE2018-87832.). Permission is included in Appendix A.

5.2 Introduction

Manipulation of droplets is common practice today in many manufacturing processes where it is done to perform some task, i.e. transporting solid objects or similar [3-5]. These processes all rely critically on fine control of contact angle and droplet shape. Surface coatings [125], surfactants [126], and electric fields [54] can all be used to change how a puddle or droplet wets a surface. Many of these methods have been widely studied, and much scientific literature exists on each one as of today. Vibration has also been shown to affect the wetting states of liquids [1, 32, 56, 65, 71-73, 77-79], but coupled dynamic effects are very complex, and thus not much work has been done in the way of characterizing or applying this method in industry.

If vibration effects were well known, it could become a viable method of wetting control that is robust and reliable in situations where electro-wetting or use of surfactants may not be suitable. To control wetting using vibration, first it would be necessary to understand the physical phenomena that cause wetting changes to occur. There is much prior research that examines the wetting effects of low frequency, high amplitude vibrations, and is generally split up in two categories: vertical [32, 56, 65] and horizontal excitation [71-73, 77, 78]. Prior work done with wetting effects of high frequency vibration does exist [1, 79], but mostly looks at effects macroscopically with applications and does not elucidate the key parameters and underlying phenomena that may be causing the observed effects.

Wetting control is restricted by various factors. For instance, use of low frequency vibration (<200 Hz) to excite droplets requires high amplitudes of vibration which distort droplets to such degrees that it would render the desired effects useless for applications requiring delicate movements of particles on droplets. Many switchable adhesion studies have been done

with textured surfaces [77, 127], and while textured surfaces can aid in both wetting (Wenzel state) and de-wetting (Cassie state), these surfaces are often not practical for real-world applications due to their complexity and difficulty to manufacture. High frequency vibration of droplets on smooth surfaces could provide the desired wetting effects without some of the aforementioned drawbacks.

This work investigates the impact of high frequency vibrations (>10 kHz) on the wetting of droplets. We are primarily interested in characterizing the different variables that influence the transitions. Sweeping excitation frequencies help to pinpoint parameters where droplet effects need to be further investigated. Once characterized, the information may be used to further understand the underlying causes of the wetting effects and ultimately lead to the prediction or control of wetting of liquids in general circumstances using ultrasonic vibration.

5.3 Experimental Methods

The experimental setup is shown in Figure 49. Glass microscope slides (1 mm thick) were dip-coated with an abrasive-resistant, smooth, hydrophobic coating (FluoroSyl 3750, Cytonix Corp.). Coated glass slides were fixed with adhesive (Loctite 4310 Light Cure Adhesive, Henkel) to one side of a piezoelectric transducer (PZT). De-ionized water droplets of 10, 20, and 30 µL were pumped onto the coated glass slides with a syringe pump (Legato 180, KD Scientific) with standard deviation less than 300 nL. A function generator (33250A, Agilent Technologies) and driver/amplifier (PZD350A, Trek Inc.) were used to vibrate the glass slides in the vertical direction with a standard sine wave swept from 1 and 26 kHz over 50 seconds and amplitudes of 50 to 350 volts. Frequency sweeps within this range were used to pin-point wetting transitions for further examination. After each test, the surface was dried with compressed air

before another droplet was placed on the surface. For each set of tests, a single hydrophobic-coated glass slide glued to the top of the PZT was used to gather data. Droplets were pumped onto the same location on the glass slide for every test using a micro-stepping motorized stage to avoid any spatially varying vibration or surface effects. This assured that the starting contact angle for each test was relatively unchanged throughout testing.

A camera (NX8-S2, IDT Vision), and backlight were used to image the experiments. Images were recorded at 30 Hz. A MATLAB algorithm [119-122] was used to track the triple point location and the contact angle at two sides of the droplet (Figure 50). The droplet images are correlated to the excitation frequency of the piezoelectric transducer for frequency studies.

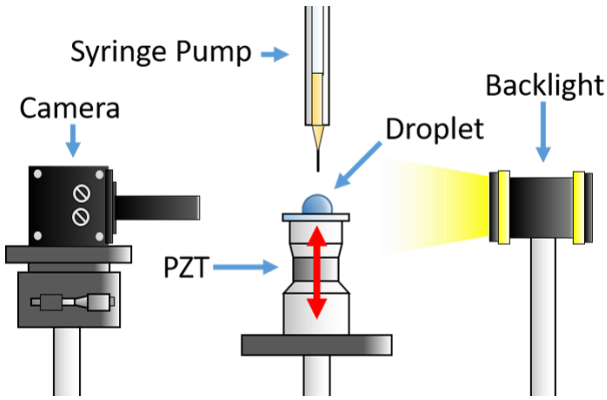

Figure 49. Experimental setup used to track contact angle and droplet position. Droplets rest on hydrophobic-coated glass slides and are vibrated vertically (direction of red arrow) with a piezoelectric transducer.

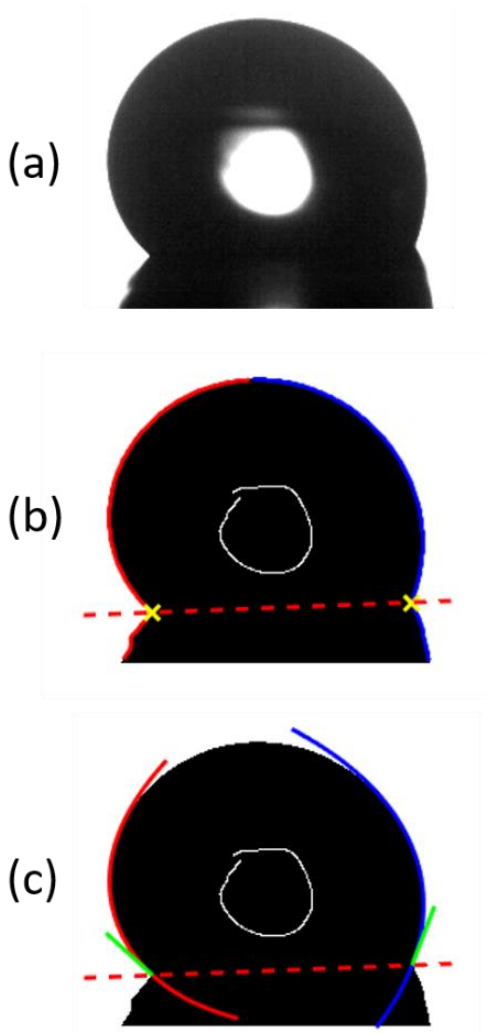

Figure 50. MATLAB algorithm used for tracking droplet position and contact angle. An image of a droplet (a) is separated into left and right sides and the contact line is plotted as a red dashed line through both yellow 'x' marks (b). Then, polynomial fitting of the droplet is used to find the contact angle of the droplet on both sides (c).

The contact angle hysteresis (CAH) for de-ionized water on the coated glass slides used for testing was determined by first pumping droplets on the surface while it is oriented horizontally. The surface is tilted while images of the droplet were recorded at 30 Hz. As the surface is tilted the droplet remains pinned, but begins to lean until the contact angle of the leading and trailing edges of the droplet reach some critical value and the droplet beings to slide down the surface. The advancing angle (θ_A) is the angle at the leading edge of the droplet just

before the leading edge becomes un-pinned, and the receding angle (θ_R) is the angle at the trailing edge of the droplet just before the trailing edge becomes un-pinned (Figure 51).

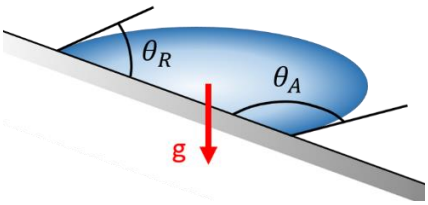

Figure 51. Advancing (θ_A) and receding (θ_R) angles of a droplet just before it slides down an inclined surface. The direction of the gravitational force is represented with a red arrow for orientation purposes.

An accelerometer (Model 352A92, PCB Piezotronics) was used to measure the acceleration of the PZT where droplets were vibrated. This was done using a dynamic signal analyzer (Model 50-21, SigLab) to acquire the frequency response of the system. The PZT was vibrated with swept sine waves (1 to 26 kHz with amplitudes of 50 to 350 volts over a duration of 50 seconds) and the dynamic analyzer computes the cross-spectrum of the driving (swept sine wave) and response (accelerometer) signals to generate the frequency response.

The repeatability of the frequency response measurement system is key to produce repeatable and reliable wetting data. This was assessed by performing consecutive (one immediately after another) frequency response measurements (described in the previous paragraph) to determine if any change in the response was occurring over time. Figure 52 shows the frequency response of the top surface of the PZT resulting from a 300 volt swept sine wave from 16 to 26 kHz. There is good agreement between all four of the consecutive tests that were performed, and only slight variation in acceleration magnitude is noticeable above 20 kHz. This suggests that there will be negligible difference in acceleration and frequency between each

individual wetting test, and pacifies a concern about charging of the piezoelectric crystals that could be a possible source of a difference if one was present.

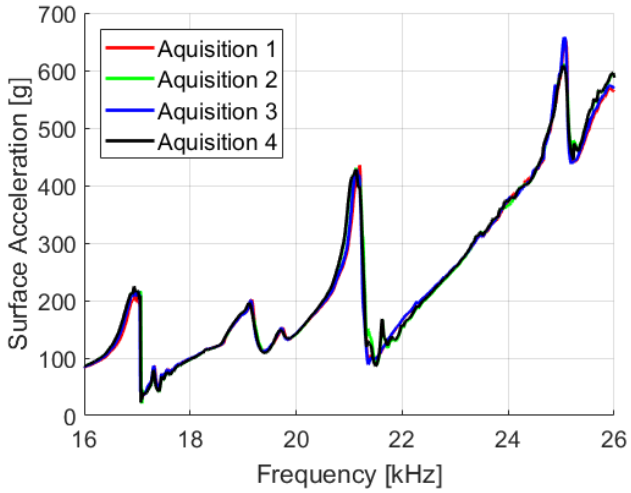

Figure 52. Frequency response of the top surface of the PZT resulting from a 300 volt swept sine wave from 16 to 26 kHz. Each acquisition plotted in the figure is a separate measurement.

Because of the intrusive nature of the frequency response measurement, extra care needs to be taken to assure accurate results. To measure the frequency response, an accelerometer is fixed to the surface with adhesive to take the measurements. The mass of the accelerometer, while small, is still many times the mass of droplets in the testing range. It could be possible that this added mass of the accelerometer could shift the frequency of the resonance peaks or change the magnitude of these peaks from wetting tests and frequency response measurements. To determine if this was the case, frequency response measurements were obtained using an accelerometer as explained previously. Then, the mass of the accelerometer was doubled by fixing extra mass to the top of the accelerometer with adhesive and frequency response measurements were obtained again with doubled mass. These data sets were then compared to

determine if the mass of the accelerometer had a noticeable effect on the frequency response of the surface.

Figure 53 shows frequency response measurements of the top surface of the PZT. The response to a 100 volt sine wave is shown as a red line, and the response to the same 100 volt sine wave when the mass of the accelerometer is doubled is shown as a green line. The response to a 300 volt sine wave is shown as a blue line, and the response to the same 300 volt sine wave when the mass of the accelerometer is doubled is shown as a black line. Comparison of both 100 volt responses, and both 300 volt responses yields good agreement. The added mass in both cases seems to lower the frequency of the peak as well as lower the magnitude of the acceleration, but it seems insignificant enough that data collected from wetting tests would not require any frequency shift for processing.

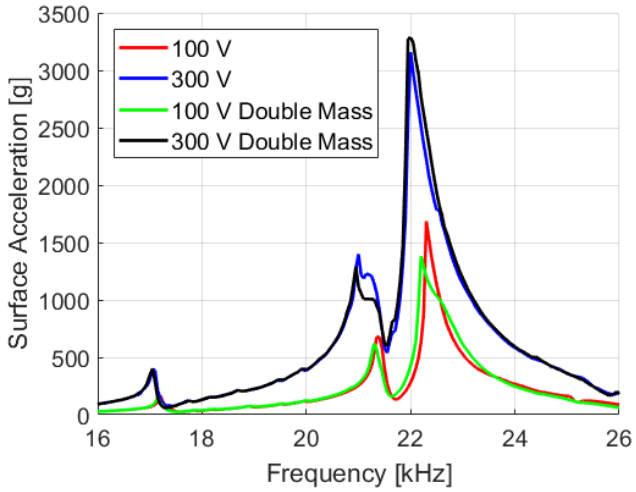

Figure 53. Frequency response measurements of the top surface of the PZT. The response to a 100 volt sine wave is shown as a red line, and in green when the mass of the accelerometer is doubled. The response to a 300 volt sine wave is shown as a blue line, and in black when the mass of the accelerometer is doubled.

5.4 Results and Discussion

Figure 54 shows how the droplet appearance and contact angle change with frequency. As the frequency is increased, the contact angle decreases. Over the sweeping frequency range (1 to 26 kHz), droplets do not oscillate in the form of volume modes, but vivisible traveling ripples form on the surface of droplets while spreading begins to occur at frequencies near 22 kHz (Figure 54, b and c).

The wetting transitions occur abruptly (as seen in Figure 55). Once vibration ceases the contact angle recovers slightly, but it maintains a new, lower equilibrium contact angle. However, when the droplet is removed with a burst of compressed air, the surface is dried, and a new droplet is deposited on the surface, the subsequent droplet returns to the original equilibrium droplet state to within 4°. Wetting transitions occur over a range of vibration amplitude and droplet volume, but the magnitude of the transition varies slightly depending on certain factors.

The amplitude of the sine wave that drives the PZT affects the wetting transition of droplets vibrated on the hydrophobic glass slides. As the voltage is increased, and droplet volume kept constant, droplets would transition to a lower contact angle. Figure 55 shows contact angle data for droplets of 30 µL that were vibrated with varying amplitude swept sine waves from 1 to 26 kHz. At excitation frequencies near 22 kHz, droplets vibrated with a 200 volt sine wave transitioned to the lowest contact angle, while droplets vibrated with a 50 volt sine wave had the least change in contact angle during the transition. After vibration was ceased, droplets did not return to their equilibrium state. At higher voltages, there is a less substantial contact angle transition at a lower frequency (~14.5 kHz).

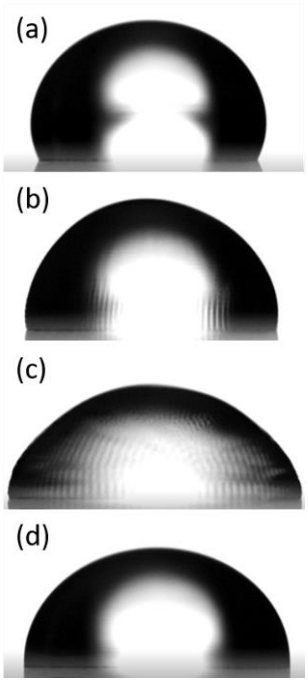

Figure 54. Droplet wetting transition: The droplet placed on the surface in its original equilibrium state (a) is vibrated with a sine wave frequency sweep from 1 to 26 kHz. If the initiation of the wetting transition (b) is taken as t = 0 seconds, the droplet is spread out (c) at 0.3 seconds, and comes to rest at its new equilibrium state (d) once vibration is ceased.

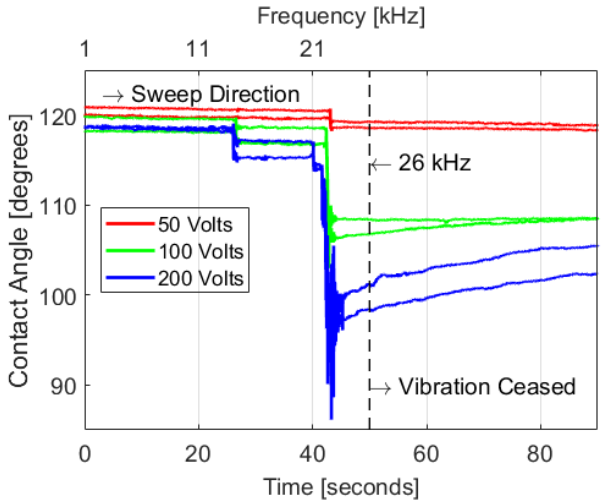

Figure 55. Excitation frequency plotted vs. contact angle for droplets of 30 µL and varying amplitude of excitation voltage as excitation frequency is swept from 1 to 26 kHz and then ceased. The vertical dashed line represents the cessation of vibration.

By keeping droplet volume (and thus droplet shape) constant, it would be expected that wetting – if caused or influenced by droplet mode excitations – would occur at the same excitation frequency even if the excitation amplitude was varied. The resonance frequencies for volume modes of sessile droplets vibrated vertically on a flat plate with dependence on contact angle (Equation (1)) is known analytically [83].

$$f_n = \frac{\pi}{2}\left(\frac{n^3\gamma(cos^3\theta - 3cos\theta + 2)}{24m\theta^3}\right)^{1/2} \tag{25}$$

It could be possible, and has been the case in prior research, that droplet volume resonance modes cause contact angle fluctuations that generate large contact line forces which in turn cause de-pinning of the contact line and its subsequent motion [70]. However, no evidence was seen for volume vibration modes in the droplets during transitions. High speed imaging of wetting transitions shed some light on what occurs at speeds too fast for the eye to see. It is clear that in the case of these high frequency transitions, surface modes, rather than volume modes are present (Figure 56).

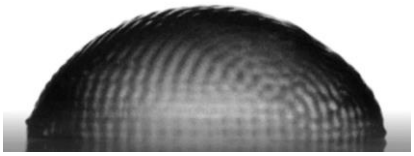

Figure 56. Single image of a droplet undergoing a wetting transition at high speed. The droplet maintains its hemispherical shape, but patterns of surface waves are present along its surface.

Volume resonance modes for droplets sized in the tens of microliters are on the order of 10 – 100 Hz, but with wetting transitions occurring in the kilohertz range, volume modes can most likely

be ruled out, and this hypothesis would be verified if different volume droplets wet at the same frequency.

Varying droplet volume has a similar affect to varying the amplitude of vibration. Under the same excitation amplitude, larger volume droplets transition to a lower contact angle. Figure 57 shows contact angle data for 10, 20, and 30 µL droplets that were vibrated with a 200 volt swept sine wave from 1 to 26 kHz. The transition frequency is very similar for all droplet volumes with the primary transition occurring near 22 kHz. Larger volume droplets transition at a lower frequency (~14.5 kHz), but to a lesser degree than the transition near 22 kHz. Droplet volume did play a role in the magnitude of the change with 30 µL droplets transitioning to the lowest contact angle, while the 10 µL droplets had the least change in contact angle during the transition. Again, after vibration was ceased, droplets did not return to their original equilibrium state.

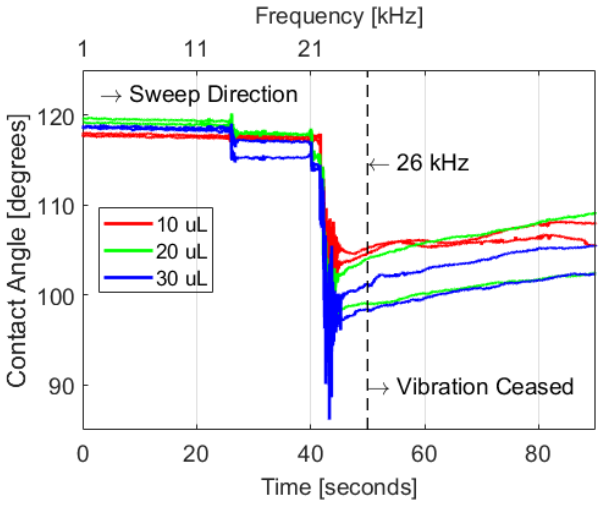

Figure 57. Excitation frequency plotted vs. contact angle for droplets of varying volume and a constant 200 volt amplitude excitation voltage as excitation frequency is swept from 1 to 26 kHz and then ceased. The vertical dashed line represents cessation of vibration.

Larger droplets clearly undergo a more drastic wetting change. This may be explained by the presence of longer contact lines for larger volume droplets. An increase in contact line length for similar amplitude surface ripples would increase the force on the contact line caused by the oscillating contact angle. This could enhance de-pinning and allow a larger volume droplet to spread more easily. However, the wetting transition does not seem to be dependent on the droplet volume resonance modes because 10, 20, and 30 µL droplets would all transition at different excitation frequencies.

While the resonance of the liquid does not seem to have any influence on the wetting transitions, the resonance of the surface in which the droplet vibrates on may play a crucial role. When comparing the wetting transition frequency for different droplet volumes to the frequency response of the surface, resonance peaks coincide with the transitions. Figure 58 shows 10, 20, and 30 µL droplets that were vibrated with a 200 volt swept sine wave from 1 to 26 kHz and compares this to the frequency response of the same swept sine excitation. The largest magnitude peak of acceleration at 22 kHz corresponds to the same 22 kHz wetting frequency. A smaller magnitude peak at 14.5 kHz corresponds to a partial wetting transition that occurs for the larger volume droplets in this case. Because wetting transitions coincide with resonance peaks of the solid surface, the higher accelerations and displacements of the solid surface that occur at resonance are likely to be the governing effect behind the transitions that are being studied in this case. Another interesting observation is that the wetting transitions occur at frequencies on the rising edge of the resonance peak, which would suggest that solid surface resonance may not actually be necessary to transition a droplet, but once a threshold of acceleration or vibration amplitude is reached, the transition may take place.

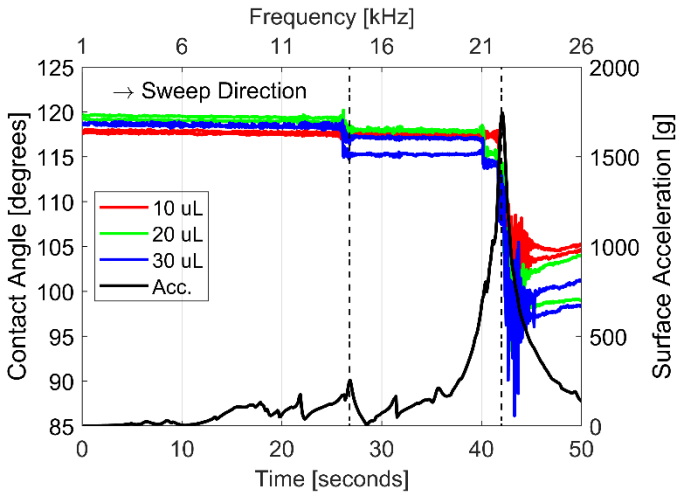

Figure 58. Data from Figure 57 plotted vs. the frequency response of the surface excited with a 200 volt swept sine wave at the location where droplets are placed for testing. Vertical dashed lines are used to show that peaks of surface acceleration coincide with wetting transitions.

Wetting transitions occur in the same manner when sweeping frequencies from high to low. Droplets vibrated with a swept sine wave from 26 to 1 kHz transitioned at 23.5 kHz and followed the same trends noted in frequency sweeps from 1 to 26 kHz. The only difference was the slightly different transition frequency, which can be attributed to the rising edge of the acceleration peak occurring on the higher frequency side of the frequency response peak. The lower frequency transition that sometimes occurred at 14.5 kHz when sweeping excitation frequencies from 1 to 26 kHz did not occur when sweeping from 26 to 1 kHz. When sweeping with this excitation pattern, the larger magnitude acceleration peak at 22 kHz is encountered initially and transitions the droplet to an equilibrium state that cannot be lowered further when it encounters lower magnitude accelerations at other harmonic frequencies.

The advancing and receding angles of de-ionized water on FluoroSyl 3750 are 118 and 88 degrees respectively, and this specifies the CAH (range of meta-stable contact angles) of the surface. It appears that wetting transitions that occur were only able to lower the contact angle of droplets to the calculated receding angle.

Much additional work needs to be done to better understand the effects of high frequency vibration on wetting of droplets. Examination of the high-speed, micro-scale effects that occur during wetting transitions would help to understand the dynamics of droplet oscillations that may be causing the transitions to occur. Varying droplet density without changing surface tension (by using a salt-water solution) in testing would help to understand whether the enhanced wetting transitions are caused by increased inertial forces, or if it is solely caused by a size effect such as increased contact line length. Transducers with different frequency responses will be used in testing to study whether the frequency at which wetting transitions occur can be controlled.

5.5 Conclusion

Forced wetting of water droplets was accomplished using surface vibrations to excite droplets on a hydrophobic surface over a range of high frequencies. Droplet volume and excitation amplitude both affect the amount of contact angle change when a transition occurs, but the surface acceleration or displacement of the solid surface seems to govern the frequency at which the transitions take place. More work needs to be done to isolate and study these variables to better understand the phenomena behind the wetting transitions.

CHAPTER 6:

DROPLET SPREADING WITH ULTRASONIC VIBRATION

6.1 Abstract

In the prior chapter, we observed a decrease in apparent contact angle when droplets were excited with high frequency vibration (from 1-26 kHz). Now, this phenomenon is investigated to evaluate the conditions under which a droplet's contact line moves when ultrasonically vibrated. In order to reduce imaging measurement errors, droplet diameter change is measured rather than contact angle. Droplets of various fluids with volumes ranging from 2 to 70 µL are vibrated on a hydrophobic-coated (FluoroSyl) glass substrate fixed to a piezoelectric transducer with a ramping stepped sine wave at various frequencies between 21 and 42 kHz. Droplets of all tested liquids begin to spread near a consistent threshold value of surface acceleration around 20,000 m/s^2. The extent of spreading is proportional to the instantaneous acceleration of the surface of the vibrating transducer. The relative diameter increase of droplets for a specific level of surface acceleration appears to be independent of volume, but seems to differ slightly between liquids proportionally to the liquid-air surface tension. A very similar spreading response is observed for droplets when vibrated using an alternate transducer with different frequency response characteristics. Increasing the fluid viscosity smoothens the spreading response slightly, but does not affect the diameter change directly.

6.2 Introduction

In prior work discussed in the previous chapter, liquid droplets were vibrated on a smooth hydrophobic surface with a constant amplitude sine wave signal applied to a vibrating transducer. Vibration frequencies between 1 and 26 kHz were swept, causing droplets to spread out on the vibrating surface. These wetting transitions were found to occur at local peaks in the amplitude of vibration corresponding to modal vibrations of the transducer (Figure 58). However, the physical change in droplet shape was not well understood. The spreading of droplets was perceived as a change in the measured contact angle, but unlike prior work studying the spreading induced by low frequency vibrations [32, 56, 65], spreading due to ultrasonic vibration does not appear to be a result of contact angle oscillation in excess of the advancing angle. This is unless the contact angle oscillations occur in a very short length and time scale not apparent with the equipment available during this study. The work in the previous chapter showed that it is unlikely for the wetting transitions to be caused by excitation of droplet vibration modes due to the occurrence of wetting transitions at similar vibration frequencies for droplets of varying volumes. However, it is possible that transitions could have been caused by droplet capillary-modes or simply by reaching a threshold acceleration level that causes a droplet to flatten.

To better study and characterize the wetting effects of ultrasonic vibration and hopefully simplify the analysis, droplet contact line diameter was tracked instead of apparent contact angle. Revisiting the work in the previous chapter, it is apparent that the relative diameter change (D/D_i) also seemed to be related to the droplet volume (Figure 59) and driving signal voltage (Figure 60), as it was when plotted against contact angle change. However, the spreading of droplets transpired over a short period of time (~1 second) while sweeping a broad frequency

range, and occurred near resonances where there are larger uncertainties in the magnitude of the acceleration produced by the vibration. For these reasons mainly, it was important to use more precise experimental methods.

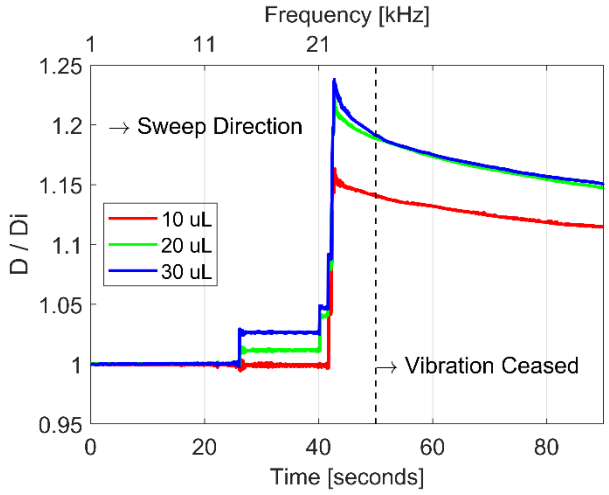

Figure 59. Data from Figure 57 for different volume droplets subjected to a frequency sweep plotted as the ratio of droplet diameter to initial droplet diameter.

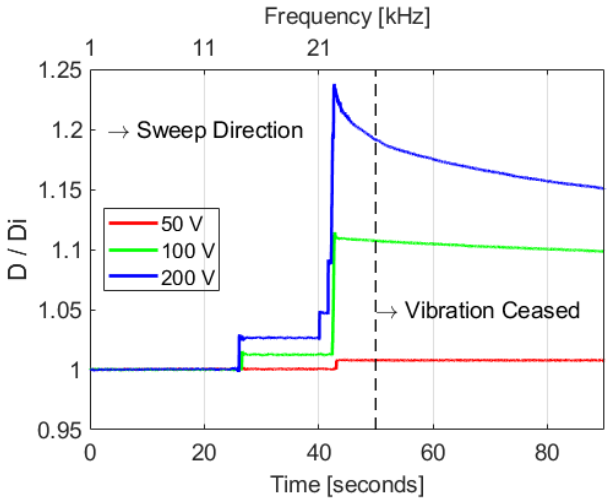

Figure 60. Data from Figure 55 for 30 µL droplets subjected to a swept sine wave at varying voltage. This data is plotted as the ratio of droplet diameter to initial droplet diameter.

To better understand the cause of the wetting effects, the problem had to be simplified as much as possible, and the variables that influence the dynamics of ultrasonically vibrated droplets needed to be characterized. In this chapter, revised experimentation of droplet spreading is investigated. The vibration of droplets is controlled more precisely by varying the excitation amplitude signal (voltage) driving the piezoelectric transducer and not by tuning the vibration frequency. This will allow more accurate measurement of surface acceleration levels using an accelerometer to better study the effects of surface acceleration on droplet spreading. Different piezoelectric transducers are used in testing to attempt to rule out vibration frequency dependencies. Lastly, a larger range of droplet volumes, as well as different liquids are used to study the geometrical effects more thoroughly and investigate the impact of material properties on the effect of spreading using ultrasonic surface vibration.

6.3 Experimental Methods

Ultrasonic droplet spreading was studied by pumping droplets of liquid ranging from 2 to 70 µL with a syringe pump (Legato 180, KD Scientific) on to glass substrates coated with a hydrophobic coating (FluoroSyl). The glass substrates were coated in FluoroSyl by the methods outlined in chapter 4. Glass substrates were then mounted on the cap of the transducer with adhesive using the recommended method as described in chapter 3. A sine wave signal with an amplitude of 1 V and a user-variable frequency is produced by a function generator (33250A, Agilent), and input to a signal conditioner/digital-analog converter (DAQ) (USB-6343, LabVIEW). A trigger switch initiates the ramping of the driving signal amplitude (voltage) with a step function gain of 0.05 V/second while simultaneously initiating image acquisition. The ramped signal is output from the DAQ into a high frequency amplifier (PZD350A, Trek) with a

gain of 100x, and then to the vibrating transducer (Figure 61). The resulting sine wave signal that powers the transducer has a stepped amplitude that increases from 0 to 300 V in 5 V increments over 60 seconds (Figure 62).

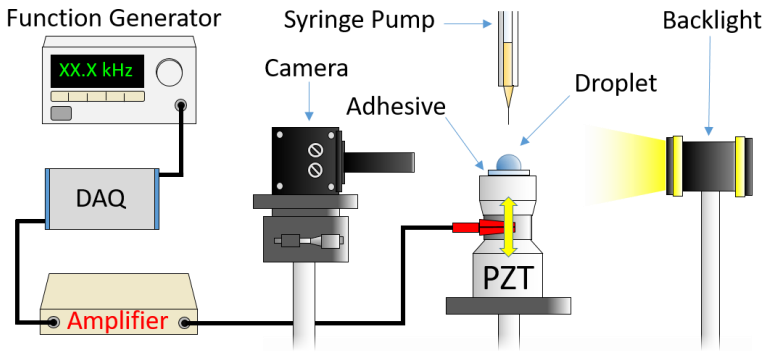

Figure 61. Droplets are vibrated via an ultrasonic transducer with a stepped sine wave signal of increasing amplitude (5 V/second) from 0 to 300 V and user-variable frequency. Backlit images of vibrating droplets are recorded at 30 frames per second.

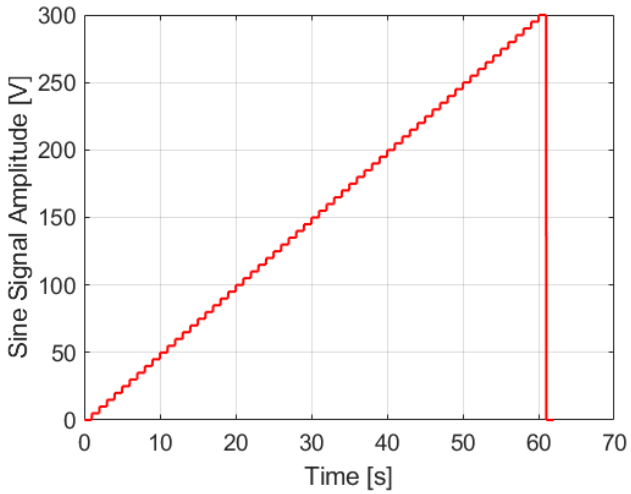

Figure 62. Amplitude of sine signal driving the piezoelectric transducer over duration of a single droplet spreading test. The droplet is not vibrated for 1 second at the beginning and end of each test.

Droplets are imaged at 30 frames per second with a high speed camera (NX8-S2, IDT Vision) using a backlight to produce a high-contrast droplet surface profile. Droplets are initially

imaged for 1 second with no excitation at the beginning of each individual test. At 1 second, the amplitude of the sine wave driving the piezoelectric transducer begins to ramp. As the amplitude of the signal powering the transducer increases, droplets can eventually begin to spread until vibration is ceased at 61 seconds into the test. At this point, droplets that spread out during excitation remain in a spread state with a larger contact line diameter than the original droplet. The droplet retracts to a degree if the droplet contact angle is lower than the receding angle of the contact angle hysteresis range for the liquid-surface combination. A MATLAB edge detection algorithm (similar to the algorithm used in the previous work) was used to post-process images by tracking the droplet's diameter at the contact line. This was repeated with a new droplet for each volume tested at a given frequency. Tests were conducted across a range of ultrasonic vibration frequencies from 21 - 42 kHz with the same ultrasonic transducer unless otherwise noted. After sufficient droplet spreading data was taken on one substrate, the glass substrate was cleaned and an accelerometer was fixed to the surface with adhesive (following the recommended method outlined in chapter 4). The frequency response of the surface was measured with a dynamic analyzer (as outlined in chapter 4) to characterize the vibration intensity at voltages of 50, 100, 150, 200, 250, and 300 V in precisely the spot where droplets were vibrated during testing. Acceleration at intermediate voltages were estimated by linear interpolation between the measured values at a specific frequency. Four different liquids were used throughout testing: deionized water, a 3:5 volume ratio water/glycerol mixture, ethylene glycol, and propylene glycol. Using multiple liquids allowed the investigation of effects that may be due to the varying material properties. The vibration frequencies, droplet volumes, liquid type, and piezoelectric transducer used in testing throughout this chapter to investigate the spreading effects of ultrasonic vibration are recorded in Table 4 through Table 8.

Table 4. Droplet spreading test parameters for deionized water.

Liquid	Droplet Volume [µL]	Frequency [kHz]	PZT
Deionized Water	10, 20, 30, 50, 70	24.0	1
Deionized Water	10, 20, 30, 50, 70	25.2	1
Deionized Water	10, 20, 30, 50, 70	26.0	1
Deionized Water	10, 20, 30, 50, 70	27.4	1
Deionized Water	10, 20, 30, 50, 70	28.2	1
Deionized Water	10, 20, 30, 50, 70	28.8	1
Deionized Water	10, 20, 30, 50, 70	29.4	1
Deionized Water	10, 20, 30, 50, 70	30.2	1
Deionized Water	10, 20, 30, 50, 70	30.6	1
Deionized Water	10, 20, 30, 50, 70	31.0	1
Deionized Water	10, 20, 30, 50, 70	31.4	1
Deionized Water	10, 20, 30, 50, 70	31.8	1
Deionized Water	10, 20, 30, 50, 70	32.2	1
Deionized Water	10, 20, 30, 50, 70	32.6	1
Deionized Water	10, 20, 30, 50, 70	33.2	1
Deionized Water	10, 20, 30, 50, 70	34.0	1
Deionized Water	10, 20, 30, 50, 70	34.8	1
Deionized Water	10, 20, 30, 50, 70	36.0	1
Deionized Water	10, 20, 30, 50, 70	37.6	1
Deionized Water	10, 20, 30, 50, 70	38.8	1
Deionized Water	10, 20, 30, 50, 70	41.0	1
Deionized Water	2, 4, 6, 8, 10	21.6	1
Deionized Water	2, 4, 6, 8, 10	24.2	1
Deionized Water	2, 4, 6, 8, 10	26.8	1
Deionized Water	2, 4, 6, 8, 10	27.4	1
Deionized Water	2, 4, 6, 8, 10	28.0	1
Deionized Water	2, 4, 6, 8, 10	28.6	1
Deionized Water	2, 4, 6, 8, 10	29.0	1
Deionized Water	2, 4, 6, 8, 10	29.4	1
Deionized Water	2, 4, 6, 8, 10	29.8	1
Deionized Water	2, 4, 6, 8, 10	30.2	1
Deionized Water	2, 4, 6, 8, 10	30.6	1
Deionized Water	2, 4, 6, 8, 10	31.0	1
Deionized Water	2, 4, 6, 8, 10	31.6	1
Deionized Water	2, 4, 6, 8, 10	32.2	1
Deionized Water	2, 4, 6, 8, 10	35.4	1
Deionized Water	2, 4, 6, 8, 10	38.6	1
Deionized Water	2, 4, 6, 8, 10	42.0	1

Table 5. Droplet spreading test parameters for 3:5 volume ratio water/glycerol mixture.

Liquid	Droplet Volume [µL]	Frequency [kHz]	PZT
3:5 Water/Glycerol	10, 30, 50	24.0	1
3:5 Water/Glycerol	10, 30, 50	24.8	1
3:5 Water/Glycerol	10, 30, 50	25.6	1
3:5 Water/Glycerol	10, 30, 50	26.0	1
3:5 Water/Glycerol	10, 30, 50	26.6	1
3:5 Water/Glycerol	10, 30, 50	27.0	1
3:5 Water/Glycerol	10, 30, 50	30.6	1
3:5 Water/Glycerol	10, 30, 50	28.0	1
3:5 Water/Glycerol	10, 30, 50	28.8	1
3:5 Water/Glycerol	10, 30, 50	29.4	1
3:5 Water/Glycerol	10, 30, 50	29.8	1
3:5 Water/Glycerol	10, 30, 50	30.4	1
3:5 Water/Glycerol	10, 30, 50	30.8	1
3:5 Water/Glycerol	10, 30, 50	31.2	1
3:5 Water/Glycerol	10, 30, 50	32.0	1
3:5 Water/Glycerol	10, 30, 50	32.6	1
3:5 Water/Glycerol	10, 30, 50	33.2	1
3:5 Water/Glycerol	10, 30, 50	34.0	1

Table 6. Droplet spreading test parameters for ethylene glycol.

Liquid	Droplet Volume [µL]	Frequency [kHz]	PZT
Ethylene Glycol	10, 20, 30, 50. 70	24.6	1
Ethylene Glycol	10, 20, 30, 50. 70	26.8	1
Ethylene Glycol	10, 20, 30, 50. 70	28.4	1
Ethylene Glycol	10, 20, 30, 50. 70	29.0	1
Ethylene Glycol	10, 20, 30, 50. 70	29.4	1
Ethylene Glycol	10, 20, 30, 50. 70	29.6	1
Ethylene Glycol	10, 20, 30, 50. 70	29.8	1
Ethylene Glycol	10, 20, 30, 50. 70	30.0	1
Ethylene Glycol	10, 20, 30, 50. 70	30.4	1
Ethylene Glycol	10, 20, 30, 50. 70	31.2	1
Ethylene Glycol	10, 20, 30, 50. 70	33.2	1
Ethylene Glycol	10, 20, 30, 50. 70	35.6	1
Ethylene Glycol	10, 20, 30, 50. 70	38.8	1
Ethylene Glycol	10, 20, 30, 50. 70	41.0	1

Table 7. Droplet spreading test parameters for propylene glycol.

Liquid	Droplet Volume [µL]	Frequency [kHz]	PZT
Propylene Glycol	10, 20, 30, 50. 70	24.8	1
Propylene Glycol	10, 20, 30, 50. 70	27.2	1
Propylene Glycol	10, 20, 30, 50. 70	28.6	1
Propylene Glycol	10, 20, 30, 50. 70	29.0	1
Propylene Glycol	10, 20, 30, 50. 70	29.4	1
Propylene Glycol	10, 20, 30, 50. 70	29.8	1
Propylene Glycol	10, 20, 30, 50. 70	30.2	1
Propylene Glycol	10, 20, 30, 50. 70	30.6	1
Propylene Glycol	10, 20, 30, 50. 70	31.2	1
Propylene Glycol	10, 20, 30, 50. 70	33.4	1
Propylene Glycol	10, 20, 30, 50. 70	36.2	1
Propylene Glycol	10, 20, 30, 50. 70	38.8	1
Propylene Glycol	10, 20, 30, 50. 70	42.0	1

Table 8. Droplet spreading test parameters for deionized water vibrated with an alternate PZT.

Liquid	Droplet Volume [µL]	Frequency [kHz]	PZT
Deionized Water	10, 20, 30, 50, 70	24.4	2
Deionized Water	10, 20, 30, 50, 70	25.8	2
Deionized Water	10, 20, 30, 50, 70	27.0	2
Deionized Water	10, 20, 30, 50, 70	28.2	2
Deionized Water	10, 20, 30, 50, 70	29.0	2
Deionized Water	10, 20, 30, 50, 70	29.8	2
Deionized Water	10, 20, 30, 50, 70	30.6	2
Deionized Water	10, 20, 30, 50, 70	32.0	2
Deionized Water	10, 20, 30, 50, 70	33.0	2
Deionized Water	10, 20, 30, 50, 70	33.8	2
Deionized Water	30, 50, 70	34.6	2
Deionized Water	10, 20, 30, 50, 70	36.0	2
Deionized Water	10, 20, 30, 50, 70	37.2	2
Deionized Water	10, 20, 30, 50, 70	38.4	2
Deionized Water	10, 20, 30, 50, 70	39.6	2
Deionized Water	10, 20, 30, 50, 70	40.6	2

Prior to the discussion of results, the measurement certainty using the methods and equipment described above is first addressed.

6.4 Measurement Error

Despite all the progress made in chapter 3 to improve the repeatability of the measurements, it is still possible to have significant variation in experimental data given the complexity of this problem. Measurement error in droplet spreading testing is manifest in one of two ways: error in droplet diameter measurement, and error in acceleration measurement. Error in droplet diameter measurement primarily comes from the digital nature of image processing. Camera resolution defines how accurately the droplet is represented as a digital image. In this case, pixels on the image sensor of the high-speed camera are square with a side length of 8.6 µm and the optical magnification is 1:1, so 8.6 µm would be the approximate error introduced when measuring droplet diameter. Droplet diameters used in testing are on the scale of millimeters, while the droplet diameter measurement error is on the scale of micrometers. This would then result in an error of 0.1% when measuring the relative diameter change, or the ratio of instantaneous diameter to the initial diameter (D/D_i). Droplet diameter measurement can also be affected if the droplet moves toward or away from imaging equipment, as well as blur the profile of the droplet. However, in this case, if the droplet moves significantly enough to change the size of the droplet, the edges are blurred and the edge detection algorithm cannot calculate the diameter properly. For these reasons, the measurement of droplet diameter are assumed to be relatively errorless and ignored.

Acceleration measurement is a significant cause for data inaccuracies. This error can be attributed to various aspects of the measurement methods. The shortcomings of accelerometer measurement for characterization of ultrasonic vibration are discussed in depth in chapter 3, but are due to the inherent transducer accuracy (greater than 10% error in the frequency range used). The accelerometer data sheet only reports a measurement error for frequencies up to 20 kHz, but

experimental data was taken from testing in the 30 - 40 kHz range where higher levels of surface acceleration were generated by the ultrasonic transducers used in testing. For this reason, it could be assumed that the error could be larger than the ±10% documented in the data sheet. However, the best case scenario of ±10% error in measuring acceleration using the accelerometer is assumed for the entire testing frequency range.

Acceleration measurement error can also be introduced through adhesive cure changes or unnoticed delamination of coupled surfaces. However, as noted previously in Chapter 3, if ample time was given for adhesives to cure, the variation in acceleration measurements over time can be ignored.

Due to vibration mode shapes of the testing surfaces at specific frequencies, droplets may move around during testing. Because surface acceleration is measured in one location (where droplets are initially placed for testing) with an accelerometer, a droplet that moves along the surface will be subject to a different level of acceleration than that which is measured. As previously determined in Chapter 3, the spatial variation can result in large acceleration measurement discrepancies (20% difference between the center and edge as measured in Figure 34) across the top surface of the piezoelectric transducer. Testing done at frequencies in which droplets moved along the surface significantly were not included in final data sets, however, droplets vary in size throughout testing and also move slightly and spread out when acceleration levels are high enough. This results in different droplet footprints on the vibrating surface, and while the spatial difference is not the same as in Figure 33, a 5% acceleration measurement error is assumed due to spatial variation in the frequency response.

During droplet testing, the driving voltage to the piezoelectric transducer is increased in steps of 0.5 V per second from 0 to 300 V. Each driving voltage corresponds to a unique surface

acceleration level that vibrates the droplet at a given frequency during testing. After droplet testing, the accelerometer was mounted to the testing surface to measure the surface acceleration, but was only done so at 50 V increments (50, 100, 150, 200, 250, 300 V). In order to determine the acceleration between the increments, linear interpolation of the frequency response was used at each vibration frequency. This could however introduce acceleration measurement error especially near resonance frequencies where the response is non-linear. Figure 63 shows an example of both linear and non-linear frequency response. The blue shaded region shows a non-linear response in surface acceleration, where a 50 V excitation generates 50% of the total acceleration level that is produced by a 300 V excitation. In contrast, the red shaded region shows a linear response in surface acceleration, where the increase in excitation voltage results in a very uniform increase in surface acceleration.

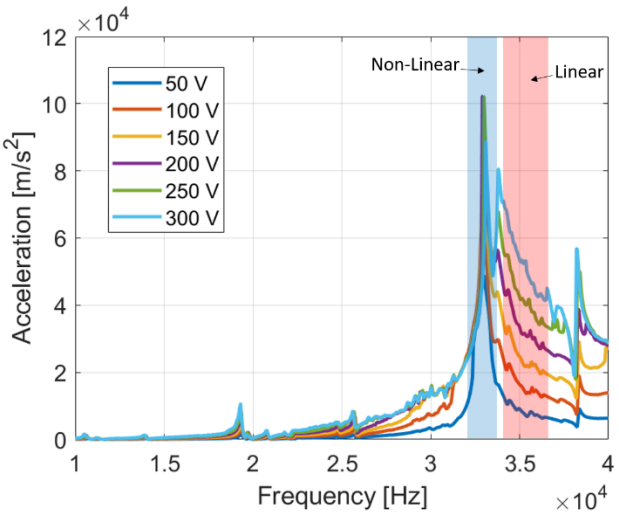

Figure 63. Linear and non-linear regions of acceleration levels for a frequency response measurement. In the non-linear region, 50% of the total acceleration measured with a 300 V excitation was achieved with a 50 V excitation. In contrast, the linear region shows a very uniform acceleration increase as the excitation voltage is increased.

Non-linearity error is difficult to quantify because of the difference in response behavior at different frequencies and excitation voltages, but could be more than 10% if the acceleration increase is non-linear. In this case, a 5% measurement error is conservatively considered for the entire data set.

A summary of the sources for the acceleration measurement error are recorded in Table 9 below. Taking in to account all the sources of error, a conservative estimation of error for measuring acceleration with an accelerometer is ± 20%. This is a significant amount of error, so it will be considered throughout the discussion in the next section.

Table 9. Summary of acceleration measurement error sources.

Error Source	Error Contribution
Accelerometer Measurement	±10%
Spatial Measurement Variation	±5%
Acceleration Interpolation	±5%

6.5 Results and Discussion

6.5.1 Droplet Spreading with Ultrasonic Vibration

During testing, as the driving voltage for the signal powering the vibrating transducer increases, waves become visible on the surface of a droplet (Figure 64). The amplitude of the surface waves increases as the magnitude of the vibration increases, and eventually a droplet will begin to spread out on the surface.

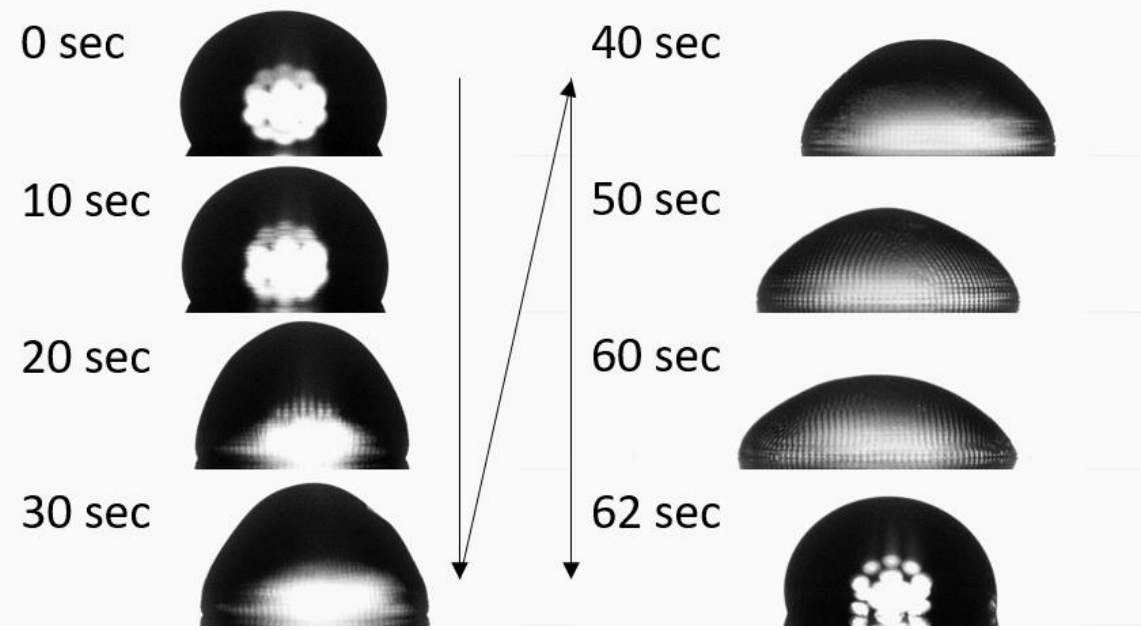

Figure 64. A 20 µL droplet is initially at rest at 0 seconds. The droplet is then excited with a 31 kHz stepped sine wave signal that started ramping at one second. The droplet spreads out as the driving signal increases, until vibration is ceased at 61 seconds, and the droplet returns to an equilibrium position at 62 seconds, but is still in a spread state compared to the initial state.

Droplets continue to spread with increasing signal amplitude until vibration is ceased at 61 seconds. The dimpled pattern on the surface of the droplet seen at 60 seconds in Figure 64 is shown in larger resolution in Figure 65. This image shown was taken at a frame rate of 30 Hz and exposure of 1 µs, so not much can be learned about the dynamics of the waves. However, images taken at frame rates similar to the vibration frequency show capillary waves that appear to originate around the contact line of the droplet and propagate on the surface toward the droplet center.

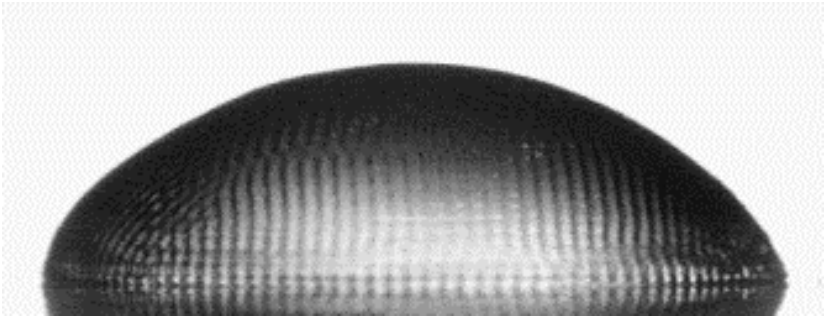

Figure 65. Dimpled surface of a spreading deionized water droplet imaged at 30 Hz with an exposure of 1 µs. Travelling capillary waves appear to form around the contact line of the droplet and propagate on the droplet's surface toward its center.

Spreading of 2 to 70 µL droplets was investigated in order to study the effects over as large a range as possible. Deionized water droplets larger than 10 µL exceed the capillary length, so gravity causes them to flatten rather than assume an idealized spherical cap characteristic of small droplets. At volumes larger than ~70 µL, the liquid volumes no longer appears as droplets, so volumes > 70 microliters are outside the scope of this present study. However, it is helpful to understand the impact of using liquid volumes that produced droplets with a diameter less than the capillary length of the liquid (K). For deionized water, the capillary length is 2.7 mm. Droplets with diameters that exceed the capillary length deviate from a spherical shape due to the effects of gravity squashing the droplet causing it to mushroom on a surface. This effect increases with droplet volume above the capillary length, which includes droplets used in this work (Table 10).

Table 10. Ratio of water droplet diameter on FluoroSyl to the capillary length (2.7 mm).

Droplet Volume [µL]	C.L. Diameter [mm]	C.L. Diameter / K
10	2.5	0.9
20	3.3	1.2
30	4.0	1.5
50	4.8	1.8
70	5.8	2.1

The initial wetting state of larger droplets may vary with droplet size, and small droplet volumes can flatten if the liquid has a low surface tension or high density. This could have effects on the behavior of vibrated droplets and could affect measurement repeatability. Deionized water droplets ranging from 2 to 70 µL were tested to evaluate whether the results differed significantly above and below the capillary length. The ratio of diameter change against the level of surface acceleration for all different combinations of droplet volume and vibration frequency for deionized water droplets is plotted in Figure 66. Droplet spreading is indicated when D/D_i exceeds unity.

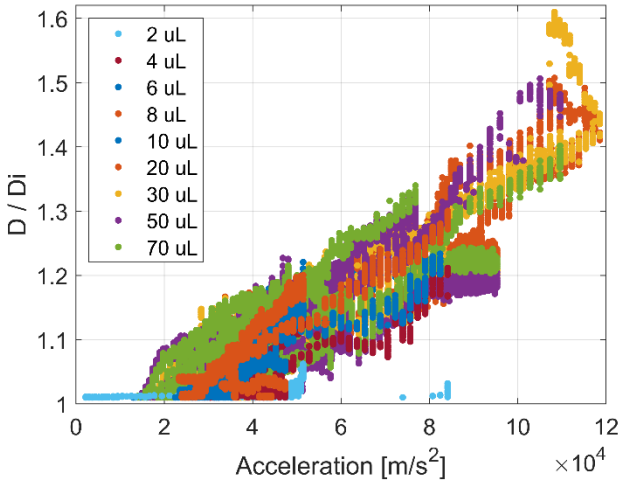

Figure 66. Droplet spreading data plotted as diameter change against surface acceleration for 2 to 70 µL deionized water droplets vibrated between 21 and 41 kHz.

Droplet spreading seems to initiate at a common value of surface acceleration (~20,000 m/s^2), and increases linearly with increasing surface acceleration. In most cases, droplets spread linearly with increasing acceleration while the driving sine wave signal was ramped. No discernable trend due to droplet volume is apparent (across the range of volumes tested), so it seems that ultrasonic spreading is not to be attributed to a threshold inertial body force (as noted

in [90] and other low frequency vibration cases) that would cause the flattening and spreading phenomenon. The lack of body or volume mode vibration is apparent when observing spreading of droplets under high frequency excitation across a wide range of droplet volumes and frequencies. This lack of dependence on droplet oscillation and volume may also suggest that the density of the liquid may not affect the spreading behavior noticeably. Droplets in the lower range of volumes tested (2 and 6 µL) do not appear to spread as much for a given level of surface acceleration. The difference is not significant, but it may suggest that the relationship between droplet spreading and surface acceleration breaks down when surface tension forces are higher than the inertial forces caused by ultrasonic vibration. This does not necessarily suggest a volume dependency, but that higher relative surface tension forces fix droplets in place like an anchor.

The 20% error in acceleration measurement for the data set in Table 4 is represented by the region between the dotted black lines on both sides of the solid black line with x-intercept of 20,000 m/s^2 plotted through the middle of the data in Figure 67.

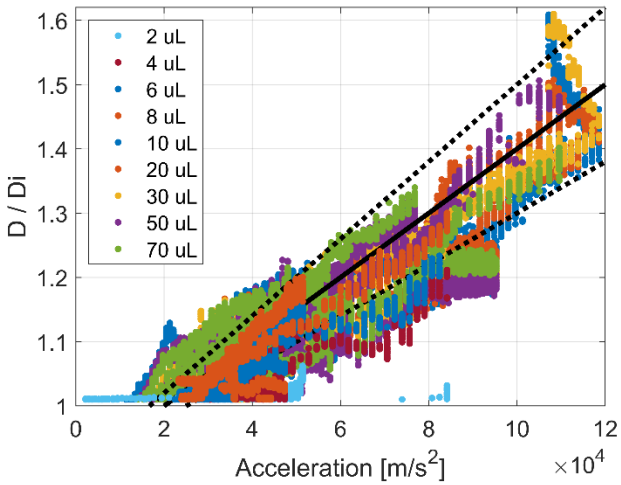

Figure 67. A representation of 20% error in measuring surface acceleration with an accelerometer, plotted as the region bound by the dotted black lines on either side of the solid black line that runs through the center of the data and has an x-intercept of 20,000 m/s^2.

Plotting the acceleration measurement error over top of the data for relative diameter change versus acceleration level demonstrates that most of the data spread could theoretically be due to the accelerometer measurement limitations. Data variation when D/D_i is near unity may be attributed to a stick-slip behavior in droplet spreading that could be caused by local surface features that act as an energy barrier to contact line motion. When acceleration levels are near the threshold for spreading, contact line pinning on surface features could require higher levels of acceleration to supply the energy for the contact line to un-pin from the barrier and advance to the next barrier. This error range will also be useful when comparing other data sets later in this chapter, so it is plotted as a reference case in other figures later on for comparison. Closer examination of droplet spreading behavior may help better understand the phenomena.

6.5.1.1 Droplet Spreading Behavior

Spreading data for each individual droplet can be examined more closely to help draw some conclusions. Figure 68 shows the time history of diameter change of three different volume droplets of deionized water as they are vibrated with increasing intensity at a specific frequency.

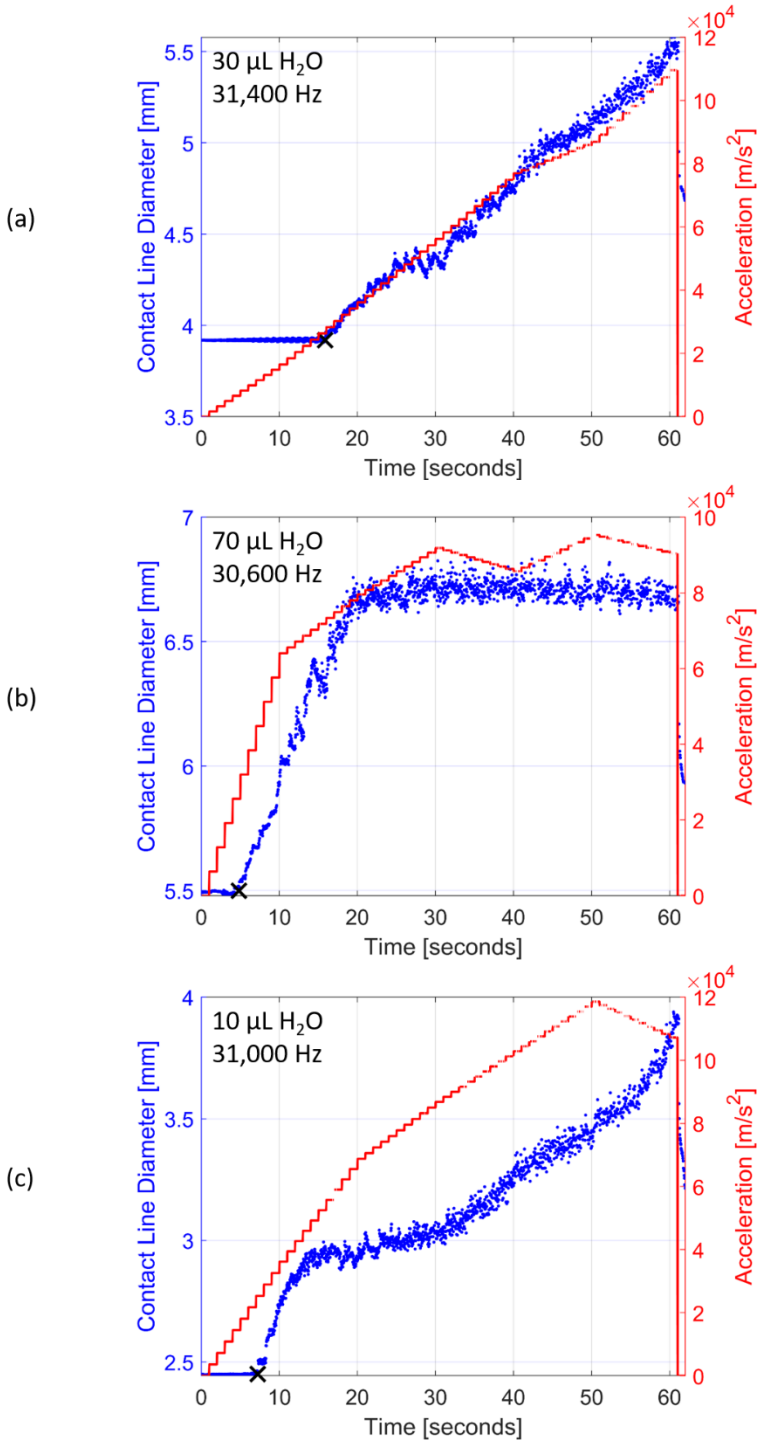

Figure 68. The spreading behavior of individual droplets shows the effect of increasing acceleration on droplet diameter. The droplet volume and vibration frequency are different in each case (a, b, and c). For each different frequency, the resulting acceleration increase is subsequently different with time, however droplets always begin to spread at ~20,000 m/s^2.

Some droplets spread linearly with substrate acceleration (Figure 68, a), and other droplets showed more erratic contact line motion characteristics (Figure 68, b and c). However, the droplet diameter increases with increasing acceleration. This results in a linear relationship between the two quantities when the data is plotted as a group like in Figure 66. While some droplets respond very smoothly (Figure 68 a) to increasing acceleration, others respond erratically—possibly due to contact line pinning (Figure 68 b, c). The erratic response may be due to the nonlinear relationships between voltage and acceleration (Figure 68 b and c). This is especially true near vibration resonances. The frequency response for the piezoelectric transducer used in this case is shown in Figure 69. The resonance frequency of this transducer is near 31 kHz where the surface acceleration levels are highest, but also highly non-linear with excitation voltage. Excluding data points at frequencies near this resonance where the acceleration behavior is non-linear could help to reduce the variation in the data set.

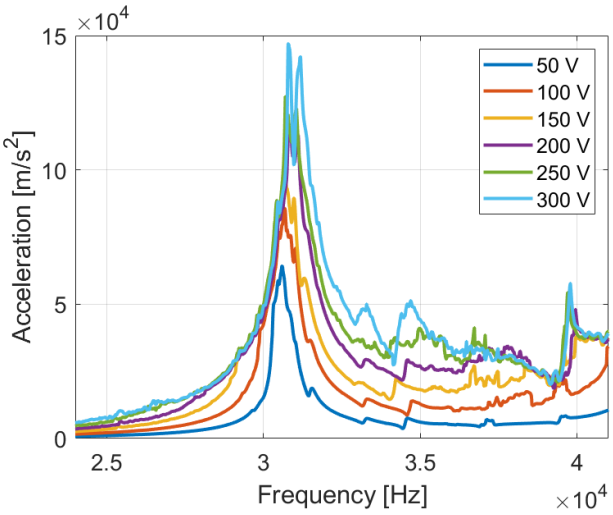

Figure 69. Frequency response of the piezoelectric transducer used in droplet spreading testing. The transducer resonance near 31 kHz results in a non-linear behavior of acceleration increase near those frequencies.

Data collected from frequencies of 30.2, 30.6, and 31.0 kHz, and droplet volumes of 6 µL and less were excluded, while the rest of the data set was replotted in Figure 70. Comparing this plot to Figure 67 shows that by excluding the few vibration frequencies near the transducer resonance, the variation in the data set has become less, and is closer to the bounds of the possible acceleration measurement error prescribed by the dotted black lines at higher levels of acceleration.

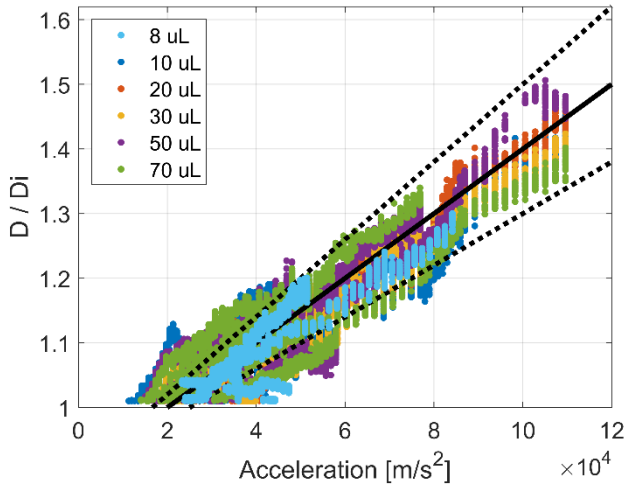

Figure 70. The same data as Figure 67 for droplets of deionized water plotted as diameter change against surface acceleration, except data for the vibration frequencies near the resonance of the transducer (30.2, 30.6, and 31.0 kHz) were excluded. This data is compared to the measurement error (denoted by the dotted black lines) for the reference case.

While acceleration and droplet diameter seem to be linearly related, the rate of increase in acceleration seems to also play a role. By examining droplet spreading behavior at frequencies where the acceleration behavior (or ramp rate) is linear, a few observations can be made. Figure 71 compares the spreading behavior of droplets vibrated at frequencies at different acceleration ramp rates for frequencies where the acceleration response is relatively linear. An acceleration

ramp rate of less than 100 g per second is plotted on the left side of the figure, while an acceleration ramp rate greater than 100 g per second is plotted on the right.

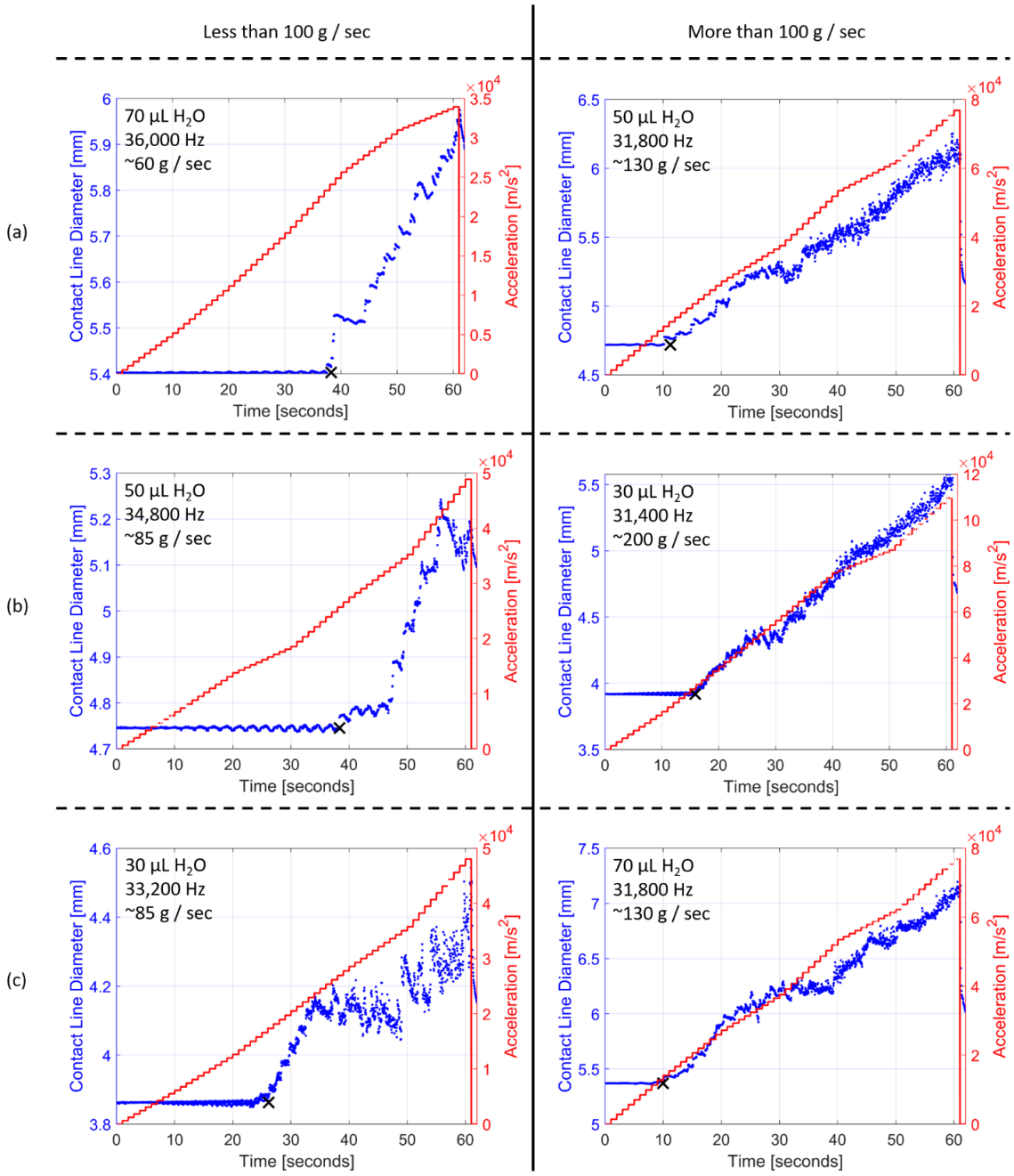

Figure 71. Spreading behavior of different volume droplets vibrated at discrete frequencies with a linear ramp rate of acceleration. A linear increase in acceleration rate significantly lower than 100 g / sec results in stick and slip droplet spreading behavior (left column), while a linear increase in acceleration rate significantly higher than 100 g / sec results in a good linear relationship between spreading and acceleration (right column).

At vibration frequencies of 33.2, 34.8, and 36.0 kHz, the acceleration ramp rate is rather linear as noted by the red line in the plots on the left side of Figure 71. The acceleration ramp rate at each of the three frequencies is also sufficiently less than 100 g per second. Droplet spreading behavior for this low ramp rate appears to be causing a stick-slip contact line motion with slightly more variation in threshold spreading acceleration. In contrast, droplet spreading behavior for a faster, linear ramp in acceleration greater than 100 g per second plotted on the right side of Figure 71 appears to result in a consistent droplet spreading initiation acceleration and the best control of droplet diameter as spreading advances. At vibration frequencies of 31.4, and 31.8 kHz, the acceleration ramp rate is again rather linear as noted by the red line in the plots on the right side of Figure 71. The acceleration ramp rate at both of these frequencies is also sufficiently greater than 100 g per second. This higher, steady rate of linear acceleration may improve the linearity of the behavior between spreading and acceleration increase.

Droplet spreading data for deionized water droplets of 10 to 70 µL at these specific vibration frequencies is plotted below as relative diameter change against surface acceleration for low and high acceleration ramp rates respectively on the left and right side of Figure 72. This figure shows that spreading data for droplets that are vibrated with a linear ramp of acceleration less than 100 g per second have variation outside the bounds of error determined by the dotted black lines, and experience large deviations for the spreading onset acceleration level. A stick-slip contact line motion behavior is difficult to visualize with the data plotted here, but droplets vibrated at these lower ramp rates do have a noticeable fluctuating diameter change. Droplets that are vibrated with a linear ramp of acceleration greater than 100 g per second experience little deviation for the spreading onset acceleration level, and are well bound well by the error region determined by the dotted black lines.

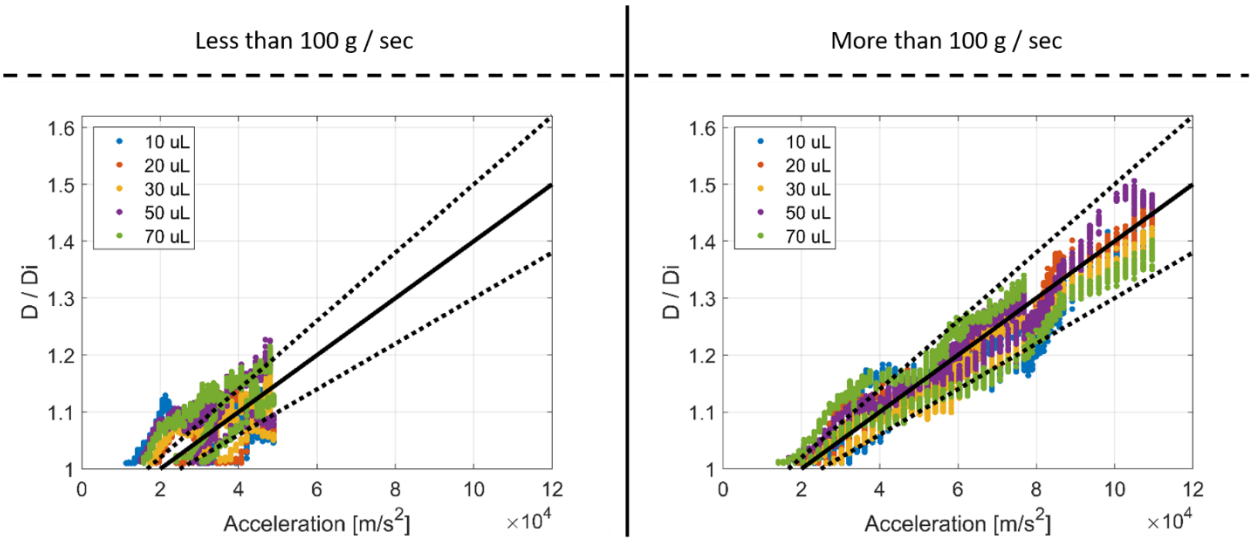

Figure 72. Data for 10 to 70 µL droplets of deionized water vibrated at frequencies of 33.2, 34.8, and 36.0 kHz where droplets are excited in a linear, but low rate of acceleration increase less than 100 g per second (left). Data for 10 to 70 µL droplets of deionized water vibrated at frequencies of 31.4, and 31.8 kHz where droplets are excited in a linear, but high rate of acceleration increase greater than 100 g per second (right). This data is compared to the measurement error (denoted by the dotted black lines) for the reference case.

A sufficient (greater than 100 g per second), but linear increase in acceleration seems to be best suited to controllably spread a droplet. However, this behavior may need its own study to quantify these observations. The acceleration ramp rate seems to cause a noticeable difference in the spreading behavior of droplets, but this behavior may also be frequency dependent. Similar spreading behavior occurred at different frequencies, however the frequencies were relatively similar. The impact of excitation frequency cannot be definitively determined using the current dataset though the relatively consistent responses across a wide range of excitation frequencies suggests that it is a secondary effect. The current data suggests that only a few (2-3) bands of vibration frequencies in the testing performed exist where acceleration increases linearly with driving signal amplitude. While additional vibration frequencies may be suitable for controlling the spreading of droplets reliably, these linear regions of acceleration increase do not reach sufficient levels of acceleration at the maximum 300 V excitation signal to observe enough

droplet spreading to demonstrate this suggestion. In order to verify this, a more powerful amplifier would be necessary. Alternatively, if the relationship between driving voltage and acceleration is known, a non-linear increase in driving signal amplitude might be used to smooth out the acceleration change over time when spreading droplets with precision is required. Though, as stated before, further testing is required to test this concept.

An empirical investigation of linear acceleration ramping rates could yield more information about the behavior of spreading droplets that could be useful for predicting droplet spreading initiation and controlling droplet diameter. However, existing data can be examined to probe this observation, as the stick and slip behavior of droplet spreading in some cases may be a result of viscous damping effects as the droplets vibrates. Other properties such as surface tension and density may also play a role.

6.5.2 Liquid Property Effects

Four different liquids were tested to study the spreading effects of varying mechanical properties (viscosity and surface tension in particular): deionized water, a 3:5 volume ratio water-glycerol mixture, ethylene glycol, and propylene glycol. The density, surface tension, and dynamic viscosity of all four fluids is presented in Table 11.

The density of all four liquids is relatively the same with only a 20% difference between all liquids. There is approximately a factor of 2 difference in the range of surface tensions, and more than an order of magnitude difference in dynamic viscosity.

Table 11. Properties of four different liquids used in testing.

	Deionized Water	**Water-Glycerol (3:5)**	**Ethylene Glycol**	**Propylene Glycol**
Density $[kg/m^3]$	997	1173	1110	1040
Surface Tension $[N/m]$	0.072	0.067	0.048	0.076
Dynamic Viscosity $[Pa * s]$	0.0009	0.02	0.0162	0.042

Varying fluid properties may change the resulting effects of spreading droplets with ultrasonic vibration. As droplets spread, the contact line advances outward. A fluid advancing along a boundary is subject to a shear stress (τ) in the direction opposite motion. For a Newtonian fluid, the shear stress is proportional to the velocity gradient at the surface and is given by

$$\tau(y) = \mu \frac{\partial u}{\partial y} \tag{26}$$

where μ is the dynamic viscosity of the liquid, and $\partial u/\partial y$ is the velocity gradient of the moving liquid. The shear stress manifests physically as a shear force (F) that opposes the advancing liquid on the solid surface. Visualized macroscopically, in the case of a droplet that spreads out symmetrically in all directions, this shear stress equates to a shear force of

$$F = \left(\mu \frac{\partial u}{\partial y}\right) A \tag{27}$$

where *A* is the instantaneous area of fluid in a net outward movement at the contact line. By examination of equation (27), if a droplet were to spread out on a surface by instantaneously increasing its liquid-solid contact area at the contact line, the rate of diameter change would be slowed by an increasing shear force. This increasing shear force would affect the rate at which droplets spread, but not necessarily affect the final spread diameter.

Droplets of a water/glycerol mixture with a volume ratio of 3:5 were used to test the hypothesis. The resulting mixture has a surface tension of 67 mN/m and density of 1173 kg/m^3 that are very similar to water (~20% different), but has a viscosity of 20 cP which is 22 times larger [128]. Measurements of this mixture permit a semi-isolated study of viscous effects by allowing other possible influencing factors to remain relatively unchanged. The ratio of diameter change to surface acceleration for the 54 different combinations of droplet volume and vibration frequency in Table 5 is plotted in Figure 73.

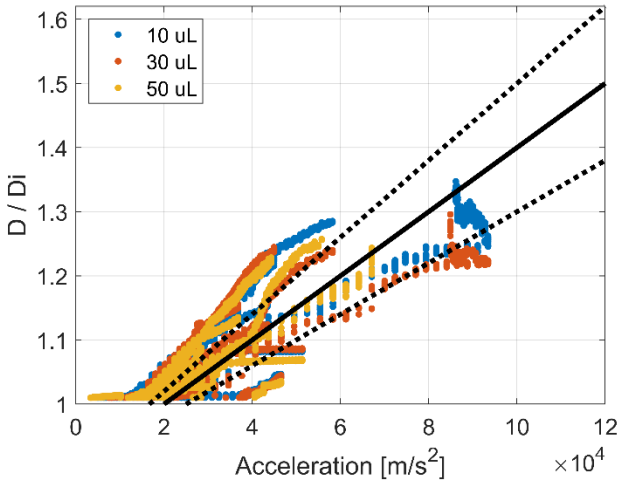

Figure 73. Data plotted as change in diameter against surface acceleration for 10 to 50 µL droplets of a 3:5 water-glycerol mixture vibrated at frequencies between 24 and 34 kHz. This data is compared to the measurement error (denoted by the dotted black lines) for the reference case.

Again, droplets of the water-glycerol mixture begin to spread at a threshold acceleration value of about 20,000 m/s^2, and appear to do so linearly with acceleration just as deionized water droplets (Figure 73). There is a significant amount of variation in the data for water-glycerol droplets, just as for the deionized water droplets. However, this data may suggest a slight increase in diameter change for a specific acceleration level when compared to the data range for deionized water droplets bound by the dotted black lines.

The spreading response of water-glycerol droplets also appears to be smoother when compared to water droplets from the previous data set (Figure 66). This could be due to the viscous damping of the surface perturbations on the droplet as it spreads. As a droplet spreads, microscopic contact line oscillations occur, but at a very small scale that is difficult to pick up with the imaging resolution. The higher viscous damping in the water-glycerol mixture may act like a ratchet, not allowing the contact line to recede as much between each oscillation.

The same ultrasonic transducer was used in both cases, but new hydrophobic substrates were mounted to the top of the piezoelectric transducer for set of data taken for a specific liquid. Coupling the piezoelectric transducer and the substrate with adhesives is not a completely repeatable fixturing method because the frequency response can change slightly as noted in a previous chapter. In addition, droplets were placed in the same initial position on the testing substrate during the duration of each individual set of tests (i.e., all the droplets of water-glycerol mixture that were tested), but this initial position can change slightly between each set of individual tests (i.e., between testing with deionized water droplets and water-glycerol droplets) due to the syringe pump mount and stepper motor positioning. The combination of different mounted substrates, slightly different droplet positioning, and different vibration frequencies used between data sets results in differing acceleration levels used to excite droplets from the

different data sets. Unfortunately the different levels of excitation acceleration is not avoidable. The acceleration levels would only be the same between all data sets that were collected if a single substrate was used for all the data sets, and the same vibration frequencies were used. However, separate data sets were required due to the time dependent factors like adhesive curing changes, substrate delamination, and coating degradation that could affect the repeatability of measurements over time.

To further investigate the effects caused by the change of liquids, droplets of deionized water and droplets of water-glycerol mixture with a volume ratio of 3:5 were again vibrated, but were both imaged in high speed to observe the dynamic spreading behavior more closely. Droplets of deionized water and water-glycerol were separately placed on the same location of the same substrate and excited by a piezoelectric transducer with a high amplitude, 300 V driving signal at 28.1 kHz. Imaging of droplets was done at a high speed of 1,000 fps to observe the fast transition in slow motion and improve temporal resolution. Excitation occurred at t = 0.5 seconds, and droplets quickly (~20 ms) spread to a quasi-equilibrium state (Figure 74).

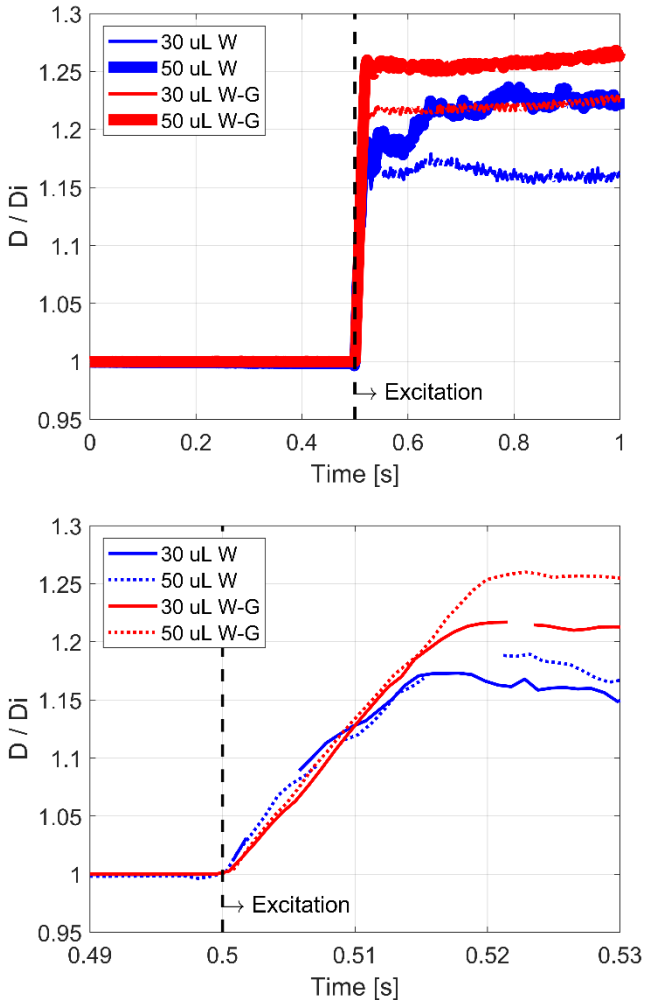

Figure 74. Spreading of droplets using a piezoelectric transducer pulsed with a sine wave signal of 300 V and 28.1 kHz imaged at a high frequency of 1,000 Hz. Droplets of a water-glycerol mixture and droplets of water spread at the same rate. Both figures are the same except for the time scale.

Water-glycerol droplets sustained a larger relative diameter increase under the same vibration conditions as the same volume deionized water droplet (Figure 74 top), but the spreading rate of various volume droplets of the water-glycerol mixture were similar to lower viscosity water droplets. (The examples plotted in Figure 74, are but a subset of the supporting observations). Additionally, close examination of the vibration pulse shows a slightly delayed response for water-glycerol droplets (Figure 74 bottom). This delay is on the order of a

thousandth of a second, while the spreading occurs on the order of a hundredth of a second. This delayed response to vibration seems insignificant unless rapid droplet spreading actuation was necessary for a specific application.

The larger extent of spreading for water-glycerol droplets is likely not due to viscosity, but rather the slight difference in surface tension. Deionized water has a higher surface tension (72 mN/m) than the 3:5 volume ratio water-glycerol mixture (67 mN/m). A high surface tension means that water droplets will be less wetting when compared to water-glycerol droplets due to the minimization of energy (Figure 75).

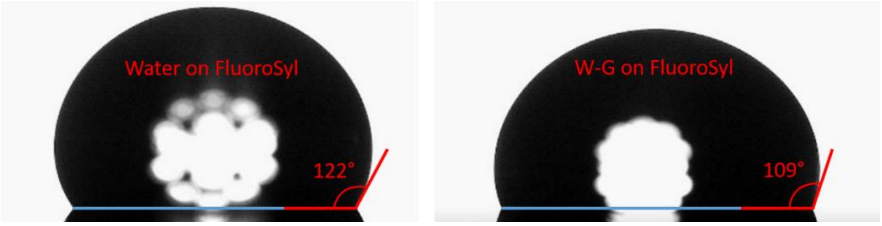

Figure 75. 30 µL droplets of deionized water (left) and a 3:5 volume ratio of water-glycerol (right) on FluoroSyl. Deionized water has a higher surface tension, and so it wets the coating less than the mixture of water-glycerol. Deionized water and water-glycerol have static contact angles of 122° and 109° respectively on FluoroSyl. This figure also demonstrates the different shape of the same volume droplets of different liquid on the same surface.

In a static condition, water droplets wet FluoroSyl with an average contact angle of 122°, while water-glycerol wets with a contact angle of 109°. The difference in the liquid's surface tensions lowers the wetting state of water-glycerol, so it is logical that this difference would also manifest as a larger spreading of water-glycerol droplets under the same acceleration. The surface energy difference is interesting and would be insightful to isolate and study. However, no other smooth hydrophobic coating tested other than FluoroSyl provides repeatable wetting conditions while spreading droplets with ultrasonic vibration, so the liquid properties would have to be changed instead.

The ratio of diameter change to surface acceleration for droplets of ethylene glycol is plotted on the left side of Figure 76. This figure shows the resulting relative diameter change for a given level of surface acceleration for 10 to 70 µL droplets of ethylene glycol as they are vibrated at frequencies between 24.6 and 41 kHz. While excitation frequencies varied in this range, data shown for ethylene glycol droplets was taken on the same testing surface in the same location on the surface.

The ratio of diameter change to surface acceleration for propylene glycol is plotted on the right side of Figure 76. This figure shows the resulting relative diameter change for a given level of surface acceleration for 10 to 70 µL droplets of propylene glycol as they are vibrated at frequencies between 24.8 and 42 kHz. The testing substrate and location were the same for all propylene glycol data shown, but these were different than the testing substrate and location used for ethylene glycol data.

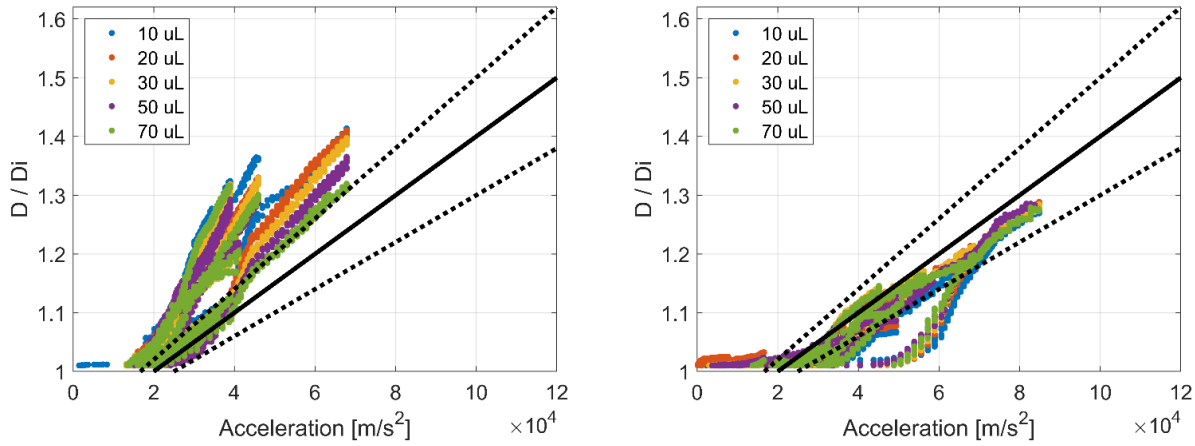

Figure 76. On the left, data is plotted as change in diameter against surface acceleration for 10 to 70 µL droplets of ethylene glycol vibrated between 24.6 and 41 kHz. On the right, data is plotted as change in diameter against surface acceleration for 10 to 70 µL droplets of propylene glycol vibrated between 24.8 and 42 kHz. This data is compared to the measurement error (denoted by the dotted black lines) for the reference case.

As with droplets of other liquids, droplets of ethylene glycol (Figure 76, left) and propylene glycol (Figure 76, right) begin to spread once a threshold surface acceleration level of approximately 20,000 m/s^2 is exceeded, and in a both cases there is a linear increase of the relative droplet diameter to acceleration. However, in the case of both liquids, and especially for ethylene glycol, the relative droplet diameter increase for a given level of surface acceleration seems to be different when comparing the measurement error region for deionized water between the dotted black lines. Droplets of ethylene glycol seem to initiate spreading at comparable acceleration levels as droplets of deionized water, but the increase of relative diameter is steeper in pitch consistently throughout the data set. Droplets of propylene glycol also initiate spreading at similar accelerations with the exception of one set of data points at a specific frequency of 29.8 kHz that coincides with the nonlinear frequency response at the resonance of the piezoelectric transducer. At this nonlinear response, the acceleration levels have higher errors and so this apparent outlier may represent measurement error. The increase in relative diameter is much less than ethylene glycol for a given level of acceleration, and also seems to increase at a pitch less than deionized water droplets as well. While the cause of this difference is not fully understood, it very likely has to do with contact angle and surface tension. Ethylene glycol droplets have a larger relative diameter increase for a given level of surface acceleration, and has a low surface tension of 42 mN/m. Propylene glycol has a low relative diameter increase for a given level of surface acceleration, and has a high surface tension of 76 mN/m. Deionized water and water-glycerol droplets have moderate surface tensions of 72 and 67 mN/m respectively, and droplets of these two liquids have a moderate relative diameter increase for a given level of surface acceleration (with the lower surface tension water-glycerol droplets having a slightly larger relative diameter increase). Droplets of ethylene glycol and propylene glycol, as well as

droplets of the water/glycerol mixture spread more smoothly compared to deionized water droplets. This could be attributed to the higher viscosity of the smoothly spreading liquids, and is indicative of less stick-slip behavior that would allow better control of droplet spreading and wetting using ultrasonic vibration.

While there is no apparent dependence of viscosity or droplet volume on droplet spreading initiation, surface tension and contact angle do seem to have an impact. However, this impact was not directly measureable in this data set due to the large variations apparent in the droplet spreading plots resulting from measurement error and multiple other variables like vibration frequency that may have an effect on the spreading behavior.

6.5.3 Vibration Frequency and Transducer Resonance

Droplets of deionized water were vibrated using a different sized ultrasonic transducer (PZT 2) with a different characteristic frequency response (Figure 77, left) compared to the transducer (PZT 1) used for previously vibrating droplets. Figure 77 shows the non-linear acceleration/voltage response behavior at some frequencies of each piezoelectric transducer that seems to have a significant impact on droplet spreading behavior. Conditions in Table 8 were tested with this larger transducer and are similar to the conditions in Table 4 with the exception of the transducer.

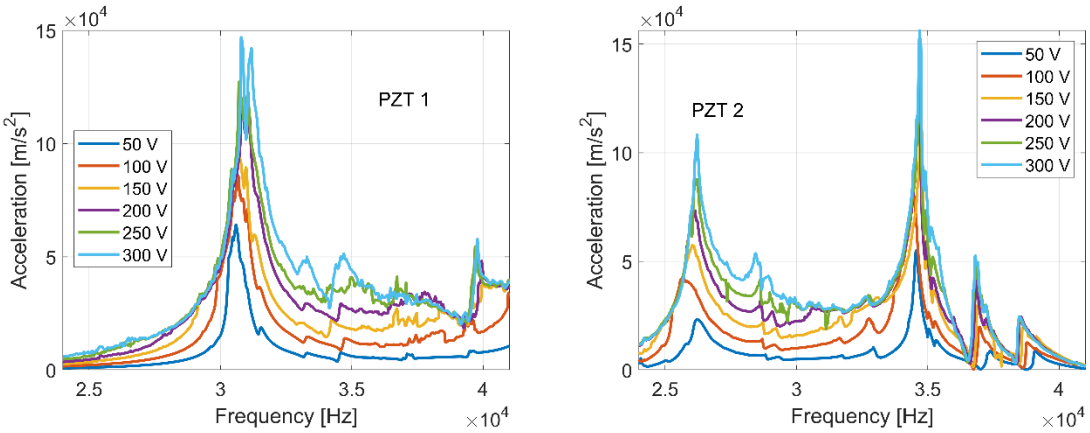

Figure 77. Frequency response of PZT 1 (left), and PZT 2 (right), as the driving signal is amplified from 0-300 V.

The parameters in Table 8 were used to vibrate droplets of water with the second ultrasonic transducer. The ratio of diameter change to surface acceleration magnitude for the 78 different combinations of droplet volume and vibration is plotted in Figure 78. The resulting relationship between the change in diameter and surface acceleration was very similar to the results of deionized water droplet spreading on the first piezoelectric transducer (denoted by the region between the dotted black lines in Figure 78 that specify the measurement error). Droplets begin to spread after a threshold acceleration of about 20,000 m/s^2 is exceeded, and the change in diameter is similar for a given acceleration level for deionized water droplets on both piezoelectric transducers, even though peak acceleration levels tested with the larger transducer were lower. Again, these data show no obvious volume dependence on spreading behavior. In relation, the main conclusion of this comparison was that there is no spreading dependency on droplet vibration mode.

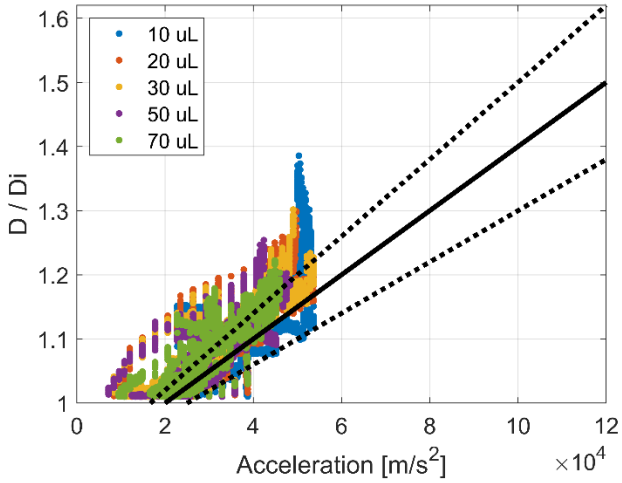

Figure 78. Data plotted as change in diameter against surface acceleration for 10 to 70 µL droplets of deionized water vibrated at frequencies between 24.4 and 40.6 kHz but using a different piezoelectric transducer than all other data sets. The data plotted is for water droplets vibrated on PZT 2, and is compared to the measurement error (denoted by the dotted black lines) for the reference case.

The use of different ultrasonic transducers with unique frequency responses initiated and spread droplets of the same liquid and volume, at similar accelerations, but at different frequencies. Figure 79 plots the spreading acceleration of all droplet volumes tested (10-70 µL) as black circles against the frequency response to various amplitudes of transducer driving signal, and shows that droplets begin to spread when accelerations are sufficiently high (> ~20,000 m/s^2), and that these acceleration levels are usually a result of characteristic transducer resonance, but can also occur off of a resonance if a sufficient level of driving amplitude is applied to the transducer. Additionally, Figure 79 demonstrates that acceleration levels that are sufficiently high enough to initiate droplet spreading are most consistent at frequencies away from a vibration resonance.

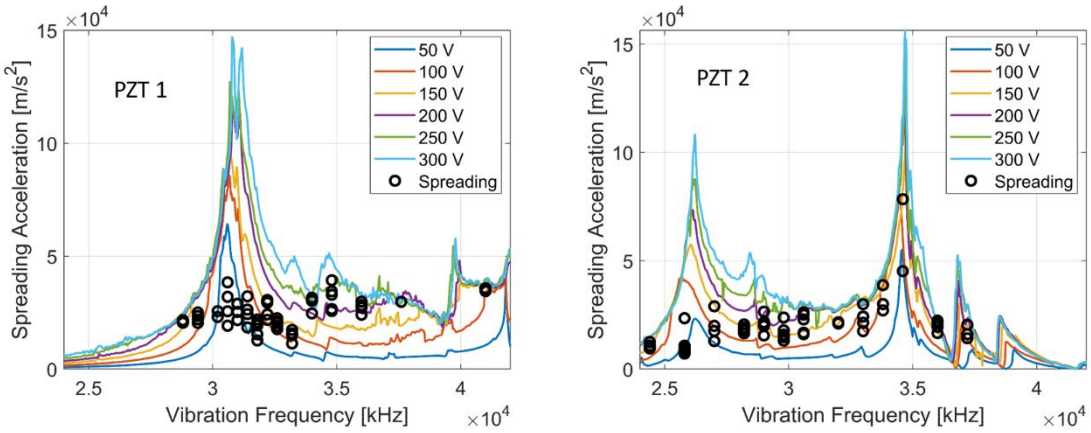

Figure 79. Frequency response difference between PZT 1 (left), and PZT 2 (right) at varying driving amplitudes. The acceleration at which droplet spreading was initiated is noted by the circles on the plot.

The data in the last few sections has provided significant insight on the spreading behavior of droplets vibrated at ultrasonic frequencies. However, the universal threshold acceleration of ~20,000 m/s^2 that seems to trigger the spreading of droplets is not well understood. Like with any empirical data set, the data can be difficult to discern trends, but there are some common methods of analysis that can be used to try and discern trends from empirical data.

6.6 Non-Dimensional Analysis

The vertical acceleration caused by the transducer is a dominant variable in the spreading behavior based on the previous discussion. One particular point of interest in this data is the consistent threshold level acceleration of 20,000 m/s^2. This threshold acceleration level initiates the spreading of droplets in every set of experiments. For this reason, the acceleration level recorded when each droplet began to spread (a_s) could be used to non-dimensionalize the spreading phenomenon.

6.6.1 Non-Dimensional Parameters

While many engineering problems rely on analytical solutions, many problems rely on experimental data to obtain a solution. Non-dimensional analysis using the Buckingham pi theorem can be applied to engineering problems by following a few steps outlined in [129]. The Buckingham pi theorem is based on dimensional homogeneity and assumes that for any physically meaningful equation involving k variables such as $u_1 = f(u_2, u_3, \dots, u_k)$, the dimensions on the left side of the of the equation must be the same as any term that stands by itself on the right side of the equation. This equation can then be rearranged into a set of dimensionless products (pi terms) so that $\Pi_1 = \phi(\Pi_2, \Pi_3, \dots, \Pi_{k-r})$. If an equation involving k variables that are unique and dimensionally homogeneous, it can be reduced to a relationship among $k - r$ independent dimensionless pi-terms, Π, where r is the minimum number of reference dimensions required to describe the variables.

To determine the Buckingham pi terms, all variables or parameters that may be important to the problem are first listed. The initiation of droplet spreading is of particular interest as it seems to occur a common value of surface acceleration (~ 20,000 m/s^2) for all different testing parameters. For the initiation of droplet spreading with ultrasonic vibration, important parameters could be any of the following:

- Spreading acceleration (a_s)
- Vibration frequency (f)
- Hysteresis ($H = \cos(\theta_{Advancing}) - \cos(\theta_{Receding})$)
- Liquid density (ρ)
- Liquid viscosity (μ)
- Liquid surface tension (σ)

- Contact angle (θ)
- Droplet volume (V)
- Droplet diameter (d)
- Droplet height (h)

As the level of surface acceleration seems to dictate the initiation and control of droplet spreading, it seems to be the most important parameter among the others to include in non-dimensional analysis. Surface tension does not seem to affect the onset of spreading, but it was included in the analysis as a variable in case the analysis says otherwise. It is important that all variables be independent, so after this is taken into account, the resulting final list of variables becomes:

- Liquid density (ρ)
- Liquid viscosity (μ)
- Liquid surface tension (σ)
- Contact angle (θ)
- Droplet diameter (d)
- Spreading acceleration (a_s)
- Vibration frequency (f)

Because contact angle (θ) is a dimensionless variable, it is added to the surface tension variable to form a sing variable $\sigma * cos$ (θ). All variables are expressed in terms of basic dimensions of mass, length and time.

- $d = L$
- $\rho = ML^{-3}$
- $\sigma * \cos(\theta) = MT^{-2}$

- $\mu = ML^{-1}T^{-1}$
- $f = T^{-1}$
- $a_s = LT^{-2}$

The required number of pi terms needed is determined by $\Pi = k - r$ which ends up being 3 in this case. Because the initiation of droplet spreading is of importance, it would be helpful to determine the functional relationship between the diameter of the droplet (d) and the rest of the independent variables, $d = f(\rho, \sigma * \cos(\theta), \mu, f, a_s)$. So, the dependent variable is droplet diameter (d), while 3 variables that will appear in each pi term (repeating variables) are selected as liquid density (ρ), liquid viscosity (μ), and spreading acceleration (a_s). The 3 pi terms were then formed by multiplying one of the non-repeating variables by the product of the repeating variables. Each raised to an exponent that makes the combination dimensionless. The resulting 3 pi terms are then:

$$\Pi_1 = \frac{(d)(\rho^{2/3})(a_s^{1/3})}{(\mu^{2/3})} \tag{28}$$

$$\Pi_2 = \frac{(\sigma * cos(\theta))(\rho^{1/3})}{(\mu^{4/3})(a_s^{1/3})} \tag{29}$$

$$\Pi_3 = \frac{(f)(\mu^{1/3})}{(\rho^{1/3})(a_s^{2/3})} \tag{30}$$

Thus the initiation of spreading could be studied by using the relationship:

$$\frac{(d)(\rho^{2/3})(a_s^{1/3})}{(\mu^{2/3})} = \phi\left(\frac{(\sigma * cos(\theta))\left(\rho^{\frac{1}{3}}\right)}{(\mu^{\frac{4}{3}})\left(a_s^{\frac{1}{3}}\right)}, \frac{(f)(\mu^{\frac{1}{3}})}{\left(\rho^{\frac{1}{3}}\right)\left(a_s^{\frac{2}{3}}\right)}\right) \quad (31)$$

6.6.2 Pi-Term Comparison

The pi terms were compared to determine if there is an experimental solution to the onset of spreading for ultrasonically vibrated droplets of any liquid and size. The comparison of pi terms was done by plotting two pi terms at a time, one on each axis. In the case of plotting Π_1 against Π_2, and Π_2 against Π_3, no relationship for the onset of spreading was found. However, plotting Π_1 against Π_3 in Figure 80 reveals a possible relationship for the onset of droplet spreading.

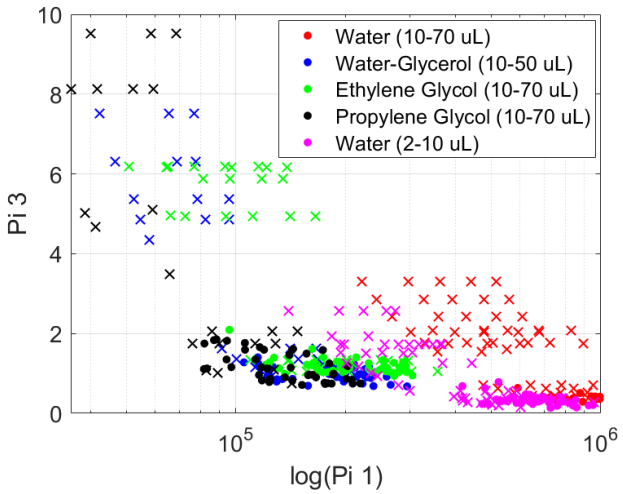

Figure 80. Π_1 plotted against Π_3 for droplets of all liquid types tested. Data plotted as solid circles represent the onset of spreading for any corresponding liquid droplet, while the data plotted as an "x" represent droplets for any corresponding liquid that did not begin to spread.

Data plotted as solid circles is calculated with the surface acceleration level at the time of droplet spreading initiation. This data, when plotted for all different liquid types as solid circles,

seems to forms a sloping line on the graph. Data plotted as an x is calculated with the maximum surface acceleration level experienced by droplets that did not spread (while the PZT was excited with 300 V amplitude sine wave at the specific frequency), or by a lower value of surface acceleration that did not cause droplets to spread. Droplets that did not spread remain above the line formed by the solid circles in the plot of Π_1 versus Π_3. As noted in the previous section, surface tension influences how much a droplet spreads under a given surface acceleration, but it does not seem to influence the initiation of spreading. It makes logical sense that Π_2 was not helpful in determining a solution to droplet spreading initiation because this term contains surface tension, however Π_1 and Π_3 do not. Using this figure could help predict whether or not a droplet would spread out under a given level of surface acceleration if the vibration frequency and physical properties of the droplet were known. This information could be helpful for applications where droplet shape needs to be manipulated, but it may be beneficial to understand droplet spreading in a less abstract way by looking at the possible forces generated by the vibration dynamics that could be influencing the transition.

6.6.3 Droplet Inertia Force and Surface Tension

Based on the previous discussion, the vertical acceleration caused by the transducer is a dominant variable in the spreading behavior, and this seems to be independent of droplet volume and frequency. This means that the droplet vibration mode would not be responsible for the spreading of droplets in contrast to investigations of low frequency droplet spreading [56, 65]. This can be further verified. If the droplet vibration mode were important to ultrasonic spreading, an up and down motion of the surface would result in a droplet inertia force shown as the yellow arrow in Figure 81.

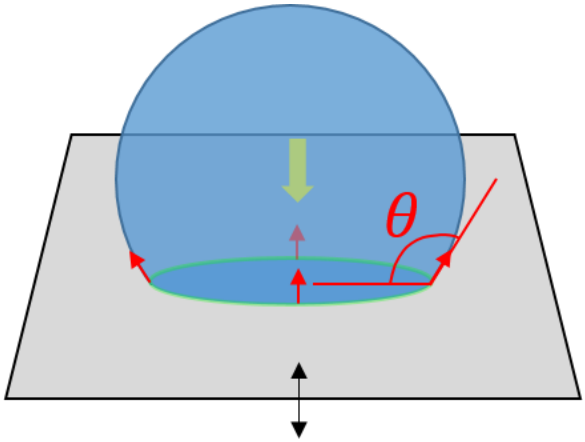

Figure 81. The droplet inertial force (yellow arrow) and surface tension (red arrows) on a droplet vibrated vertically on a flat plate.

The inertial force would be countered by the interfacial surface tension of the liquid that is responsible for the wetting state of the droplet and are shown as red arrows in Figure 81. This force acts around the entire contact line of the droplet at an angle θ. If the droplet followed the displacement of the surface, the acceleration would cause an increase in its inertia force. If this force becomes large enough compared to the surface tension force, the droplet could squash and spread. The ratio of droplet inertial force to surface tension is then

$$\frac{\rho V a_s}{\pi d \sigma \cos \theta} \tag{32}$$

where ρ is the liquid density, V is the droplet volume, a_s is the acceleration level when spreading initiates, d is the diameter of the droplet at the contact line, σ is the liquid surface tension, and θ is the initial contact angle of the droplet. If the initiation of spreading is a result of the droplet inertia force exceeding the surface tension force to some extent, this ratio would be the same for all volumes of droplets that spread. However, plotting the ratio against the vibration frequency at

the onset of droplet spreading does not reveal droplet dependency (Figure 82). Large differences (factor of 5-10) between the ratios for the data plotted suggest that this is not an explanation for the initiation of spreading. Therefore the ratio of inertial to capillary forces does not correlate with contact line motion.

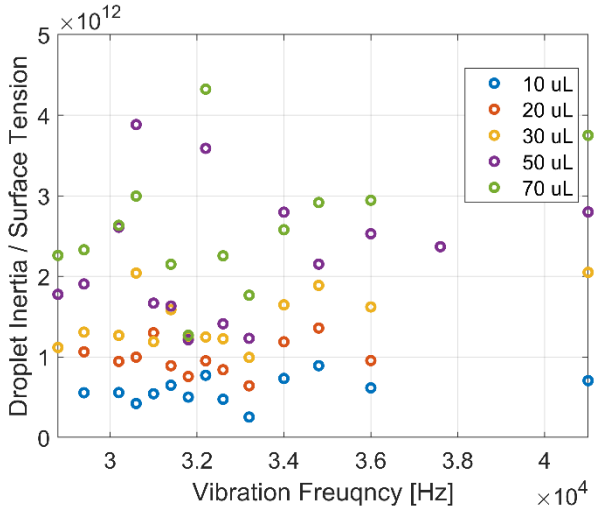

Figure 82. The ratio of droplet inertia to surface tension plotted against vibration frequency for various volume droplets of water. This does not discern a dependence of droplet vibration mode or volume on spreading.

6.7 Measurement Limitations

Imaging equipment can also impose difficulties when analyzing a vibrating droplet. Significant levels of acceleration that cause surface perturbations on a vibrating droplet cause oscillations of the contact angle and contact line. These are not macroscopically apparent, but contact angle oscillations can be resolved reasonably well (Figure 83, left) with high image rates and low exposure times (1 μs in this case). The oscillation in contact angle and contact line are not detected using the edge-detection algorithm to post-process images (Figure 83, right) due to the shape profile fit by the algorithm. The small surface waves traveling at high velocities makes it difficult to fully resolve the contact line motion spatially and temporally, however they are an

important effect to capture. Imaging equipment used resolves to 8.68 µm per pixel, and so capillary waves with amplitude on the order of this resolution are difficult to resolve. Additionally, the minimum exposure time of 1 µs is insufficient to eliminate all blurring of the droplet profile, especially at the contact line.

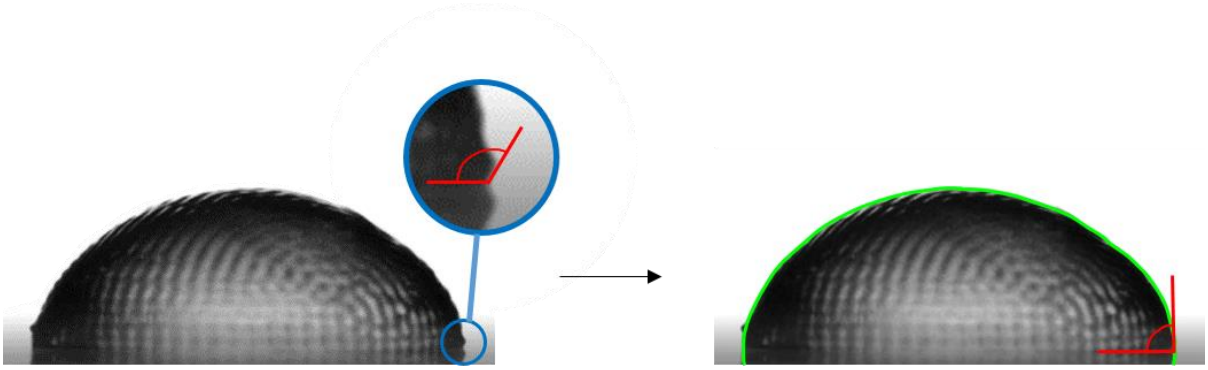

Figure 83. Magnification of contact angle oscillations at the triple point (left), and calculation of apparent contact angle by image processing. The length of exposure for this image was 1 µs.

Considering the theories developed for low frequency excitation of droplets [57, 78, 83], vibration of droplets at 20 kHz would initiate surface waves oscillating the contact angle at 20 kHz. The period of each oscillation would be the reciprocal of the vibration frequency: 50 µs. Depending on the amplitude of the waves, the contact angle would fluctuate from peak to peak in 25 µs, and would produce contact angle measurement error. Higher frequency vibration will exacerbate this error. Finally, the maximum frame rate of 90,000 frames per second of the available imaging equipment poses two main issues: aliasing at vibration frequencies higher than 30 kHz, and the necessity to crop the image sensor (and subsequently, the droplet) vertically at image rates higher than 4,000 frames per second.

Despite not being able to easily resolve the capillary waves on the liquid surface of ultrasonically vibrated droplets, the amplitude of the capillary waves at the onset of spreading can be approximated by

$$A = \frac{a_s}{f^2} \tag{33}$$

where A is the maximum amplitude of the solid surface, a_s is the solid surface acceleration at the initiation of spreading, and f is the vibration frequency. With the onset of spreading observed to occur at 20,000 m/s^2, the amplitude of surface waves would range from 35 μm at 24 kHz to 11 μm at 41 kHz. Waves with this amplitude and a wavelength only 3 to 6 times larger (96 μm at 24 kHz, to 65 μm at 41 kHz, determined in a previous section) propagating from the contact line of a droplet would generate sufficient oscillation in the contact angle of the droplet, and may be the cause for spreading. However, these parameters need to be measured to know for sure.

6.8 Conclusion

Ultrasonic vibration of droplets was shown to be a promising method for controlling the spreading of droplets on a smooth surface. The spreading behavior is independent of droplet volume and thus droplet vibration mode, but depends on the acceleration level due to vibration. Droplet diameter increase (spreading) is roughly linear with surface acceleration levels but depends on the liquid-air surface tension. A threshold acceleration of ~20,000 m/s^2 is necessary to initiate the spreading of droplets, and seemed to be independent of any physical property over the range tested, with the exception of droplets smaller than 4 μL (dominated by surface tension forces) where the trend may be beginning to break down. Droplet spreading is most controllable

with higher acceleration ramp rates that prevents a stick and slip droplet spreading behavior. Droplet spreading was found to be more erratic at the higher levels of acceleration tested.

The threshold value of 20,000 m/s^2 was comparable across the conditions tested. However, droplets of a water-glycerol mixture, with its lower surface tension, spread slightly more than water droplets for a given acceleration level. Similarly, other liquids tested with a lower surface tension compared to water spread slightly more than water for a given acceleration level and conversely for liquids with a higher surface tension compared to water. This effect was most likely caused by the different surface tensions of the various liquids altering the droplet wetting state before and during vibration. The increase in fluid viscosity did contribute to smoother spreading behavior, however. Spreading is also independent of vibration frequency, and can changes based on the characteristic frequency response of the transducer exciting the droplet. The use of pi terms determined from non-dimensional analysis of analytical data may be useful to determine whether or not droplet spreading will occur under a given surface acceleration level.

Acceleration measurement methods and imaging limitations may be a significant source of error in the empirical relationship between droplet spreading and acceleration, so improvements to testing and measurement methods would be beneficial to aid in discerning trends more accurately and with less spread in the future.

CHAPTER 7:

CONCLUSION AND FUTURE WORK

7.1 Conclusion

Ultrasonic vibration of droplets is not commonly studied due to the difficulties it poses to spatial and temporal quantification. Most studies that use high frequency vibration to affect wetting changes on surfaces, examine the effects qualitatively [1]. Here, we attempted to semi-quantitatively characterize the effects of ultrasonic vibration on droplets wetting a smooth hydrophobic surface, and harness the effects in a controllable manner. There were many limitations to this study that will need continued investigation, however the data acquired during this testing was gainful in uncovering new facets and parametric relationships to investigate.

Ultrasonic vibration was shown to affect the wetting state of droplets on a smooth, hydrophobic-coated surface by causing a droplet to spread. Droplet spreading was shown to be controllable by imaging deionized water droplets ranging from 10 to 70 µL on hydrophobic surfaces as they were vibrated at a constant frequency with ramped amplitude signal driving ultrasonic piezoelectric transducers. The spreading behavior was empirically related to the surface acceleration level caused by ultrasonic vibration. The initiation of droplet spreading occurs abruptly when a universal threshold surface acceleration of approximately 20,000 m/s^2 is exceeded for all surface and liquid combinations tested. Spreading behavior seems to be independent of droplet volume and excitation frequency unlike previous work with low frequency vibration [56, 65]. The most controllable droplet spreading is achieved with a linear

increase in surface acceleration at a sufficiently high acceleration increase rate. A substantial increase in liquid viscosity retards the spreading response, but not detrimentally, while a lower surface tension fluid increases the relative spreading of the same volume droplets.

Seven different hydrophobic fluoropolymer coatings were characterized in hopes of finding a robust coating that yielded repeatable wetting conditions, even under long term exposure to water and vibration. Most coatings used for studying the effects of ultrasonic vibration on droplets suffered from a degrading effect that caused a change in the contact angle hysteresis of the surface. In the case of coatings just exposed to water alone, the degradation was reversible by heating the coating to 160° C, but the degradation resulting from ultrasonic vibration of wet coatings was not. Only the FluoroSyl coating was found to be robust enough to maintain wetting state over long periods of water exposure and vibration.

Acceleration measurement error with an adhesive-mount accelerometer was reduced significantly and made somewhat repeatable by following careful guidelines for mounting and measurement determined by much investigation. Optimal cure times and methods for adhesives used in coupling vibrating components were determined. The acceleration level over the surface of the transducers that were used in studying the vibration of droplets varies significantly, and is not always piston-like. Three-dimensional surface vibration modes that may be a source of acceleration measurement error were discovered using laser Doppler vibrometry.

7.2 Future Work

Much additional work is needed to better understand the effects of high frequency vibration on wetting of droplets. Examination of the high-speed, micro-scale effects that occur during wetting transitions would help to understand the dynamics of droplet oscillations that may

be causing spreading to occur. Surface energy seems to have a significant impact on the spreading behavior of droplets excited with ultrasonic vibration. Studying the effects of surface tension by using a different surface energy coating could help to elucidate the cause of spreading. Varying droplet density without changing surface tension (by using a salt-water solution), while most likely insignificant, could help to eliminate droplet vibration modes as a cause of spreading. Additional transducers, with different frequency responses, could be used to determine whether the spreading of droplets can be predicted, by first measuring the frequency response of the surface, and then determining what vibration frequency and amplitude will cause a given diameter change for a droplet. This will be integral to the integrity of this model to predict droplet spreading using ultrasonic vibration. Using this model for droplet spreading would be useful in investigation of reversible wetting on textured surfaces. If hydrophobic textured surfaces are used to vibrate droplets and cause similar spreading behavior to smooth surfaces, this relationship could be used to alter the droplet shape and apparent contact angle on the textured surface. This could be helpful in overcoming the barriers to contact line motion and transition droplets reversible between the Cassie and Wenzel states on the textured surface.

To better understand these relationships, it may be helpful to make some adjustments in future testing. Polishing the aluminum cap of the piezoelectric transducer and then applying coatings directly to the cap may help to pacify inconsistencies caused by partial or full adhesive delamination of coated substrates used in testing. This however would not eliminate the need to still fix the accelerometer with adhesive unfortunately, but would be beneficial to eliminate one of the inconsistencies. The use of glass substrates is not recommended, as sudden delamination can cause whole data sets to be useless, and gradual changes in the adhesive bond during the

course of testing will affect the accuracy of acceleration measurement, and the repeatability of droplet spreading.

The inherent uncertainty of an accelerometer to measure acceleration – especially around the natural frequencies of the transducer where the magnitude of acceleration is non-linear makes this method of measurement inadequate. The measurement of surface acceleration with an accelerometer is limited to one dimension and may not characterize the motion of the surface well enough, to use in an empirical relationship with droplet spreading. The use of more sophisticated measurement equipment is necessary to aid in the investigation and characterization of droplet wetting phenomena caused by high frequency vibration. A laser Doppler vibrometer would be essential to obtain real-time, non-contact 3-D measurements of surface vibrations to measure surface displacement, velocity, and acceleration, as well as helpful information of mode shapes that occur at the onset, and duration of ultrasonic spreading. LDV measurements may help improve accuracy. Vibration characterization using LDV would need to be measured with the same conditions as testing. Without the use of LDV, it may be possible to focus on spreading data away from peaks where acceleration is still high enough, to obtain a better empirical relationship between parameters.

Using deionized water droplets of 10 µL or less in future testing will assure a consistent initial droplet wetting condition. If implemented, this could help to reduce measurement repeatability and inaccuracy, but the higher relative evaporation rates will necessitate the use of a humidity control chamber.

Surface energy seems to play a crucial role in the spreading of droplets using ultrasonic vibration. While FluoroSyl was a relatively reliable coating for vibrating droplets at ultrasonic frequencies, another robust, low hysteresis hydrophobic coating or surface would be beneficial to

use in testing to study the effects of varying surface tension without changing other fluid properties.

The approximation of the amplitude and wavelength of surface waves at the onset of droplet spreading in the previous chapter suggests that small-scale contact angle oscillations may be a key cause for ultrasonic spreading. High speed investigation of water droplets ultrasonically vibrated on FluoroSyl-coated glass substrates revealed a dynamic contact angle as high as ~138 º as the droplet spreads. This is substantially larger than the advancing angle of 114 º as previously measured. This suggests that droplet spreading under ultrasonic vibration could be a result of contact angle oscillation, just as under low frequency vibration. However, higher resolution study of the dynamic contact angle (especially at the onset of spreading) will be necessary to be certain.

The possibility of asymmetry in the spreading behavior of droplets suggests the use of overhead imaging to deal with both movement and asymmetric spreading. Imaging equipment and post-processing could be used and the droplet perimeter could be used as a parameter instead of diameter.

Varying the amplitude of the sine wave signal that excites the transducer at discrete frequencies near the resonance frequency of the transducer also allows the droplet diameter at the contact line to be controlled reversibly. Increasing the amplitude of this signal past a threshold value at different vibration frequencies causes the droplet to spread in a controlled manner to an equilibrium diameter that increases with the amplitude of the signal. Subsequently decreasing the amplitude of the signal will cause the droplet to controllably retract back to the receding angle of the liquid on the surface (Figure 84).

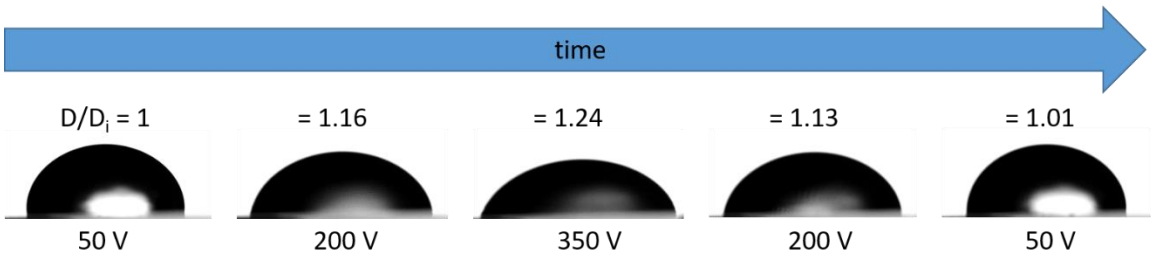

Figure 84. Spreading progression of a droplet vibrated with a sine wave at a frequency 20.5 kHz. Images are ordered from left to right in the sequence of time as a droplet is vibrated with 50 V, 200 V, 350 V, 200 V, 50 V amplitude sine wave. The ratio of instantaneous diameter to initial diameter is shown above each droplet for reference.

Reversible control of droplets is also demonstrated by increasing or decreasing vibration frequency in fine increments near the resonance frequency of the transducer. In this case, increasing and then decreasing the frequency causes the magnitude of surface acceleration to also increase and then decrease, causing the droplet to spread and then retract back to the receding angle of the liquid on the surface (Figure 85).

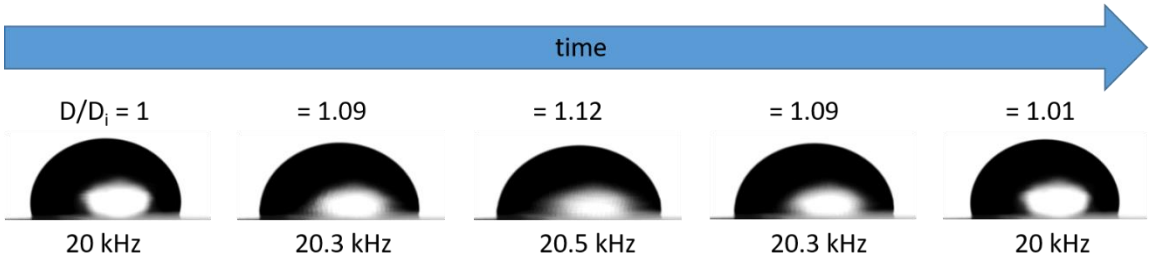

Figure 85. Spreading progression of a droplet vibrated with a sine wave with amplitude of 350 V. Images are ordered from left to right in the sequence of time as a droplet is vibrated with 20 kHz, 20.3 kHz, 20.5 kHz, 20.3 kHz, 20 kHz frequencies. The ratio of instantaneous diameter to initial diameter is shown above each droplet for reference.

The reversible control of droplet spreading using these methods would be an interesting addition to the previous work.

REFERENCES

[1] Eslamian, M. and F. Zabihi, *Ultrasonic Substrate Vibration-Assisted Drop Casting (SVADC) for the Fabrication of Photovoltaic Solar Cell Arrays and Thin-Film Devices.* Nanoscale Research Letters, 2015. **10**(1): p. 462.

[2] Galleguillos-Silva, R., Y. Vargas-Hernández, and L. Gaete-Garretón, *Wettability of a surface subjected to high frequency mechanical vibrations.* Ultrasonics Sonochemistry, 2017. **35**: p. 134-141.

[3] Chong, J., J.D. Whitehill, and A. Neild, *Low-volume filling of microplate wells using vibration.* Analytical Biochemistry, 2012. **425**(1): p. 10-12.

[4] Destgeer, G., et al., *Particle Separation inside a Sessile Droplet with Variable Contact Angle Using Surface Acoustic Waves.* Analytical Chemistry, 2017. **89**(1): p. 736-744.

[5] Daniel, S., M.K. Chaudhury, and P.G. de Gennes, *Vibration-Actuated Drop Motion on Surfaces for Batch Microfluidic Processes.* Langmuir, 2005. **21**(9): p. 4240-4248.

[6] Soltman, D., et al., *Methodology for Inkjet Printing of Partially Wetting Films.* Langmuir, 2010. **26**(19): p. 15686-15693.

[7] Silva-Bermudez, P., G. Ramirez, and S.E. Rodil, *11 - Corrosion resistant coatings for dental implants*, in *Bio-Tribocorrosion in Biomaterials and Medical Implants*, Y. Yan, Editor. 2013, Woodhead Publishing. p. 250-308.

[8] Keagy, J.A., et al., *CO2 promotes penetration and removal of aqueous hydrocarbon surfactant cleaning solutions and silylation in low-k dielectrics with 3nm pores.* The Journal of Supercritical Fluids, 2007. **42**(3): p. 398-409.

[9] Chappuis, J., *Lubrication by a new principle: The use of non-wetting liquids.* Wear, 1982. **77**(3): p. 303-313.

[10] Hegemann, D., H. Brunner, and C. Oehr, *Plasma treatment of polymers for surface and adhesion improvement.* Nuclear Instruments and Methods in Physics Research Section B: Beam Interactions with Materials and Atoms, 2003. **208**: p. 281-286.

[11] Cheng, Y.-T. and D.E. Rodak, *Is the lotus leaf superhydrophobic?* Applied Physics Letters, 2005. **86**(14): p. 144101.

[12] Hu, D.L., B. Chan, and J.W.M. Bush, *The hydrodynamics of water strider locomotion.* Nature, 2003. **424**: p. 663.

[13] Hamilton Iii, W.J. and M.K. Seely, *Fog basking by the Namib Desert beetle, Onymacris unguicularis.* Nature, 1976. **262**: p. 284.

[14] *Theory Of Surface Tension*, in *Surface And Colloid Science*, J.F. Padday, Editor. 1969, John Wiley & Sons, Inc.: New York.

[15] Gibbs, J.W., *Thermodynamics*. The Collected Works Of J. Willard Gibbs, Ph.D., LL.D. Vol. 1. 1928, New York: Longmans, Green and Co.

[16] *The Thermodynamics Of Fluid Interfaces*, in *Surface And Colloid Science*, F.C. Goodrich, Editor. 1969, John Wiley & Sons, Inc.: New York.

[17] Amin, R., et al., *Gas–gas experimental interfacial tension measurement.* Fluid Phase Equilibria, 2010. **295**(2): p. 230-236.

[18] Young, T., *III. An essay on the cohesion of fluids.* Philosophical Transactions of the Royal Society of London, 1805. **95**: p. 65-87.

[19] Meglio, J.M.D., *Contact Angle Hysteresis and Interacting Surface Defects.* EPL (Europhysics Letters), 1992. **17**(7): p. 607.

[20] Bayer, I.S. and C.M. Megaridis, *Contact angle dynamics in droplets impacting on flat surfaces with different wetting characteristics.* Journal of Fluid Mechanics, 2006. **558**: p. 415-449.

[21] Marmur, A., *Solid-Surface Characterization by Wetting.* Annual Review of Materials Research, 2009. **39**(1): p. 473-489.

[22] Fitzpatrick, R., *Surface Tension*, in *Theoretical Fluid Mechanics*. 2017, IOP Publishing. p. 3-1-3-21.

[23] Bonn, D., et al., *Wetting and spreading.* Reviews of Modern Physics, 2009. **81**(2): p. 739-805.

[24] Schrader, M.E., *Young-Dupre Revisited.* Langmuir, 1995. **11**(9): p. 3585-3589.

[25] de Gennes, P.G., F. Brochard-Wyart, and D. Quere, *Capillarity and Wetting Phenomena: Drops, Bubbles, Pearls, Waves*. 2004, New York, NY: Springer.

[26] Della Volpe, C., et al., *An Experimental Procedure to Obtain the Equilibrium Contact Angle from the Wilhelmy Method.* Oil & Gas Science and Technology - Rev. IFP, 2001. **56**(1): p. 9-22.

[27] *Wettability And Contact Angles*, in *Surface And Colloid Science*, R.E. Johnson, Editor. 1969, John Wiley & Sons, Inc: New York.

[28] Cubaud, T. and M. Fermigier, *Advancing contact lines on chemically patterned surfaces.* Journal of Colloid and Interface Science, 2004. **269**(1): p. 171-177.

[29] Gao, L. and T.J. McCarthy, *Contact Angle Hysteresis Explained.* Langmuir, 2006. **22**(14): p. 6234-6237.

[30] Krasovitski, B. and A. Marmur, *Drops Down the Hill: Theoretical Study of Limiting Contact Angles and the Hysteresis Range on a Tilted Plate.* Langmuir, 2005. **21**(9): p. 3881-3885.

[31] Bracco, G. and B. Holst, *Surface science techniques*. 2013, Berlin; New York: Springer.

[32] Andrieu, C., C. Sykes, and F. Brochard, *Average spreading parameter on heterogeneous surfaces.* Langmuir, 1994. **10**(7): p. 2077-2080.

[33] Wenzel, R.N., *Resistance of solid surfaces to wetting by water.* Industrial & Engineering Chemistry, 1936. **28**(8): p. 988-994.

[34] Cassie, A. and S. Baxter, *Wettability of porous surfaces.* Transactions of the Faraday society, 1944. **40**: p. 546-551.

[35] Kim, D., N.M. Pugno, and S. Ryu, *Wetting theory for small droplets on textured solid surfaces.* Scientific Reports, 2016. **6**: p. 37813.

[36] Koishi, T., et al., *Coexistence and transition between Cassie and Wenzel state on pillared hydrophobic surface.* Proceedings of the National Academy of Sciences, 2009. **106**(21): p. 8435-8440.

[37] Li, Y., et al., *Biomimetic Surfaces for High-Performance Optics.* Advanced Materials, 2009. **21**(46): p. 4731-4734.

[38] Andreas, S., et al., *The dream of staying clean: Lotus and biomimetic surfaces.* Bioinspiration & Biomimetics, 2007. **2**(4): p. S126.

[39] Kwon, G., et al., *On-Demand Separation of Oil-Water Mixtures.* Advanced Materials, 2012. **24**(27): p. 3666-3671.

[40] Truesdell, R., et al., *Drag Reduction on a Patterned Superhydrophobic Surface.* Physical Review Letters, 2006. **97**(4): p. 044504.

[41] Nakajima, A., *Design of hydrophobic surfaces for liquid droplet control.* Npg Asia Materials, 2011. **3**: p. 49.

[42] Yuan, Q. and Y.-P. Zhao, *Multiscale dynamic wetting of a droplet on a lyophilic pillar-arrayed surface.* Journal of Fluid Mechanics, 2013. **716**: p. 171-188.

[43] Hang, T., et al., *Super-hydrophobic nickel films with micro-nano hierarchical structure prepared by electrodeposition.* Applied Surface Science, 2010. **256**(8): p. 2400-2404.

[44] Ebert, D. and B. Bhushan, *Durable Lotus-effect surfaces with hierarchical structure using micro- and nanosized hydrophobic silica particles.* Journal of Colloid and Interface Science, 2012. **368**(1): p. 584-591.

[45] Lee, G.C., et al., *Induced liquid-solid contact via micro/nano multiscale texture on a surface and its effect on the Leidenfrost temperature.* Experimental Thermal and Fluid Science, 2017. **84**: p. 156-164.

[46] Hitchcock, S.J., N.T. Carroll, and M.G. Nicholas, *Some effects of substrate roughness on wettability.* Journal of Materials Science, 1981. **16**(3): p. 714-732.

[47] Liu, T.L. and C.-J.C. Kim, *Turning a surface superrepellent even to completely wetting liquids.* Science, 2014. **346**(6213): p. 1096.

[48] Fuqua, P.D., et al. *Fabrication of true 3D microstructures in glass/ceramic materials by pulsed UV laser volumetric exposure techniques*. in *Optoelectronics '99 - Integrated Optoelectronic Devices*. 1999. SPIE.

[49] Kanungo, M., et al., *Effect of Roughness Geometry on Wetting and Dewetting of Rough PDMS Surfaces.* Langmuir, 2014. **30**(25): p. 7358-7368.

[50] Vieu, C., et al., *Electron beam lithography: resolution limits and applications.* Applied Surface Science, 2000. **164**(1): p. 111-117.

[51] Gong, W., et al., *Wetting transition energy curves for a droplet on a square-post patterned surface.* Science Bulletin, 2017. **62**(2): p. 136-142.

[52] Bormashenko, E., *Progress in understanding wetting transitions on rough surfaces.* Advances in Colloid and Interface Science, 2015. **222**: p. 92-103.

[53] Ran, C., et al., *Wetting on Nanoporous Alumina Surface: Transition between Wenzel and Cassie States Controlled by Surface Structure.* Langmuir, 2008. **24**(18): p. 9952-9955.

[54] Frieder, M. and B. Jean-Christophe, *Electrowetting: from basics to applications.* Journal of Physics: Condensed Matter, 2005. **17**(28): p. R705.

[55] Adera, S., et al., *Non-wetting droplets on hot superhydrophilic surfaces.* Nature Communications, 2013. **4**: p. 2518.

[56] Whitehill, J., et al., *Droplet spreading using low frequency vibration.* Applied Physics Letters, 2011. **98**(13): p. 133503.

[57] Noblin, X., A. Buguin, and F. Brochard-Wyart, *Vibrated sessile drops: transition between pinned and mobile contact line oscillations.* Eur Phys J E Soft Matter, 2004. **14**(4): p. 395-404.

[58] Liu, G., et al., *Water Droplet Motion Control on Superhydrophobic Surfaces: Exploiting the Wenzel-to-Cassie Transition.* Langmuir, 2011. **27**(6): p. 2595-2600.

[59] Kelvin, L., *Oscillations of a liquid sphere.* mathematical and Physical papers, 1890. **3**: p. 384-386.

[60] Rayleigh, L., *The Theory of Sound, 2nd*. 1894, Macmillan, London.

[61] Lamb, H., *Hydrodynamics*. 1932: Cambridge university press.

[62] Santesson, S. and S. Nilsson, *Airborne chemistry: acoustic levitation in chemical analysis.* Analytical and Bioanalytical Chemistry, 2004. **378**(7): p. 1704-1709.

[63] Tian, Y., R.G. Holt, and R.E. Apfel, *A new method for measuring liquid surface tension with acoustic levitation.* Review of Scientific Instruments, 1995. **66**(5): p. 3349-3354.

[64] Adachi, M., et al., *Precise Density Measurements for Electromagnetically Levitated Liquid Combined with Surface Oscillation Analysis.* International Journal of Thermophysics, 2008. **29**(6): p. 2006-2014.

[65] Whitehill, J.D., A. Neild, and M.H. Stokes, *Forced spreading behavior of droplets undergoing low frequency vibration.* Colloids and Surfaces A: Physicochemical and Engineering Aspects, 2012. **393**: p. 144-152.

[66] Li, Y., R.J. Baker, and D. Raad, *Improving the performance of electrowetting on dielectric microfluidics using piezoelectric top plate control.* Sensors and Actuators B: Chemical, 2016. **229**: p. 63-74.

[67] Brunet, P., J. Eggers, and R.D. Deegan, *Motion of a drop driven by substrate vibrations.* The European Physical Journal Special Topics, 2009. **166**(1): p. 11-14.

[68] Noblin, X., R. Kofman, and F. Celestini, *Ratchetlike motion of a shaken drop.* Phys Rev Lett, 2009. **102**(19): p. 194504.

[69] Brunet, P., J. Eggers, and R.D. Deegan, *Vibration-Induced Climbing of Drops.* Physical Review Letters, 2007. **99**(14): p. 144501.

[70] Noblin, X., A. Buguin, and F. Brochard-Wyart, *Vibrations of sessile drops.* The European Physical Journal Special Topics, 2009. **166**(1): p. 7-10.

[71] Manor, O. and L.M. Pismen, *Effect of high-frequency in-plane substrate vibration on a three-phase contact angle.* Physics of Fluids, 2015. **27**(6): p. 062101.

[72] Dong, L., A. Chaudhury, and M. Chaudhury, *Lateral vibration of a water drop and its motion on a vibrating surface.* The European Physical Journal E: Soft Matter and Biological Physics, 2006. **21**(3): p. 231-242.

[73] Mettu, S. and M.K. Chaudhury, *Motion of Liquid Drops on Surfaces Induced by Asymmetric Vibration: Role of Contact Angle Hysteresis.* Langmuir, 2011. **27**(16): p. 10327-10333.

[74] Lyubimov, D.V., T.P. Lyubimova, and S.V. Shklyaev, *Non-axisymmetric oscillations of a hemispherical drop.* Fluid Dynamics, 2004. **39**(6): p. 851-862.

[75] Daniel, S., et al., *Ratcheting Motion of Liquid Drops on Gradient Surfaces.* Langmuir, 2004. **20**(10): p. 4085-4092.

[76] Daniel, S. and M.K. Chaudhury, *Rectified Motion of Liquid Drops on Gradient Surfaces Induced by Vibration.* Langmuir, 2002. **18**(9): p. 3404-3407.

[77] Bormashenko, E., et al., *Resonance Cassie−Wenzel Wetting Transition for Horizontally Vibrated Drops Deposited on a Rough Surface.* Langmuir, 2007. **23**(24): p. 12217-12221.

[78] Celestini, F. and R. Kofman, *Vibration of submillimeter-size supported droplets.* Physical Review E, 2006. **73**(4): p. 041602.

[79] Vukasinovic, B., M.K. Smith, and A. Glezer, *Dynamics of a sessile drop in forced vibration.* Journal of Fluid Mechanics, 2007. **587**: p. 395-423.

[80] Brunet, P., et al., *Droplet displacements and oscillations induced by ultrasonic surface acoustic waves: a quantitative study.* Phys Rev E Stat Nonlin Soft Matter Phys, 2010. **81**(3 Pt 2): p. 036315.

[81] Wang, Z. and J. Zhe, *Recent advances in particle and droplet manipulation for lab-on-a-chip devices based on surface acoustic waves.* Lab on a Chip, 2011. **11**(7): p. 1280-1285.

[82] Whitehill, J., et al., *Collection of suspended particles in a drop using low frequency vibration.* Applied Physics Letters, 2010. **96**(5): p. 053501.

[83] Sharp, J.S., D.J. Farmer, and J. Kelly, *Contact Angle Dependence of the Resonant Frequency of Sessile Water Droplets.* Langmuir, 2011. **27**(15): p. 9367-9371.

[84] Noblin, X., A. Buguin, and F. Brochard-Wyart, *Vibrated sessile drops: Transition between pinned and mobile contact line oscillations.* The European Physical Journal E, 2004. **14**(4): p. 395-404.

[85] Rodríguez-Valverde, M.A., F.J. Montes Ruiz-Cabello, and M.A. Cabrerizo-Vílchez, *A new method for evaluating the most-stable contact angle using mechanical vibration.* Soft Matter, 2011. **7**(1): p. 53-56.

[86] Smith, T. and G. Lindberg, *Effect of acoustic energy on contact angle measurements.* Journal of Colloid and Interface Science, 1978. **66**(2): p. 363-366.

[87] Decker, E.L. and S. Garoff, *Using Vibrational Noise To Probe Energy Barriers Producing Contact Angle Hysteresis.* Langmuir, 1996. **12**(8): p. 2100-2110.

[88] Thomson, J., *XLII. On certain curious motions observable at the surfaces of wine and other alcoholic liquors.* The London, Edinburgh, and Dublin Philosophical Magazine and Journal of Science, 1855. **10**(67): p. 330-333.

[89] Greenspan, H.P., *On the motion of a small viscous droplet that wets a surface.* Journal of Fluid Mechanics, 2006. **84**(1): p. 125-143.

[90] Bormashenko, E., et al., *Vibration-induced Cassie-Wenzel wetting transition on rough surfaces.* Applied Physics Letters, 2007. **90**(20): p. 201917.

[91] Lei, W., et al., *Vibration-induced Wenzel-Cassie wetting transition on microstructured hydrophobic surfaces.* Applied Physics Letters, 2014. **104**(18): p. 181601.

[92] Shokrollahi, S., F. Adel, and H. Ahmadian, *An investigation into the accelerometer mounting effects on signal transmissibility in modal measurements*. Vol. 24. 2017.

[93] *352A92 Accelerometer Datasheet*. Available from: http://www.pcb.com/contentstore/mktgContent/LinkedDocuments/Vibration/TM_352A91_352A92_lowres.pdf.

[94] Zhou, S.-W. and C.A. Rogers, *Heat Generation, Temperature, and Thermal Stress of Structurally Integrated Piezo-Actuators.* Journal of Intelligent Material Systems and Structures, 1995. **6**(3): p. 372-379.

[95] Asmatulu, R., et al., *Effects of UV degradation on surface hydrophobicity, crack, and thickness of MWCNT-based nanocomposite coatings.* Progress in Organic Coatings, 2011. **72**(3): p. 553-561.

[96] Yang, X.F., et al., *Blistering and degradation of polyurethane coatings under different accelerated weathering tests.* Polymer Degradation and Stability, 2002. **77**(1): p. 103-109.

[97] Gutiérrez-Cano, V., et al., *Thermal degradation of hydrophobic graphite-based thin film nano-coatings observed by Raman spectroscopy.* Thin Solid Films, 2018. **648**: p. 8-11.

[98] Han Yeong, Y., et al., *Temperature and humidity effects on superhydrophobicity of nanocomposite coatings.* Applied Physics Letters, 2012. **100**(5): p. 053112.

[99] Mahadik, S.A., et al., *Durability and restoring of superhydrophobic properties in silica-based coatings.* Journal of Colloid and Interface Science, 2013. **405**: p. 262-268.

[100] Ji, W.-G., et al., *Reducing the water absorption in epoxy coatings by silane monomer incorporation.* Corrosion Science, 2006. **48**(11): p. 3731-3739.

[101] Vosgien Lacombre, C., et al., *Water uptake in free films and coatings using the Brasher and Kingsbury equation: a possible explanation of the different values obtained by electrochemical Impedance spectroscopy and gravimetry.* Electrochimica Acta, 2017. **231**: p. 162-170.

[102] Zhou, Q. and Y. Wang, *Comparisons of clear coating degradation in NaCl solution and pure water.* Progress in Organic Coatings, 2013. **76**(11): p. 1674-1682.

[103] Boinovich, L., A.M. Emelyanenko, and A.S. Pashinin, *Analysis of Long-Term Durability of Superhydrophobic Properties under Continuous Contact with Water.* ACS Applied Materials & Interfaces, 2010. **2**(6): p. 1754-1758.

[104] Zhou, Q., Y. Wang, and G.P. Bierwagen, *Flow accelerated degradation of organic clear coat: The effect of fluid shear.* Electrochimica Acta, 2014. **142**: p. 25-33.

[105] Yuan, Z., et al., *A novel fabrication of a superhydrophobic surface with highly similar hierarchical structure of the lotus leaf on a copper sheet.* Applied Surface Science, 2013. **285**: p. 205-210.

[106] Youngblood, J.P., et al., *Coatings Based on Side-chain Ether-linked Poly(ethylene glycol) and Fluorocarbon Polymers for the Control of Marine Biofouling.* Biofouling, 2003. **19**(sup1): p. 91-98.

[107] Rao, A.V., et al., *Mechanically stable and corrosion resistant superhydrophobic sol–gel coatings on copper substrate.* Applied Surface Science, 2011. **257**(13): p. 5772-5776.

[108] Liu, Y., et al., *Superhydrophobic Nanocomposite Coating for Reliability Improvement of Microelectronics.* IEEE Transactions on Components, Packaging and Manufacturing Technology, 2013. **3**(7): p. 1079-1083.

[109] Arunkumar, P., et al., *Hydrophobic Organic Skin as a Protective Shield for Moisture-Sensitive Phosphor-Based Optoelectronic Devices.* ACS Applied Materials & Interfaces, 2017. **9**(8): p. 7232-7240.

[110] Lu, H.W., et al., *A diffuse-interface model for electrowetting drops in a Hele-Shaw cell.* Journal of Fluid Mechanics, 2007. **590**: p. 411-435.

[111] Bonhye, K. and K. Chang-Jin, *Evaluation of repeated electrowetting on three different fluoropolymer top coatings.* Journal of Micromechanics and Microengineering, 2013. **23**(6): p. 067002.

[112] Arcella, V., A. Ghielmi, and G. Tommasi, *High Performance Perfluoropolymer Films and Membranes.* Annals of the New York Academy of Sciences, 2006. **984**(1): p. 226-244.

[113] Liu, G., et al., *Water Droplet Motion Control on Superhydrophobic Surfaces: Exploiting the Wenzel-to-Cassie Transition RID A-6986-2010 RID A-6607-2008.* Langmuir, 2011. **27**(6): p. 2595-2600.

[114] Simal, S., et al., *Use of ultrasound to increase mass transport rates during osmotic dehydration.* Journal of Food Engineering, 1998. **36**(3): p. 323-336.

[115] Bellex, *Cytop Catalog*. 2009.

[116] Cytonix. *FluoroPel Coatings Selection Guide*. Available from: https://www.cytonix.com/Articles.asp?ID=252.

[117] Cytonix. *FluorAcryl 3298 Datasheet*. Available from: https://www.cytonix.com/Articles.asp?ID=277.

[118] Cytonix. *FluoroSyl 3750 Datasheet*. Available from: https://www.cytonix.com/FluoroSyl-3750-p/fsm3750_60ml.htm.

[119] Trujillo-Pino, A., et al., *Accurate subpixel edge location based on partial area effect.* Image and Vision Computing, 2013. **31**(1): p. 72-90.

[120] Trujillo-Pino, A., *Accurate subpixel edge location*. 2017. p. Detection of subpixel edges with very high precision in grey level images.

[121] Gal, O., *fit_ellipse*. 2003. p. Find the best fit for an ellipse using a given set of points (a closed contour).

[122] Andersen, N.K., *Drop Shape Analysis*. 2016. p. Fit contact angle by double ellipses or polynomials.

[123] Pierce, E., F.J. Carmona, and A. Amirfazli, *Understanding of sliding and contact angle results in tilted plate experiments.* Colloids and Surfaces A: Physicochemical and Engineering Aspects, 2008. **323**(1): p. 73-82.

[124] Feng, L., et al., *Super-Hydrophobic Surfaces: From Natural to Artificial.* Advanced Materials, 2002. **14**(24): p. 1857-1860.

[125] Nakajima, A., K. Hashimoto, and T. Watanabe, *Recent Studies on Super-Hydrophobic Films.* Monatshefte für Chemie / Chemical Monthly, 2001. **132**(1): p. 31-41.

[126] Rosen, M.J., *Wetting and Its Modification by Surfactants*, in *Surfactants and Interfacial Phenomena*. 2004.

[127] Bormashenko, E., et al., *Cassie−Wenzel Wetting Transition in Vibrating Drops Deposited on Rough Surfaces: Is the Dynamic Cassie−Wenzel Wetting Transition a 2D or 1D Affair?* Langmuir, 2007. **23**(12): p. 6501-6503.

[128] Pagliaro, M. and M. Rossi, *Glycerol: properties and production.*

[129] Munson, B.R., A.P. Rothmayer, and T.H. Okiishi, *Fundamentals of Fluid Mechanics, 7th Edition*. 2012: Wiley.

APPENDIX A:

COPYRIGHT PERMISSIONS

The permission below is for the use of material in Chapter 4 and Chapter 5.

ASME Journals Digital Submission Tool
Guidelines and Information

Rights and Permissions

Assignment of Copyright
ASME requests that authors/copyright owners assign copyright to ASME in order for a journal paper to be published by ASME. Authors exempt from this request are direct employees of the U.S. Government, whereby papers are not subject to copyright protection in the U.S., or non-U.S. government employees, whose governments hold the copyright to the paper.

For more information on copyright, please view the Copyright Transfer information page.

Retained Rights of Authors
Authors retain all proprietary rights in any idea, process, procedure, or articles of manufacture described in the Paper, including the right to seek patent protection for them. Authors may perform, lecture, teach, conduct related research, display all or part of the Paper, and create derivative works in print or electronic format. Authors may reproduce and distribute the Paper for non-commercial purposes only. Non-commercial applies only to the sale of the paper per se. For all copies of the Paper made by Authors, Authors must acknowledge ASME as original publisher and include the names of all author(s), the publication title, and an appropriate copyright notice that identifies ASME as the copyright holder.

Permissions
Once your paper has been published by ASME, you may wish to submit it for inclusion in a non-ASME publication or to incorporate some or all of its elements in another work. Since ASME is the legal holder of copyright for its papers, it will be necessary for you to secure the permission of the copyright holder to have its material published in another source.

In this case, for permission to have your paper - in whole or in part, as is or adapted - published elsewhere, please submit your request here

Questions
The ASME Publishing staff is available to discuss current ASME policy on permissions and rights. Please feel free to contact us with any questions or comments at: permissions@asme.org.